

# POLITECNICO DI TORINO

Master thesis in Biomedical Engineering



## Impact of Stenosis Length and Severity on Clinical Functional Parameters in an Atherosclerotic Coronary Model

**Supervisor:** Prof. Umberto Morbiducci

**Co-supervisors:** Dr. Diego Gallo

Ing. Maurizio Lodi Rizzini

**Master student**

Alessandra Porta

**Academic year 2017/2018**



# INDEX

ABSTRACT .....	5
SOMMARIO .....	7
CHAPTER 1 .....	9
THE CARDIOVASCULAR SYSTEM .....	9
1.1 The heart .....	10
1.2 Blood vessels .....	12
1.2.1 Structural elements of the artery wall .....	14
1.2.2 Anatomy of vessels wall .....	15
1.2.3 Classification of arteries .....	18
1.3 Blood tissue .....	19
1.4 Blood rheology .....	21
1.4.1 Blood density .....	21
1.4.2 Blood viscosity .....	22
1.4.3 Rheological Newtonian model .....	23
1.4.4 Rheological non-Newtonian models .....	24
1.5 Wall Shear Stress (WSS) .....	28
CHAPTER 2 .....	30
CORONARY SYSTEM AND ASSOCIATED PATHOLOGIES .....	30
2.1 Coronary anatomy .....	30
2.2 Physiology of the coronary flow .....	34
2.3 Atherosclerosis .....	34
2.3.1 Main causes of atherosclerosis .....	37
2.3.2 Effects of atherosclerosis in coronary arteries .....	38
2.4 Measurement and classification of coronary stenosis .....	39
CHAPTER 3 .....	44
VIRTUAL FRACTIONAL FLOW RESERVE FOR NON-INVASIVE FUNCTIONAL ASSESSMENT OF STENOSIS IN CORONARY ARTERIES .....	44
3.1 Fractional Flow Reserve .....	44
3.1.1 Measurement of FFR .....	47
3.1.2 FFR in the most common coronary stenosis location .....	48
3.1.3 Limits of FFR and current solutions .....	51
3.2 Computation of vFFR through Computational Fluid Dynamics .....	52

3.2.1	Boundary conditions .....	55
3.2.2	vFFR computation: steady VS transient analysis .....	58
3.3	Relationship between FFR and WSS .....	59
3.4	Advantages and disadvantages of vFFR .....	59
CHAPTER 4	.....	61
METHODS	.....	61
4.1	Geometry model and generation of stenosis .....	61
4.2	Pre-processing .....	66
4.3	Sensitivity Analysis .....	72
4.4	CFD simulations .....	81
4.5	Post-processing .....	83
CHAPTER 5	.....	84
RESULTS AND DISCUSSION	.....	84
5.1	WSS and pressure at rest and hyperemia .....	84
5.2	FFR at rest and hyperemia .....	90
CONCLUSIONS	.....	96
BIBLIOGRAPHY	.....	98

# ABSTRACT

Among all the pathologies that affect the circulatory system, coronary artery diseases (CADs) are one of the main causes of death in the developed countries.

Coronary arteries represent the only source of blood supply for the myocardium: they are capable to self-regulate to maintain blood flow at levels appropriate to the needs of the cardiac muscle. In fact, when the oxygen requirements of the myocardium increase, there is an increase in coronary flow to satisfy the metabolic demand, while a decrease of cardiac activity is associated to a decrease of coronary flow.

However, these narrow vessels are commonly affected by atherosclerosis which determines a reduction in the vessel lumen with a consequent increase of resistance to blood flow, causing a decrease of perfusion in downstream regions.

The early detection and quantification of stenosis severity is important for two aspects: on the one hand, to decide if a percutaneous coronary revascularization procedure (PCI) must be planned to restore the correct vascularization of tissues and avoid the occurrence of ischaemic events, on the other hand to avoid unnecessary interventions if the lesion is not functionally significant.

Fractional Flow Reserve (FFR) has been accepted as the gold standard for the early detection and quantification of functional significance of coronary artery stenosis. This index is defined as the ratio between the mean coronary pressure distal to the stenosis and the mean aortic pressure under condition of maximal hyperemia. It is measured using pressure wires during Coronary Angiography and requires the induction of hyperemia through adenosine infusion.

Because of the invasiveness of this procedure, virtual Fractional Flow Reserve (vFFR) has emerged as an attractive alternative to the invasive FFR, ensuring operational and economic benefits at the same time. Starting from CTA (Computed Tomography Angiography) images and through the application of realistic boundary conditions, FFR is computed performing CFD simulations, which provide the relationship between flow parameters and the severity of the lesion which affects the vessel.

In this thesis, vFFR was computed to assess the functional significance of nine stenotic models, obtained introducing a concentric Gaussian stenosis in the proximal circumflex coronary artery of a non-pathological model, by varying the percentage of diameter reduction of the vessel and the extension of lesion. Three different degrees of occlusion

were simulated (30, 50, 75 %), to observe the effects given by a non-obstructive, an intermediate and an obstructive stenosis, and three different stenosis extension (3, 15, 25 mm), one for each typology according to the AHA classification (type A, B, C).

CFD steady simulations were performed in all models under two conditions of flow, rest and hyperemia, then WSS and static pressure gradient distributions were analysed and FFR was calculated to understand the relationship between stenosis geometry and the pressure drop caused by the lesion itself.

Results showed that at rest the flow does not involve any significant pressure drops in all stenotic models, regardless of the percentage of diameter reduction and stenosis extension; conversely, at hyperemia a greater impact of stenoses geometrical features on FFR values was observed. In particular, it was noticed that short stenoses ( $L = 3$  mm) are not significant even though their degree of occlusion is important, as well as those characterized by the greatest extension ( $L = 25$  mm) and mild degree of occlusion (30%). Even stenoses characterized by mild (30%) and intermediate (50%) percentage of occlusion with intermediate extension ( $L = 15$  mm) do not result as functionally significant. On the other hand, as the degree of occlusion and stenosis extension both increase, there is a decrease on FFR values, meaning that the obstruction to blood flow becomes more evident; in fact, stenoses with the highest percentage of occlusion (75%) with intermediate ( $L = 15$  mm) and the greatest extension ( $L = 25$  mm) show FFR values much lower than the cut-off value of 0.8, indicating high risk of ischaemia in downstream regions.

# SOMMARIO

Tra tutte le patologie che colpiscono il sistema circolatorio, le patologie delle arterie coronarie sono una delle principali cause di morte nei paesi sviluppati.

Le arterie coronarie rappresentano l'unica fonte di rifornimento di sangue per il miocardio: sono in grado di autoregolarsi per mantenere il flusso sanguigno a livelli adeguati alle esigenze del muscolo cardiaco. Infatti, quando il fabbisogno di ossigeno del miocardio aumenta, vi è un aumento del flusso coronarico per soddisfare la domanda metabolica, mentre una diminuzione dell'attività cardiaca è associata ad una diminuzione del flusso coronarico.

Tuttavia, questi stretti vasi sono comunemente colpiti dall'aterosclerosi che determina una riduzione del lume del vaso con un conseguente aumento della resistenza al flusso sanguigno, causando una diminuzione della perfusione nelle regioni a valle.

L'individuazione precoce e la quantificazione della severità di una lesione è importante per due aspetti: da un lato, per decidere se è necessario pianificare una procedura di rivascolarizzazione (PCI) per ripristinare la corretta vascolarizzazione dei tessuti ed evitare il verificarsi di eventi ischemici, d'altra parte per evitare interventi superflui se la lesione non è funzionalmente significativa.

Il Fractional Flow Reserve (FFR) è stato accettato come il gold standard per il rilevamento e la quantificazione della severità funzionale delle stenosi nelle arterie coronariche. Questo indice è definito dal rapporto tra la pressione coronarica media distale alla stenosi e la pressione aortica media in condizione di iperemia massimale. Viene misurato utilizzando cavi di pressione durante Angiografia Coronarica e richiede l'induzione di iperemia attraverso l'infusione di adenosina.

A causa dell'invasività di questa procedura, il virtual Fractional Flow Reserve (vFFR) è emerso come un'interessante alternativa all'FFR invasivo, assicurando al contempo benefici operazionali ed economici. A partire da immagini TCA (Tomografia Computerizzata Angiografica) e attraverso l'applicazione di condizioni al contorno realistiche, l'FFR viene calcolato effettuando simulazioni CFD, che forniscono la relazione tra i parametri di flusso e la severità della lesione che colpisce il vaso.

In questa tesi, il vFFR è stato calcolato per valutare la severità funzionale di nove modelli stenotici, ottenuti introducendo una stenosi Gaussiana concentrica nell'arteria coronaria circonflessa prossimale di un modello non patologico, variando la percentuale di

riduzione del diametro del vaso e l'estensione della lesione. Sono stati simulati tre diversi livelli di occlusione (30, 50, 75%), per osservare gli effetti dati da una stenosi non ostruttiva, intermedia e ostruttiva, e tre diverse estensioni (3, 15, 25 mm), una per ciascuna tipologia secondo la classificazione AHA (tipo A, B, C).

Sono state effettuate simulazioni CFD stazionarie in tutti i modelli con due condizioni di flusso, riposo e iperemia, poi sono state analizzate le distribuzioni del WSS e del gradiente della pressione statica ed è stato calcolato l'FFR per capire la relazione tra la geometria della stenosi e la caduta di pressione causata dalla lesione stessa.

I risultati hanno mostrato che a riposo il flusso non determina cadute di pressione significative in nessun modello stenotico, a prescindere dalla percentuale di riduzione del diametro e dall'estensione della stenosi; al contrario, in iperemia è stato osservato un maggiore impatto delle caratteristiche geometriche delle stenosi sui valori dell'FFR. In particolare, è stato notato che stenosi corte ( $L = 3\text{mm}$ ) non sono significative anche se il loro grado di occlusione è importante, così come quelle caratterizzate dall'estensione maggiore ( $L = 25\text{ mm}$ ) e livello di occlusione lieve (30%). Anche le stenosi caratterizzate da una percentuale di occlusione lieve (30%) e intermedia (50%) con estensione intermedia ( $L = 15\text{ mm}$ ) non risultano funzionalmente significative. D'altra parte, all'aumentare sia del grado di occlusione che dell'estensione della stenosi, vi è una diminuzione dei valori dell'FFR, indicando che l'ostruzione al flusso diventa più evidente; infatti, stenosi con la maggiore percentuale di occlusione (75%) ed estensione intermedia ( $L = 15\text{mm}$ ) e maggiore ( $L = 25\text{ mm}$ ) mostrano valori dell'FFR molto minori rispetto al valore di cut-off di 0.8, indicando un elevato rischio di ischemia nelle regioni a valle.

# CHAPTER 1

## THE CARDIOVASCULAR SYSTEM

The cardiovascular system, also called circulatory system, is a closed system responsible for the circulation of blood in all districts of the body through an intricate network of vessels. It allows the transport of nutrients, respiratory gases and metabolic products, permitting integration among the various tissues <sup>[1]</sup>. Blood is pumped by the heart to all tissues, releases nutrients and then it goes back to the heart.

Cardiovascular system (Figure 1.1) consists of 3 main components: heart, vessels and blood.

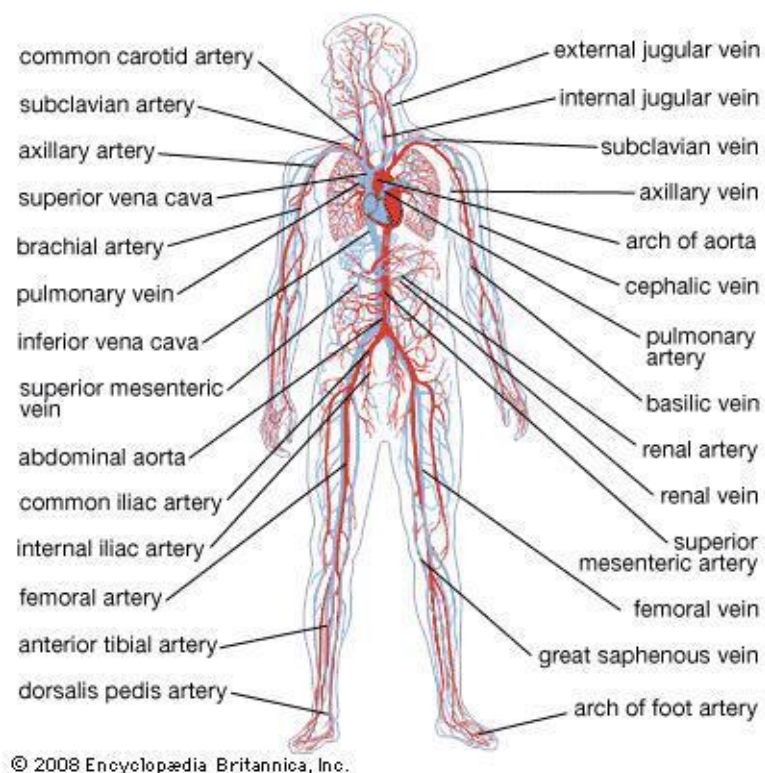


*Figure 1.1 The cardiovascular system* <sup>[1]</sup>

## 1.1 The heart

The heart is a chambered muscular organ whose role is to pump blood to all tissues. It is located obliquely within the chest cavity just left of center, with the apex pointing downward. The heart is divided into two cavities: the left cavity pumps blood throughout the body, while the right cavity throughout the lungs. Each cavity is in turn divided into two chambers: the upper ones are called atria and the lower ones, ventricles.

The heart is enclosed in a double-layered membrane called pericardium, a strong layer of dense connective tissue that surrounds the heart to hold it in its position and avoid the heart overflowing [2].

The heart wall has three layers: epicardium, myocardium and endocardium (Figure 1.2).

**Epicardium** is the outer layer of the heart wall and it represents the visceral layer of the pericardium; it is composed of loose connective tissue, including elastic fibers and adipose tissue, and its function is to protect the inner layers and to assist in the production of pericardial fluid. Found in this heart layer are the coronary blood vessels [3].

**Myocardium** is the middle layer of the heart wall and constitutes the cardiac muscle. It is composed of cardiac muscle fibers which enable heart contractions, and cardiac conduction is made possible by specialized fibers bundles, consisting of the atrioventricular bundle and Purkinje fibers, that carry electrical impulses down the center of the heart to the ventricles; these impulses trigger the muscle fibers in the ventricles to contract [3].

**Endocardium** is the thin inner layer of the heart wall composed of epithelial tissue, that lines the inner surface of the heart chambers and valves [3].

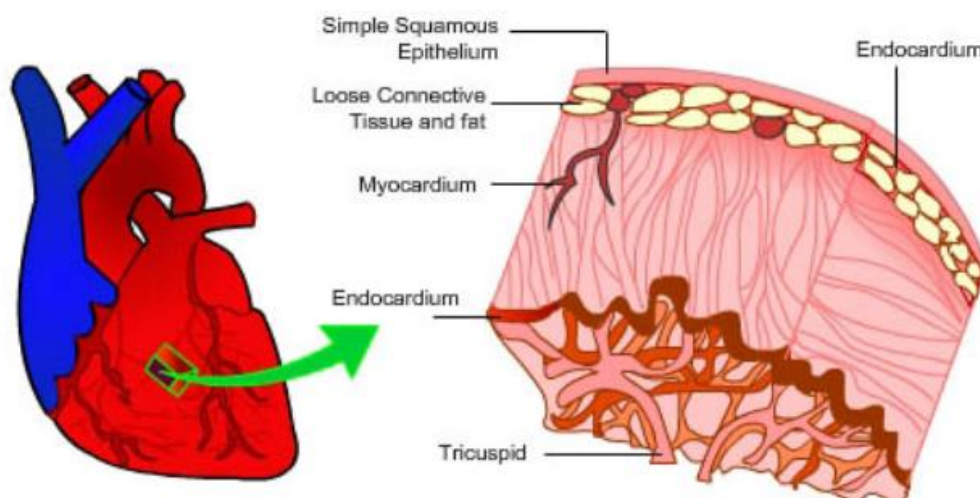


**Figure 1.2** Heart and its layers [2]

Blood flows through the heart in one direction only, thanks to the presence of valves at various openings: the tricuspid valve between the right atrium and right ventricle; the bicuspid, or mitral, valve between the left atrium and left ventricle; the semilunar valves in the aorta and the pulmonary artery.

The heart is characterized by a cardiac cycle divided into two phases: systole and diastole (Figure 1.3). Systole represents the period during which the heart contracts and pumps blood to give it the necessary velocity and pressure to reach each district of human body. Diastole is the consequently phase of relaxation and represents the period during which there is no pumping, the heart stretches and receives blood again.

The normal heart has a rate of 72 beats per minute, but in infants the rate may be as high as 120 beats, and in children about 90 beats, per minute [4].

The contraction of the heart causes the blood pressure to rise to its highest point, and relaxation of the heart brings the pressure down to its lowest point. Normal blood pressure readings for healthy young people should be below 120 mmHg for systolic pressure and 80 mmHg for diastolic pressure [5].

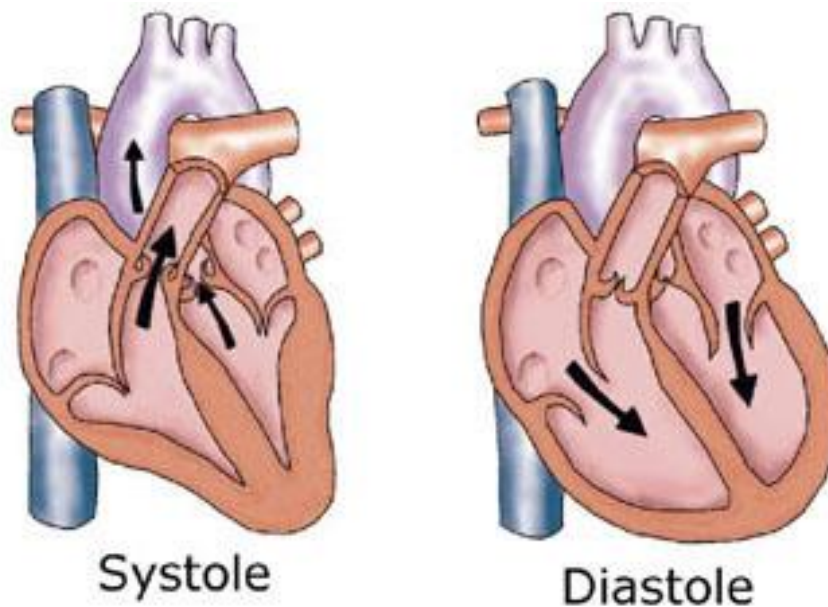


**Figure 1.3** *Systole and diastole* [6]

## 1.2 Blood vessels

Blood vessels are defined as the organs of the circulatory system used to transport blood through the body. The most important types are the arteries, capillaries and veins (Figure 1.4). Arteries are the vessel through which blood coming from the heart flows, while the veins are those through which blood flows back towards the heart. Arterial circulation is linked to venous circulation through the thick network of capillaries [7].

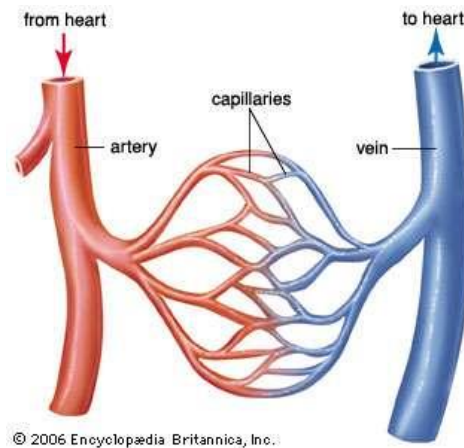


**Figure 1.4** Illustration of blood vessels [8]

There are two different circulatory loops in the human body: the systemic circulation loop and the pulmonary circulation loop (Figure 1.5).

The systemic circulation carries oxygenated blood from the left side of the heart via the aorta to all the tissues of the body, where releases nutrients and removes waste products. Deoxygenated blood returns to the right side of the heart where the pulmonary circulation begins. The pulmonary circulation transports deoxygenated blood from the right side of the heart to the lungs via the pulmonary arteries. In the lungs blood picks up oxygen, carbon dioxide is eliminated and the oxygenated blood returns to the left side of the heart via the pulmonary veins. At this point the systemic loop starts again and gives purified blood to the periphery [9].

An important difference between arteries and veins is that in the systemic circulation arteries carry oxygenated blood while veins deoxygenated blood; in the pulmonary circulation oxygenated blood is carried by veins while deoxygenated blood by arteries.

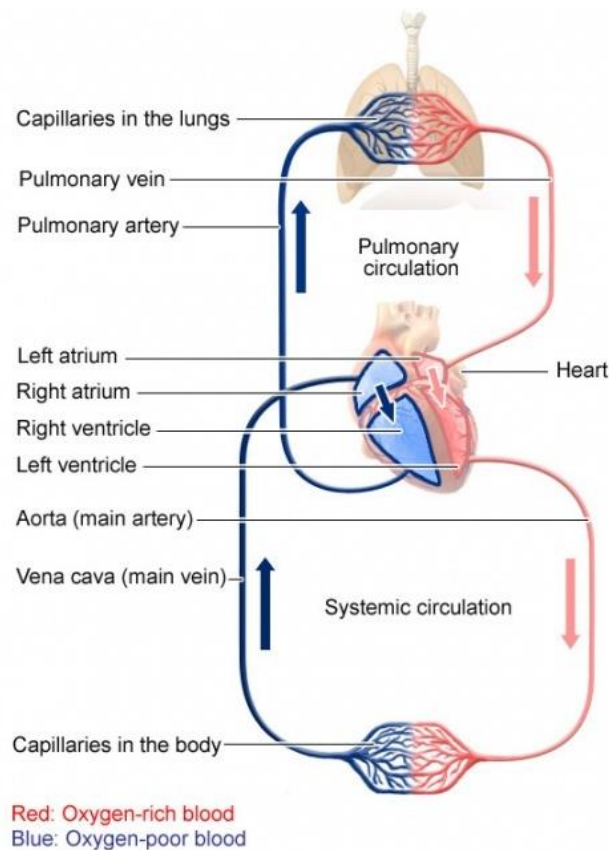


**Figure 1.5** Circulation loops <sup>[10]</sup>

The arterial tree is a complex system of vessels, which gradually thin as they move away from the heart and they are characterized by a series of branches that originate at bifurcations points. The vessel walls are compliant, they store volume during systole and return that volume during diastole, thus maintaining a nearly steady flow.

Arteries have a blood pressure higher than other parts of the circulatory system, which serves to drive blood flow along the arterial tree. The variation of pressure produces a pulsatile flow, which can be felt in different areas of the body. As the blood, flowing, moves away from the heart, it meets an increasing resistance due to the reduction of the diameter of the arteries <sup>[11]</sup>.

The veins are characterized by the presence of dovetail valves (semilunar valves) in their internal surface, that prevent blood backflow. Veins present less thick walls than the arteries and sag in absence of blood, while the arteries always retain their cylindrical shape <sup>[7]</sup>.

Capillaries are thin vessels which allow substances exchanges between the blood and the interstitial liquid that surrounds the cells. For this reason, they do not need a particular

mechanical structure, so they are characterised by a prevalence of endothelial cells that avoid capillaries collapse [7,12].

### 1.2.1 Structural elements of the artery wall

The structural elements that characterize arterial walls are [13]:

- Endothelium
- Smooth muscular cells
- Elastic fibers and collagen fibers

The **endothelium** is a tissue composed of flat cells with polygonal and stretched shape, that covers the surface of some cavities of the organism that do not communicate with the outside, such as the heart, blood vessels, lymphatic vessels, joints.

In the arterial system, endothelial cells create a smooth and continuous surface, they are arranged in parallel to the longitudinal axis of the vessel and are oriented according to blood flow direction. Endothelium has some main functions: secretion function, anti-thrombogenic function, anticoagulant function, and finally, it acts as a barrier for the indiscriminate passage of some blood constituents through the arterial wall [13].

**Muscular cells** are organized in fibers wrapped in a single step helix and their role is to provide contractility (Figure 1.6). They have modest mechanical characteristics and a high hysteresis cycle in case of cyclic stress (Figure 1.7a) [13].

**Elastin** is a fibrous protein that forms a fenestrated lamina in longitudinal direction (Figure 1.6). It is characterized by a low hysteresis (Figure 1.7b) and it has a roughly elastic linear behaviour, so it is responsible for the elastic behaviour of the vessels. Elastin is involved in physiological condition, that is for stress levels lower than 130 mmHg [13].

**Collagen** forms a messy and corrugated network in condition of low stress and becomes regular and progressively extends as stresses increases (Figure 1.6). It is characterized by a moderate hysteresis (Figure 1.7c) and it has a non-linear behaviour because its fibers come into action progressively. Collagen is involved in case of stresses higher than physiologic ones and it allows to support high solicitations keeping the wall integrity [13].

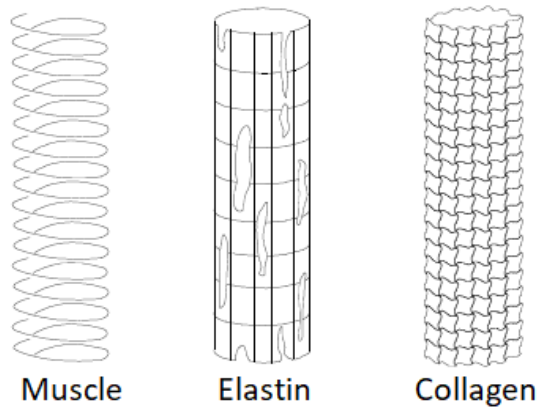


**Figure 1.6** The arterial wall components <sup>[13]</sup>

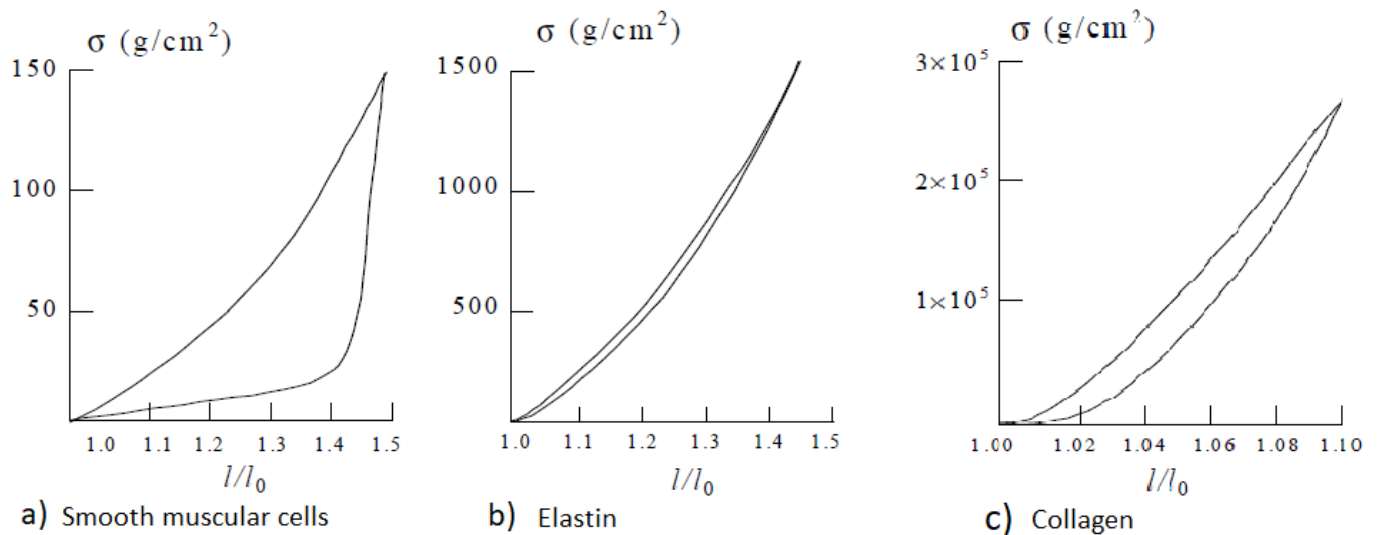


**Figure 1.7** Mechanical behaviour of a) muscular cells, b) elastin, c) collagen for cyclical stresses <sup>[13]</sup>

### 1.2.2 Anatomy of vessels wall

All vessels have a particular anatomy characterized by layers. Each layer has a different composition from the other layers because they solve different roles during the cardiac cycle.

The wall of all arteries is composed of three concentric layers <sup>[7,13]</sup> (Figure 1.8):

- Tunica intima
- Tunica media
- Tunica adventitia

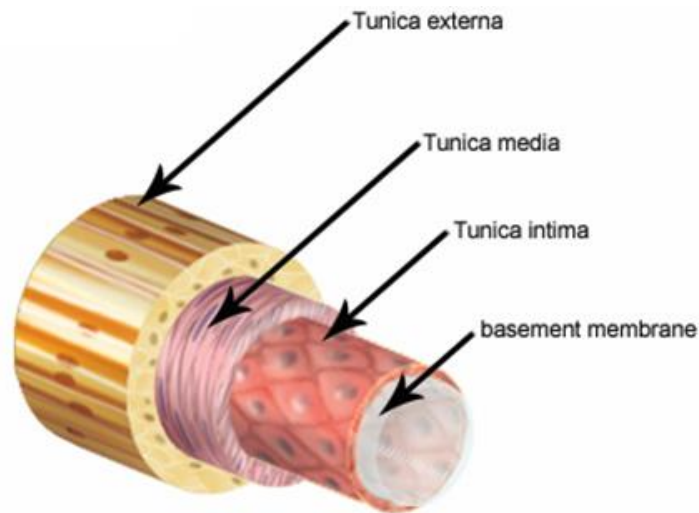


**Figure 1.8** The arterial wall structure <sup>[14]</sup>

**Tunica intima** is the inner layer, composed of a monolayer of flat and smooth endothelial cells, laid on a thin layer of connective tissue <sup>[7]</sup>. They are directly in contact with blood, so represent the only barrier between blood and the underlying thrombogenic tissues. The integrity of the endothelium is therefore of fundamental importance for the maintenance of the normal structure of the whole vessel and the endothelial damage is at least in part responsible of the beginning of atherogenesis. This layer is even composed of a thin sub-endothelial layer of collagen called basement membrane, which has a structural and filtering function in vessel/ interstitial exchanges, both in physiological condition and in course of inflammation <sup>[13]</sup>.

**Tunica media** is composed of smooth muscular cells and connective tissue rich of elastic fibers. It is normally the layer with the major thickness, however variable depending on the calibre and function. Its role is to give elasticity and contractility to the vessel <sup>[7]</sup>.

It is not very vascularized, so oxygen and nutrients arrive by diffusion from the vessels of adventitia. With advancing age, elastic fibers deteriorate and are replaced by fibrous tissue.

In physiological conditions, muscular cells regulate vasodilatation and vasoconstriction and they can synthesize different types of collagen and elastin. In course of atherosclerosis instead, they can differentiate, proliferate and migrate to the tunica intima, becoming myointimal cells. The latter express LDL receptors and produce lithic enzymes, so they represent the main causes of atherosclerosis <sup>[13]</sup>.

Tunica media in major arteries presents a higher percentage of elastin, while in average and small arteries the percentage of smooth muscular cells predominates.

**Tunica adventitia** is the external layer whose role is mainly that of containment. It is composed of bundles of smooth muscle cells and connective tissue, which contain collagen and elastic fibers, nerves and vasa vasorum.

Vasa vasorum is a network of small vessels, which penetrate no more than 1/3 of adventitia, whose role is to deliver nutrients and oxygen to arterial and venous walls and remove waste products [7,13].

Between a layer and the other there are some elastic connective laminae: the internal lamina, that separates tunica intima from tunica media, and the external lamina, that separates tunica media from adventitia. The internal lamina is a dense membrane with a fenestrated layer of elastic fibers arranged in longitudinal direction. It is through the spaces of this layer that muscular cells penetrate the tunica intima becoming myointimal cells. The external lamina is similar to the internal one but less developed; through the spaces of the layer, in case of atherosclerosis, the vessels of new synthesis penetrate the tunica media, causing an alteration of the arterial wall and its consequent structural weakening [7,13].

All vessels are characterized by these layers, but with some differences in terms of thickness, because of the different roles they solve (Figure 1.9). In fact, veins present the same three layers but have less consistent walls than arteries, their tunica media is less developed and there are few smooth muscular cells. Capillaries, instead, have a single layer of endothelial cells, they do not present smooth muscular tissue and they have very thin walls which allow the continuous passage of substances. The thinner capillaries have a smaller diameter than the red blood cells, so they deform to pass through them [13].

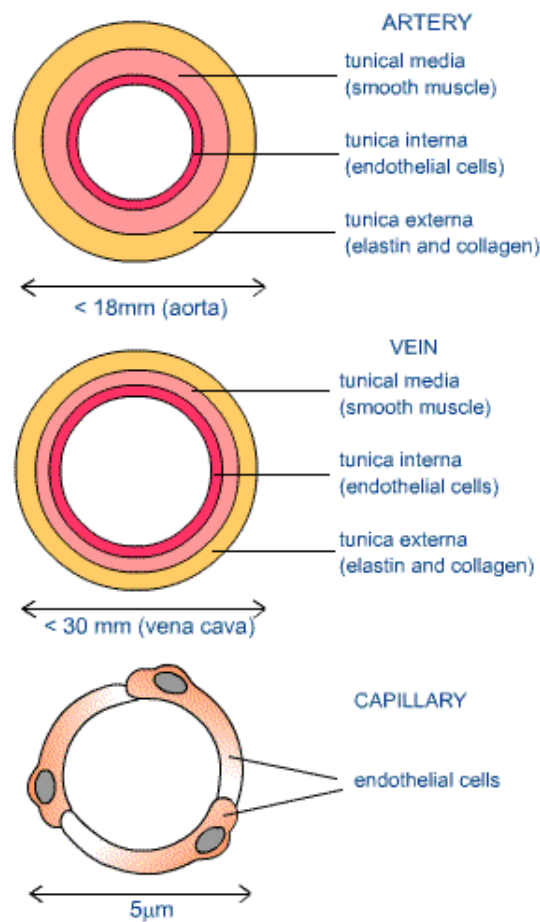


**Figure 1.9** Layers in arteries, veins and capillaries <sup>[15]</sup>

### 1.2.3 Classification of arteries

In relation to the diameter, arteries can be classified into <sup>[13]</sup> (Figure 1.10):

- Large arteries or elastic arteries
- Medium arteries or muscle arteries
- Small arteries or arterioles

**Large arteries** have a diameter from 7 mm to 3 cm and their tunica media is predominantly elastic, so they passively intervene in blood circulation <sup>[16]</sup>. Examples of major arteries are the aorta, the femoral artery, the subclavian artery, the common iliac, the carotid artery <sup>[17]</sup>.

**Medium arteries** have a diameter from 2 mm to 7 mm and their tunica media is predominantly muscular. They have contractile walls, so they actively change their lumen, regulating the quantity of blood that arrives to the tissues <sup>[16]</sup>. Most of the arteries belong to this category, for example humeral, radial, femoral arteries and even coronary arteries.

**Small arteries** have a diameter lower than 2 mm, they extend and branch out from arteries, preceding the capillaries. They have a very thin muscular wall, usually composed of one or two layers of smooth muscular cells and constitute the main site of vascular resistance [18].

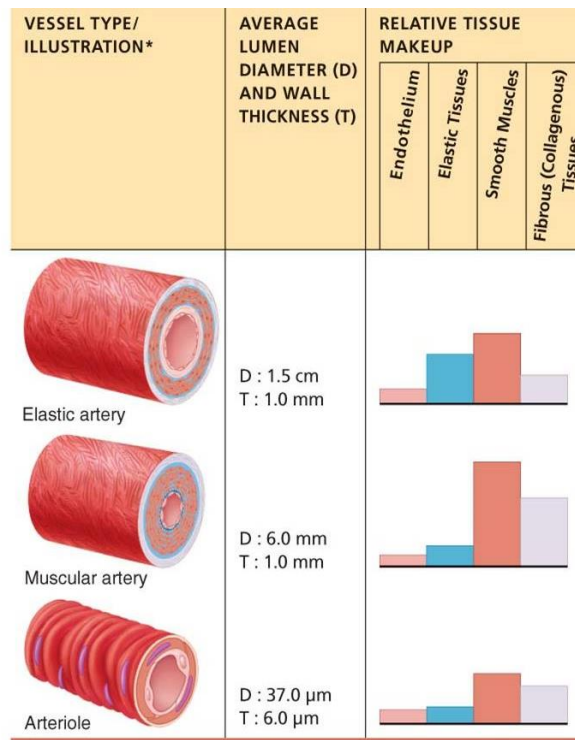


**Figure 1.10** Comparison of the structure between large, medium and small arteries [19]

### 1.3 Blood tissue

Blood is a connective tissue composed of a corpuscular component suspended on an aqueous solution called plasma.

Plasma is a slightly alkaline fluid consisting mainly on water, which contains many organic substances such us carbohydrates, lipids, proteins, amidino acids, vitamins, hormones and minerals [12,13].

The corpuscular part includes (Figure 1.11):

- Erythrocytes or red blood cells
- Leukocytes or white blood cells
- Thrombocytes or platelets

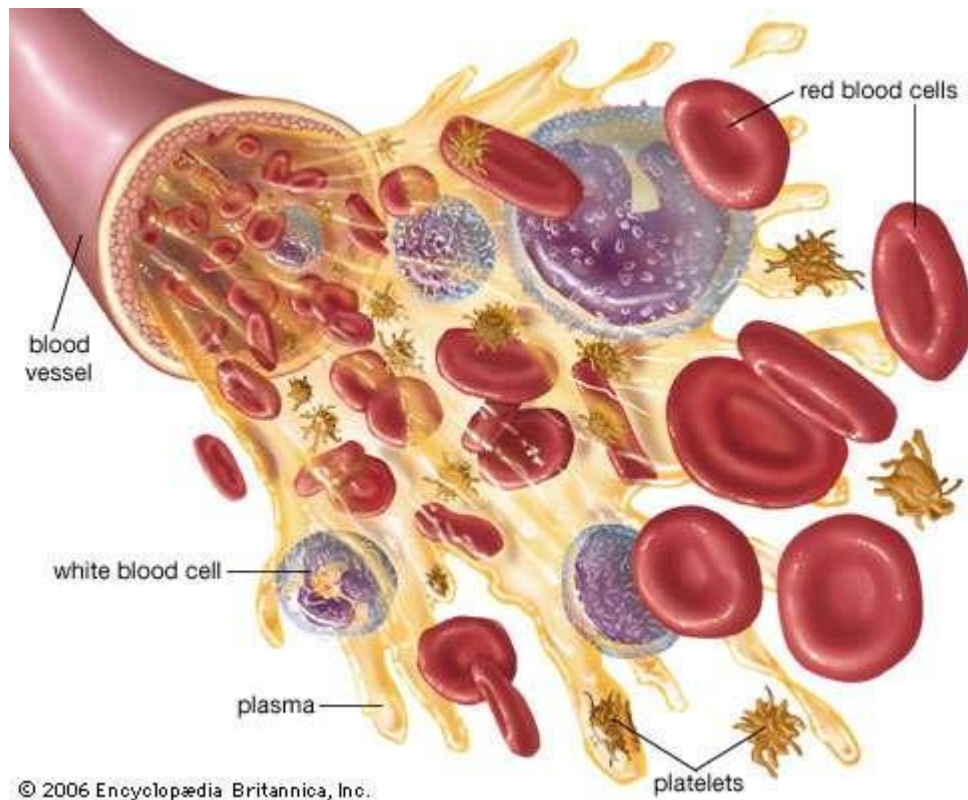


**Figure 1.11** Blood components <sup>[20]</sup>

**Erythrocytes** are the most numerous cells in the blood, they are devoid of nucleus and this lack leaves more room for haemoglobin, the protein involved in oxygen transport <sup>[13]</sup>.

**Leukocytes** are nucleated blood cells responsible for defending the organism. They include basophils, eosinophils, neutrophils, lymphocytes, monocytes.

Basophils secrete anticoagulants and vasodilators and their main function is to secrete products that mediate the hypersensitivity reaction (allergic reaction); eosinophils attack parasites and phagocyte antigen-antibody complexes; neutrophils are very active in engulfing bacteria and are present in large quantities in wound and pus; lymphocytes produce antibodies and are the main constituents of the immune system which constitute a defence against the attack of pathogenic microorganisms (viruses, bacteria, fungi and protists); monocytes are precursors of macrophages, they are the largest blood cells and also have macrophage activities <sup>[13]</sup>.

**Platelets** are blood cells coming from the bone marrow. Their main function is to stop blood loss in wounds (haemostasis): they aggregate between them promoting blood coagulation <sup>[13]</sup>.

In human body, 5.6 litres of blood circulate through the cardiovascular system to reach all districts <sup>[12]</sup>. Blood solves many important functions <sup>[13]</sup>:

- it carries oxygen (O<sub>2</sub>) to any tissue thanks to the haemoglobin, contained in each red blood cell, and it takes away the carbon dioxide (CO<sub>2</sub>) generated by cells.
- it vehicles some nutrients, like amino acids, sugars, mineral salts and it eliminates all the waste products of cells.
- it has an important role in the control of the body temperature.
- it carries some chemical substances, which are involved in the processes of cellular signalling, like growth factors, enzymes, hormones.
- it contributes to the organism defence, thanks to the white cells and antibodies.
- thanks to the coagulation process, it performs an immediate repair function of wounds, it promotes the self-renewal and the regeneration of the damaged (or old) tissue.

## 1.4 Blood rheology

Rheology is a discipline whose purpose is to study the sliding properties of different materials: some substances have intermediate flow properties between those of solid materials and fluid materials, such as emulsions, suspensions and dough.

From a mechanical point of view, blood is a suspension of corpuscular elements in a saline solution, but more precisely, blood is a biphasic fluid, constituted by a fluid phase and a solid phase.

Despite its biphasic nature, blood can be approximated as a homogeneous fluid, characterized by two quantities: density and viscosity, both function of temperature; nevertheless, the viscosity may also be function of the state of motion, which can be mainly defined as the set of all the velocity vectors of each element of the fluid domain considered <sup>[13]</sup>.

### 1.4.1 Blood density

Blood density, or volumetric mass, depends on haematocrit (*Ht*) blood, which is the percentage in volume occupied by the corpuscular elements of the total amount of blood volume. According to some experimental studies, the average value of haematocrit for an adult human is equal to 45% <sup>[13]</sup>.

The experimental expression for blood density is:

$$\rho_b = (1 - Ht)\rho_p + Ht \rho_{gr}$$

where  $\rho_p$  represents plasma density and  $\rho_{gr}$  is the density of the corpuscular fraction of blood sample. In normal conditions it can be assumed that  $\rho_p = 1035 \text{ kg/m}^3$  and  $\rho_{gr} = 1090 \text{ Kg/m}^3$ , so for an haematocrit value of 0.45 (45%), the value of blood density results equal to  $1060 \text{ kg/m}^3$  [13].

#### 1.4.2 Blood viscosity

Blood viscosity is a measure of the resistance of blood to flow, described by Newton's formula in differential form:

$$\tau_{rz} = -\mu \frac{\partial v_r}{\partial z}$$

This formula states that the shear stress  $\tau$  is directly proportional to the velocity gradient (deformation velocity)  $\frac{\partial v_z}{\partial r}$  through the constant  $\mu$  that is the dynamic viscosity of the fluid.

The velocity gradient is defined shear rate, it is indicated with the symbol  $\dot{\gamma}$  and its unit of measurement is  $\text{s}^{-1}$ . It describes the variation in radial direction of the axial velocity of the fluid. In the hypothesis of laminar motion in rectilinear cylindrical ducts, the velocity reaches the maximum value at the centre of the tube and is equal to zero at the walls.

From the law which describe the shear stress, it is possible to derive the unit of measurement for the viscosity in the I.S.:

$$\mu = \left[ \frac{\text{kg}}{\text{m} \cdot \text{s}} \right] = \left[ \frac{\text{N} \cdot \text{s}}{\text{m}^2} \right] = [\text{Pa} \cdot \text{s}]$$

However, today is of common use the unit centipoise [cP], submultiple of the unit of measurement of viscosity in the c.g.s system, where  $1\text{cP} = 10^{-3} \text{ Pa} \cdot \text{s}$ .

A range of values normally accepted for blood viscosity is  $\mu = [3; 4] \text{ cP}$  [13].

Blood viscosity is expressed using a simplified formulation of the Einstein relationship and it is given by the following formula:

$$\mu_b = \mu_p(1+2.5Ht)$$

where  $\mu_p$  represents plasma viscosity that, in normal conditions, is characterized by values in range 1.1-1.6 cP and depends on the temperature and its protein composition [13].

### 1.4.3 Rheological Newtonian model

A fluid has a Newtonian behaviour if its dynamic viscosity is independent from the shear rate. In this case, shear rate and shear stress show a linear relationship through a constant of proportionality given by the dynamic viscosity of the fluid. In the plan  $(\tau; \dot{\gamma})$  this relationship can be represented by a straight line passing through the origin, with angular coefficient given by dynamic viscosity of the fluid. (Figure 1.12).

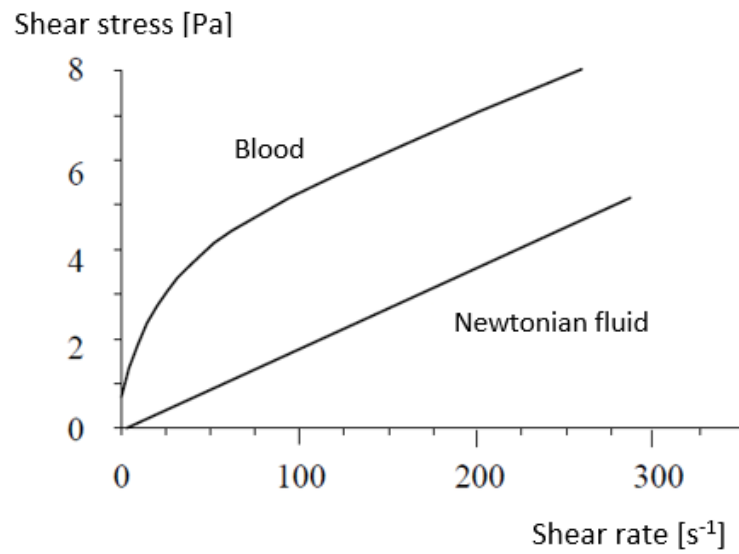


**Figure 1.12** Comparison between blood behaviour and a Newtonian fluid behaviour <sup>[13]</sup>

Blood is characterized by a different behaviour: because of its complex nature, it cannot be always defined as a homogenous fluid and thus it cannot be considered as a Newtonian fluid.

In fact, all its components have different characteristics in terms of shape, density, deformability, electrical charge, and it is for this reason that blood presents a complex rheological behaviour.

However, some experimental studies have demonstrated that blood can be considered as a homogeneous and Newtonian fluid only in vascular vessel with a diameter greater than 0.3 mm <sup>[13]</sup>. This threshold is given according to the average size of the red blood cells, which is about two orders of magnitude lower than this value. Therefore, it can be assumed that blood is a homogeneous and Newtonian fluid only in those vessels in which the dimensions of erythrocytes can be considered negligible compared to the size of the vessel, that is up to the arterioles. This assumption is true only for high values of shear rate ( $>100 \text{ s}^{-1}$ ), for which the two curves show the same slope (Figure 1.12). Conversely,

for low values of shear rate, blood behaves like pseudoplastic fluids, and this behaviour occurs for Ht > 12%. This is due to the presence of fibrinogen which determines the aggregation of the red blood cells into “rouleaux”, generally made up by fewer tens of erythrocytes, increasing blood viscosity [13].

#### 1.4.4 Rheological non-Newtonian models

A non-Newtonian fluid is a fluid characterized by a viscosity that changes depending on the applied shear stress. Consequently, it does not have a defined value of viscosity. A non-Newtonian fluid can be a viscous or a viscoelastic fluid, and it can be described by the same equation used for a Newtonian fluid, in which the dynamic viscosity is replaced by the apparent viscosity  $\mu_{app}$ :

$$\tau_{xy} = -\mu_{app} \cdot \dot{\gamma}$$

Where  $\mu_{app}$  is neither a constant nor a thermo-physical property of the fluid, but depends on the state of motion of the fluid [13].

It is clear that blood is a non-Newtonian fluid because of the complex nature of its components and even because of the interaction between particles that influenced blood viscosity. Many models have been proposed in order to describe blood behaviour and, even if none of these reflects the real behaviour, they give a good representation of its rheology.

Among non-Newtonian models there are [13]:

- Bingham model
- Casson model
- Power-Law model
- Carreau model
- Generalized Power-Law model

#### **Bingham model**

Bingham model is described by the following relationship:

$$\tau = \tau_0 + \mu_B \cdot \dot{\gamma}$$

Where  $\tau_0$  is the yield stress, which is the minimal value of the shear stress necessary to put the fluid in motion,  $\mu_B$  is Bingham's viscosity and  $\dot{\gamma}$  is the shear rate.

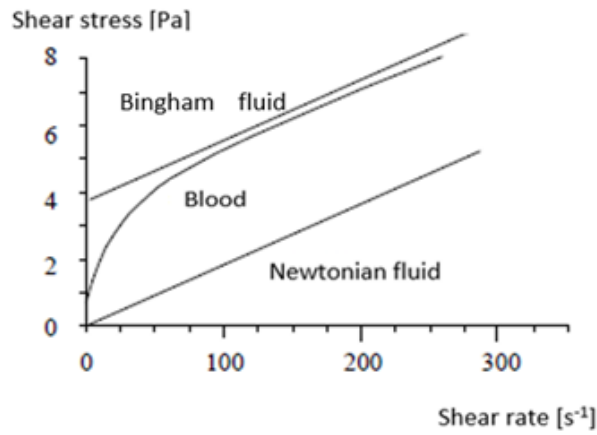


**Figure 1.13** Comparison between Bingham fluid, blood and Newtonian fluid <sup>[13]</sup>

This model is a coarse representation of blood behaviour for low values of shear rate but approximates the asymptotic behaviour quite well. Comparing Bingham fluid with Newtonian fluid, it is observed that the shear stress in the first model has the same trend of the second, but shifted of a quantity equal to  $\tau_0$  (Figure 1.13) <sup>[13]</sup>.

### **Casson model**

Casson model is described by the following relationship:

$$\sqrt{\tau} = \sqrt{\tau_0} + \sqrt{\mu_c} \cdot \sqrt{\dot{\gamma}}$$

Where  $\tau_0$  is the yield stress,  $\mu_c$  is Casson's viscosity and  $\dot{\gamma}$  is the shear rate.

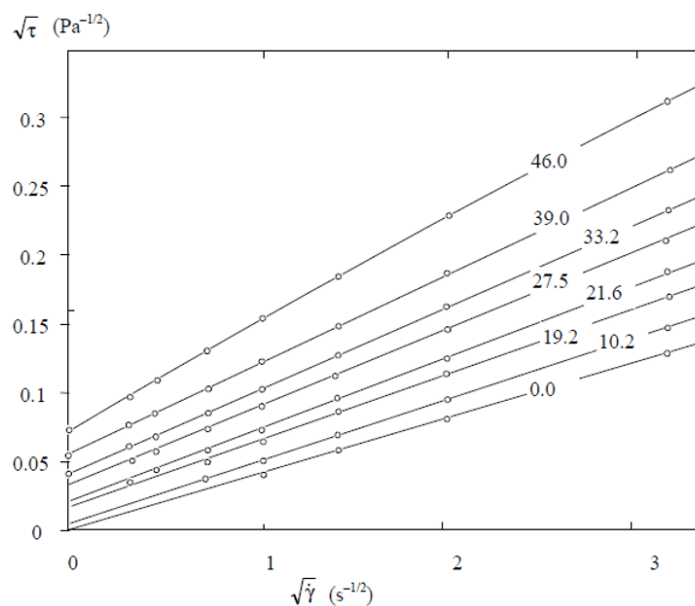


**Figure 1.14** Casson blood model for different values of  $Ht$  <sup>[13]</sup>.

The peculiar analytical form of this relationship was obtained by Casson as a graphical interpolation of experimental data, using blood samples with different haematocrit and kept at a constant temperature of 25 °C. In this way it is possible to understand the influence of the haematocrit both on the shear stress and on the shear rate.

The equation of Casson model has a linear trend (Figure 1.14): with the same value of  $\sqrt{\dot{\gamma}}$ , the value of  $\sqrt{\tau}$  increases with the increase of Ht [13].

### **Power-Law model**

Power-law model (Figure 1.15) describes the relationship between viscosity and shear rate:

$$\mu(\dot{\gamma}) = k \cdot (\dot{\gamma})^{n-1}$$

where  $k$  is the flow consistency factor and  $n$  is the Power-Law index. These are two experimental parameters which depends on some coefficients and on the values of some blood component, such as haematocrit and proteins concentrations.

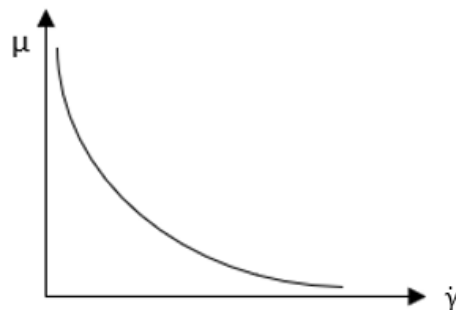


**Figure 1.15 Power-Law model**

According to Cho and Kensey [21] it is possible to considerate a Power-Law model that artificially mimics the Newtonian behaviour at strains greater than 226.5 s<sup>-1</sup>. Furthermore, according to the experimental evidence for the existence of a yield stress in human blood, a threshold value for viscosity is fixed, at strains lower than 10<sup>-5</sup> s<sup>-1</sup> [13]. The result is that the viscosity would have a plateau, so it would never go to infinity.

### **Carreau model**

The relation between viscosity and shear rate according to Carreau model, is described by:

$$\mu(\dot{\gamma}) = \mu_{\infty} + (\mu_0 - \mu_{\infty})[1 - (\lambda\dot{\gamma})^2]^{n-\frac{1}{2}}$$

where  $\lambda$  is the relaxation factor,  $n$  is the Power-Law index,  $\mu_\infty$  and  $\mu_0$  are viscosity limits for  $\dot{\gamma}=0$  and  $\dot{\gamma}=\infty$ , respectively.

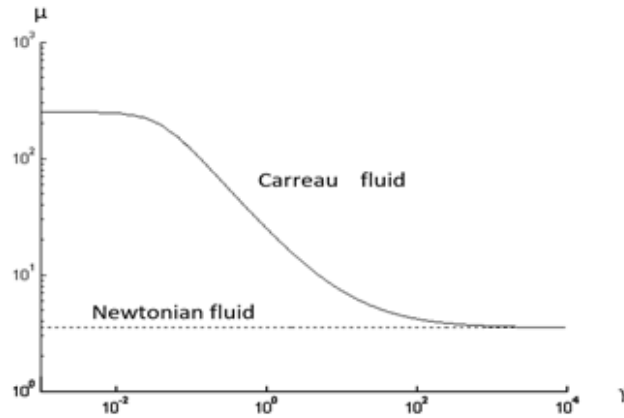


**Figure 1.16** Comparison between Carreau fluid and Newtonian fluid (logarithmic scale) <sup>[13]</sup>

As it can be seen in figure 1.16, for values of the shear rate lower than  $10^{-1} \text{ s}^{-1}$ , the viscosity is characterized by a plateau, then the curve decreases as the shear rate increases and finally, for values of the shear rate greater than  $10^2$ , the viscosity shows a plateau again, which now overlaps the trend of Newtonian fluid. The slope of the curve that describes Carreau fluid is controlled by the two parameters described above,  $\lambda$  and  $n$ . This model is commonly used to represent the shear-thinning behaviour which characterized the viscosity of blood <sup>[13]</sup>.

### **Generalized Power-Law model (Ballyk)**

This generalized model was proposed by Ballyk et al. in 1994 and it is based on Power-Law model with variable parameters. It is described by the following equation:

$$\mu(\dot{\gamma}) = \lambda(\dot{\gamma}) \dot{\gamma}^{n(\dot{\gamma})-1}$$

where:

$$\lambda(\dot{\gamma}) = \mu_\infty + \Delta\mu \exp\left[-\left(1 + \frac{\dot{\gamma}}{a}\right) \exp\left(-\frac{b}{\dot{\gamma}}\right)\right]$$

$$n(\dot{\gamma}) = n_\infty + \Delta n \exp\left[-\left(1 + \frac{\dot{\gamma}}{c}\right) \exp\left(-\frac{d}{\dot{\gamma}}\right)\right]$$

All the parameters included in the equations above were found through interpolation of experimental data <sup>[13]</sup>.

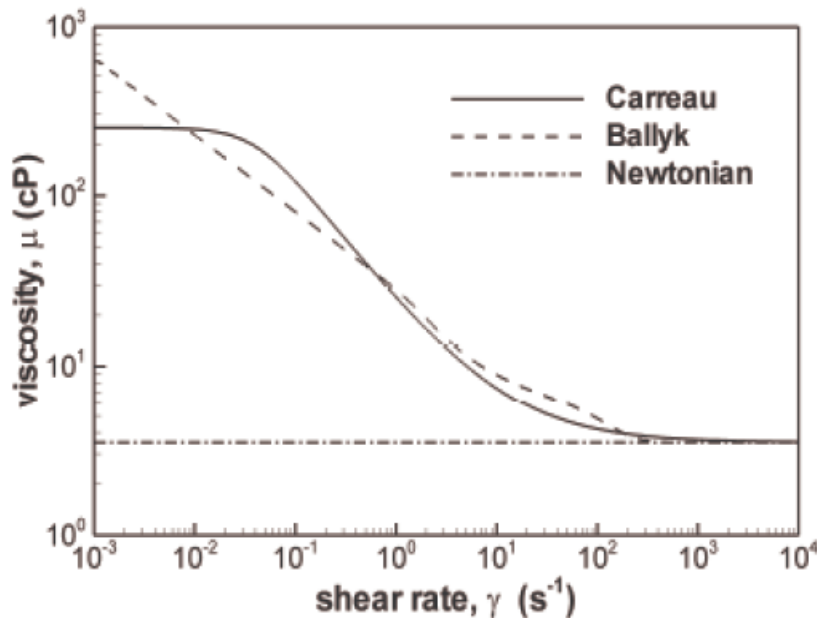


**Figure 1.17** Generalized Power-Law model and comparison with Newtonian and Carreau models <sup>[13]</sup>

Ballyk model is characterized by an improvement in viscosity representation. In fact, making a comparison between Ballyk model and Carreau model (Figure 1.17) it is possible to notice that Ballyk fluid is characterized by higher values of viscosity than Carreau at shear rates lower than  $10^{-2} \text{ s}^{-1}$  and in shear rate region ranging from 50 to  $100 \text{ s}^{-1}$  <sup>[13]</sup>. This means that in those shear rate regions Carreau underestimates the value of viscosity. As regards the comparison between Ballyk model and Newtonian model, the graph shows that the first model overlaps the second one at high values of shear rate. The Generalized Power-Law model can be considered a general model for non-Newtonian blood viscosity; from some studies in coronary arteries, it has been observed that this model is able to achieve a better approximation of WSS (wall shear stress) than Newtonian model, in case of low inlet velocity and low values of shear rate <sup>[21]</sup>.

## 1.5 Wall Shear Stress (WSS)

Wall shear stress is the shear stress in the layer of fluid next to the wall of a vessel. In non-pulsatile flow in a straight vessel, fluid does not move at the same velocity at every point in the vessel: it is faster at the center and slower close to the wall. The fluid velocity assumes a parabolic profile, which is the result of friction between the fluid and the vessel wall, and is related to the fluid viscosity. This friction creates a tangential force exerted by

the flowing fluid and is defined as "wall shear stress". The magnitude of wall shear stress depends on how fast the fluid velocity increases when moving from the vessel wall toward the center of the vessel.

Wall shear stress is defined as <sup>[13]</sup>:

$$\tau_w = \mu \left( \frac{\partial u}{\partial y} \right)_{y=0}$$

Where  $\mu$  is the dynamic viscosity,  $u$  is the flow velocity parallel to the wall and  $y$  is the distance to the wall.

WSS has a fundamental role in maintaining the normal functioning of the circulatory system, because arteries adapt to long term variation in WSS to restore optimal physiological conditions after an alteration.

# CHAPTER 2

## CORONARY SYSTEM AND ASSOCIATED PATHOLOGIES

### 2.1 Coronary anatomy

Coronary arteries are specialized vessels with a maximum diameter of 3-5 mm, responsible for the cardiac perfusion. Coronary circulation (Figure 2.1) consists of the blood vessels that supply oxygenated blood to the heart, penetrating the cardiac tissue to reach the inner parts and remove deoxygenated blood from the heart [22,23]. The first ones are known as coronary arteries, the second ones are known as cardiac veins. Coronary arteries that run on the surface of the heart are called epicardial coronary arteries. These arteries, when healthy, are capable of autoregulation to maintain coronary blood flow at levels appropriate to the needs of the heart muscle. These relatively narrow vessels are commonly affected by atherosclerosis and can become blocked, causing angina or a heart attack [9,24].

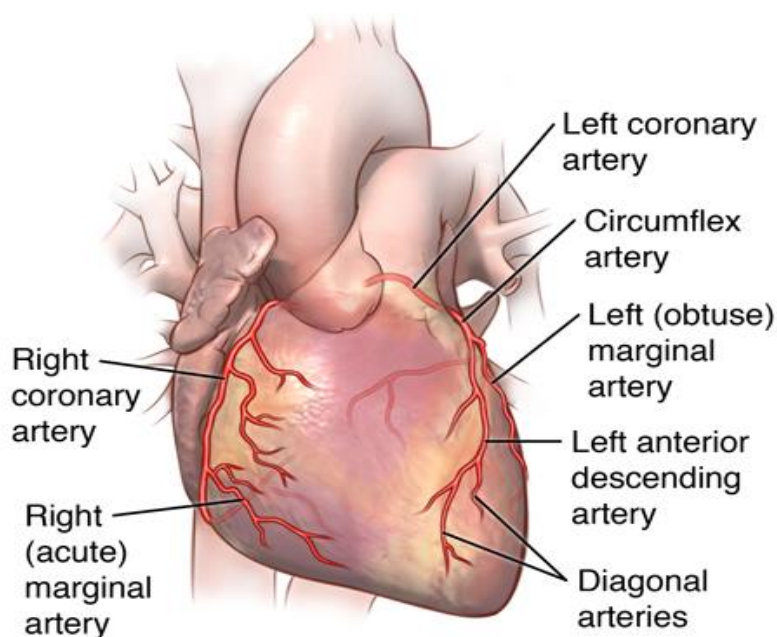


**Figure 2.1** Representation of coronary arteries [25]

Each artery has its own district of exclusive vascularization and only some parts of the heart can have a double spraying.

Coronary system is formed by two main arteries [23,26]:

- Right coronary artery (RCA)
- Left coronary artery (LCA)

They originate from the root of the aorta and their hosts are located at the aortic sinuses of Valsalva: the right coronary artery originates from the right anterior sinus, while the left coronary artery from the left anterior, at a more cranial level than the first [26].

The **right coronary artery** is divided into three sections (Figure 2.2). The first section extends from the origin up to the first right ventricular branch (RV). The second section follows the first up to the acute margin (AM) of the heart, which divides the anterior part from the posterior part of the right ventricle. The latter is the most constant branch of the RCA and runs along the ventricle until the apex. The third section begins from the acute edge of the heart and extends up to the origin of the posterior interventricular artery (PDA), at the level of the crux cordis. At this point, the right coronary artery divides into its two terminal branches, the posterior descending artery (PDA) and posterolateral branches (PLV).

The posterior descending branch is the most important branch of the RCA; it runs in the homonymous sulcus, covering about two thirds without reaching the apex of the heart, which is usually sprayed by the recurrent posterior branch of the left anterior descending artery (LAD). The right posterolateral branch (PLV) originates immediately afterwards the PDA, runs along the left posterior atrioventricular sulcus, spraying the diaphragmatic and inferior-posterior portion of the left ventricle [26].

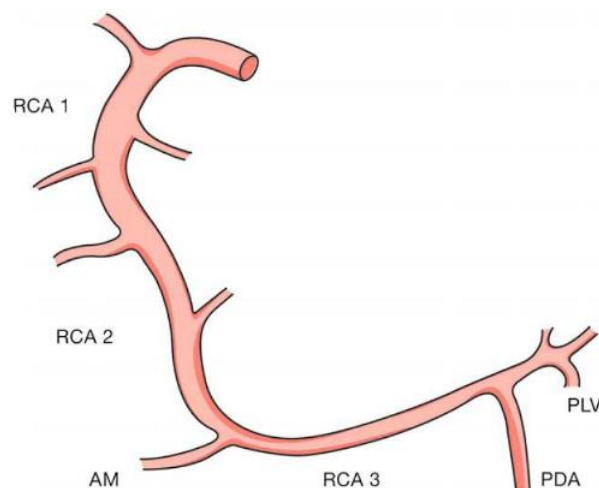


**Figure 2.2** Right coronary artery (RCA) divided in three sections (RCA1, RCA2, RCA3) [26].

The **left coronary artery** is divided into three sections (Figure 2.3): the common trunk (LM, left main), the left anterior descending artery (LAD) and the left circumflex artery (LCX).

The *common trunk* has a larger calibre than RCA; it has a diameter of 3-6 mm and it extends over a length of about 2 cm, then the vessel divides into two branches: the anterior descending artery, that runs on the anterior wall of the heart, and the circumflex artery, that runs along the lateral wall of the left ventricle. There may be cases in which the common trunk is divided into a third branch, which runs towards the apex and distributes to the anterolateral wall of the left ventricle.

The *anterior descending artery*, or anterior interventricular artery, is the most constant, in terms of origin and distribution, among all the coronary vessels. It sprays the interventricular anterior septum and the anterolateral wall of the left ventricle. The LAD is divided into three sections. The first section extends from the bi-trifurcation until the origin of the first septal branch of significant size. The second section goes from the origin of the first septal branch to the origin of the third septal branch or the second diagonal branch (DIAG). Here the third part begins and extends to the apex. Septal branches (SP) are usually three and originate at a right angle from the anterior descending artery. The diagonal branches are generally three and originate at an acute angle from the anterior descending artery and are distributed to the anterolateral wall of the left ventricle.

The *circumflex artery* runs into the posterior atrioventricular sulcus, after a short distance below the left atria. The circumflex artery is subdivided into three sections. The first goes from the origin to the first marginal branch (OM). The second follows the first up to the origin of the second marginal branch. The third and last part goes from the origin of the second marginal branch up to the point where the vessel extinguishes [26].

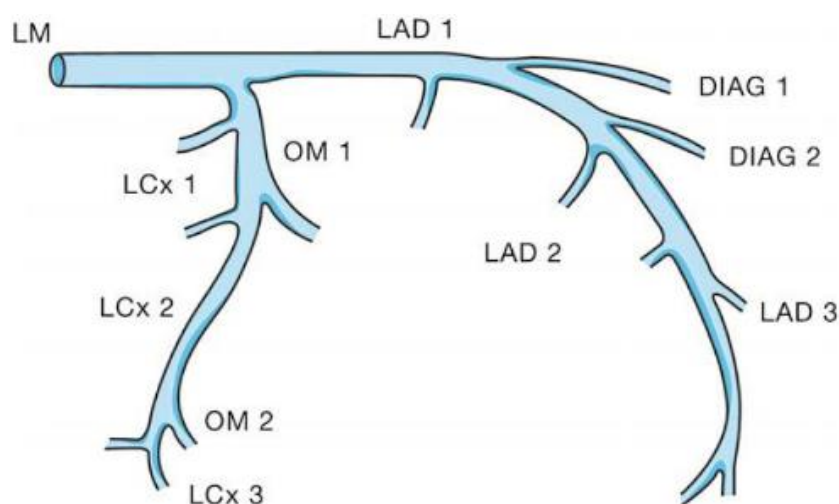


**Figure 2.3** Left coronary artery (LCA) divided in three sections (LM, LAD, LCX) [26].

According to the American Heart Association (AHA), coronary arteries are classified in 15-16 segments; this scheme includes most segments with a diameter greater than 1.5 mm (Figure 2.4).

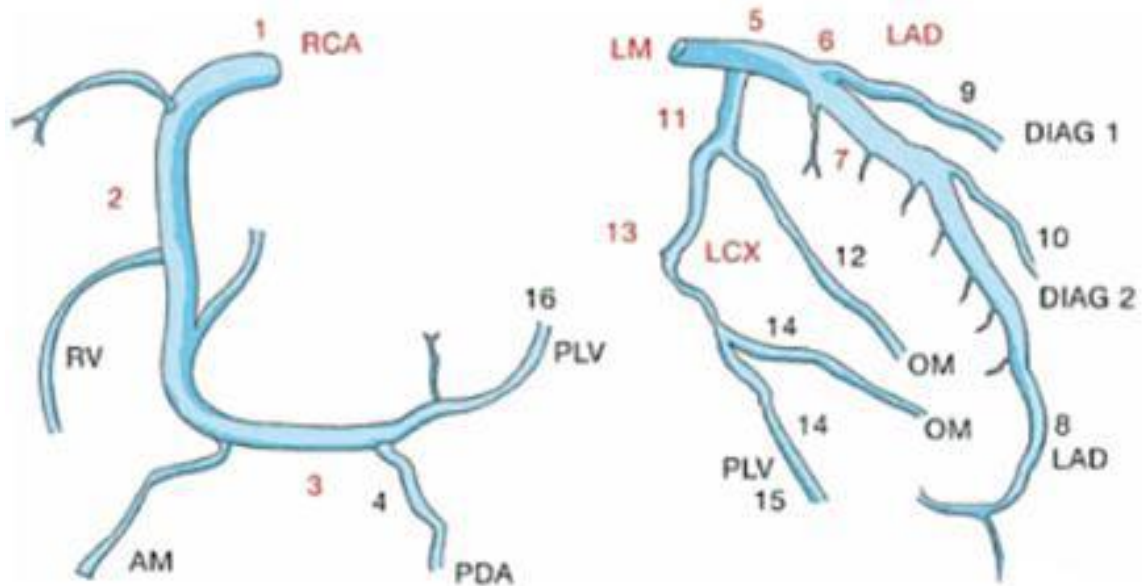


**Figure 2.4** Right and left coronary arteries, divided in segments according to the AHA classification <sup>[26]</sup>

In the classification shown, the most widespread model is reported, that is the right dominance with a frequency of about 85% on the entire population <sup>[26]</sup>. Coronary vascular anatomy may have large anatomical variations, especially as regards the terminal parts of the right coronary artery and the left circumflex artery. In case of left dominance, the circumflex artery gives origin to the left ventricular branch, or left lateral posterior (PLV), and subsequently to the left posterior descending artery (PDA), that is to say that the nourishment of the posterior left ventricle is borne by the left coronary artery. These anatomical variations are normal and do not involve any ischemic event.

Unlike other arterial vascular districts, characterized by an almost constant morphology and easily identifiable, in the case of coronaries arteries there is a remarkable variability in the distribution of the vessels and their size. This makes the coronary system of a subject different from that of another one. For this reason, some terms such as "highly developed" or "hypoplastic" are used to indicate that an artery is more or less developed but does not identify a pathology such as an injury. In case of "hypoplasia" of an important vessel, system responds on a compensatory way, enhancing other vessels <sup>[26]</sup>.

## 2.2 Physiology of the coronary flow

Coronary flow is perfectly proportional to the oxygen requirements of the myocardium: when the force of the cardiac contractions increases, there is an increase in the metabolic demand that can be satisfied only with an increase in coronary flow; vice versa, a decrease of cardiac activity is associated to a decrease of coronary flow. The ability of the coronary circulation to increase its flow when the metabolic demand increases is defined as coronary reserve.

Since the resistance to the coronary flow is determined by the microcirculation, the coronary reserve is closely related to the ability of the microcirculation to be vasodilated in response to a stimulus; in fact, blood flow through the coronary system is controlled by some local mechanisms, which regulate arterioles calibre according to the nutritional needs of the myocardium.

Coronary reserve is evaluated by measuring the coronary flow in conditions of maximal hyperemia and at rest (basal flow), and is expressed by their ratio; if this ratio is lower than 2, coronary reserve is considered as abnormal [26,27].

Maximal hyperemia is the maximum increase in blood flow that can be achieved during physical exertion, but it can even be experimentally induced for clinical purposes by the use of adenosine or dipyridamole.

At rest the coronary flow in human is about 60-80 ml/min, per 100 g of myocardial tissue, corresponding to the 5% of the total cardiac output. During intense exercise, the heart increases his cardiac output and the coronary flow increases about 3.5 times, up to 200-300 ml/min, for the nutritional supply of the heart [28]. As a result, the work of the heart, under this condition, can increase from 6 to 8 times.

In patients with ischemic heart disease, the reduction of coronary reserve is directly related to the severity of the stenosis, whereas in people with angiographically normal coronary artery disease it is a marker of myocardial dysfunction [26].

## 2.3 Atherosclerosis

Atherosclerosis (AS) is one of the main causes of death in developed countries [13]. It is a disease that affects the large and medium arteries, among which the most involved are the aorta, the coronaries and the arteries of the cerebral system.

This disease is characterized by lesions with lipid infiltrations, called atheromatous plaques, which develop on the internal surface of the arterial vessels (Figure 2.5). In its

initial state, the lesion does not determine a stenosis that can limit tissue perfusion; its manifestations take place in the form of symptoms only when the stenosis reaches a consistent development. When atherosclerosis affects coronary arteries, the most frequent consequences are angina pectoris, ischemic cardiomyopathy, myocardial infarction; when it affects the peripheral circulation, instead, it can cause cerebral infarction (stroke), lower limbs gangrene, ischemic encephalopathy, aortic and renal aneurisms [13].

Atherosclerosis is a focal pathology: atheromatous plaques, especially in the early stages of their development, are very sparse and spaced from each other. As the pathology progresses, more and more plaques are formed, they enlarge and go to occupy entire portions of arteries. The atheroma increases in volume, protrudes towards the inside of the vessel lumen and alter the normal blood flow, causing a disturbed flow [13].

The region most predisposed to atherosclerosis are those in which blood flow is turbulent, such as bifurcations and curvatures. For example, in the coronary circulation the proximal segment of the left anterior descending artery and of the left circumflex presents a particular predisposition to the development of occlusive atherosclerotic disease [26].

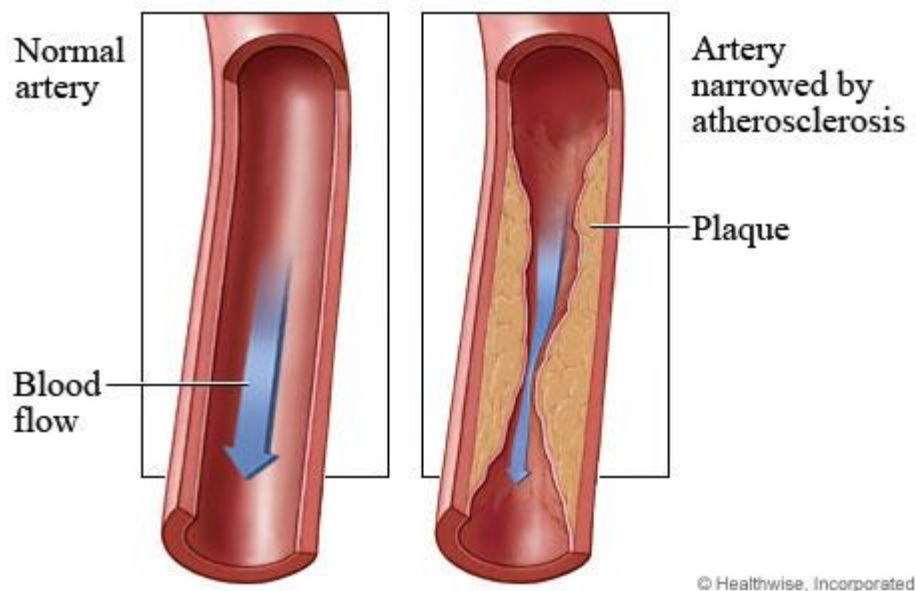


**Figure 2.5** Example of vessel affected by atherosclerotic plaque. [29]

Some atherosclerotic lesions appear predominantly dense and fibrous, others may contain large quantities of lipids and necrotic residues, while the most present combinations of these characteristics. The formation of atherosclerotic lesions is often caused by the presence of low density lipoproteins (LDL), which accumulate in some

regions of the intima by binding to some constituents of the extracellular matrix (proteoglycans) [27].

Atherogenesis in humans is a process that can last years, however it is a non-linear process in which quiescence periods alternate with episodes of rapid evolution. Intimal lesions can be divided into six types, according to their severity [30] (Figure 2.6):

- Type 1 – Foam Cells: macrophages isolated with foam cells
- Type 2 – Fatty Streak: intracellular accumulation of lipids
- Type 3 – Intermediate lesion: extracellular lipids in addition to the fatty streak
- Type 4 – Atheroma: formation of a central nucleus of lipids
- Type 5 – Fibrous Plaque: formation of a fibroatheroma
- Type 6 – Complicate Lesion

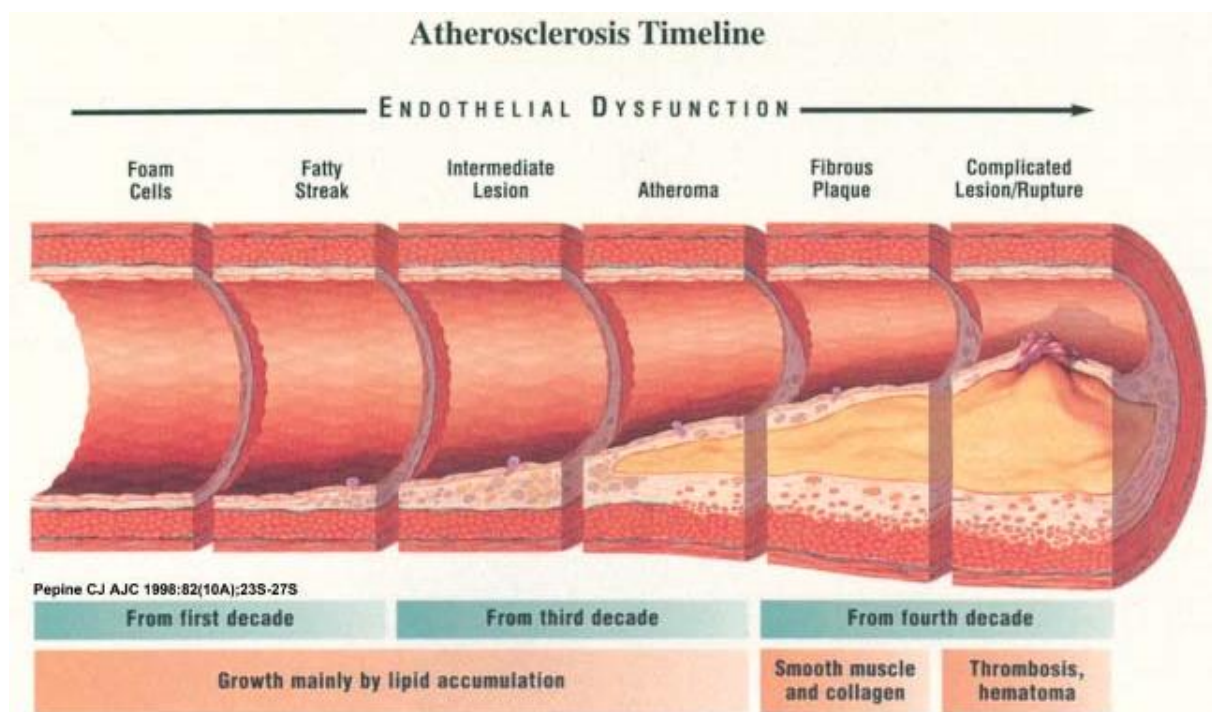


**Figure 2.6** The evolution of atherosclerosis [31]

Fatty streaks represent the earliest lesions of atherosclerosis. They are composed of foam cells filled with lipids not raised on the intimal plane which, therefore, do not cause any alteration in the blood flow. They appear as multiple yellowish maculae, flat and smaller than 1 mm in diameter, which tend to converge into elongated striations 1 cm long. They are present in some children younger than 1 year and in all adolescents over

10 years regardless of gender, race, geographical location or environmental conditions. Although fatty streaks may be plaque precursors, not all of them are destined for evolve into fibrous plaques or more advanced lesions <sup>[30]</sup>.

After the formation of fatty streaks, some adhesion molecules and receptors participate in the recruitment of mononuclear cells, leukocytes and monocytes, which adhere to the surface of endothelial cells. Then monocytes and leukocytes cross the endothelial layer and settle the tunica intima, through a mechanism promoted by LDL chemotaxis, while mononuclear phagocytes differentiate in macrophages and later in foam cells rich of lipids.

The accumulation of lipids occurs if the quantity of lipids that enters the artery is greater than that coming out through the mononuclear phagocytes, so macrophages play a vital role in the metabolism of lipids in the arterial wall during the process of atherogenesis.

During the expansion of the intimal lesion some foam cells die for apoptosis; this mechanism leads to the formation of a necrotic and thrombogenic core rich in lipids, which characterizes the most complex atherosclerotic plaques. As a consequence, macrophages produce cytokines and growth factors which stimulate the proliferation of smooth muscle cells and the production of extracellular matrix, which accumulates in atherosclerotic plaque. The atheroma is therefore formed by a lipid core and an external fibrous capsule.

The evolution of the atheroma even depends on phenomena connected to blood coagulation; in fact, if the plaque breaks, the thrombogenic core comes in contact with blood and the consequence is the formation of a thrombus which can partially or totally obstruct the blood flow <sup>[27]</sup>.

### **2.3.1 Main causes of atherosclerosis**

One of the most important factor which can cause atherosclerosis is hypercholesterolemia, that is a high plasmatic concentration of cholesterol, in form of low density lipoproteins (LDL). The concentration of LDL in the blood increases proportionally to the saturated fat content in the diet, while it increases in a smaller amount as cholesterol increases <sup>[27]</sup>.

Other risk factors that increase the likelihood of atherosclerotic plaques at the coronary level are arterial hypertension, diabetes mellitus, smoking, sedentary lifestyle, obesity, genetic factors and familiarity <sup>[22,30]</sup>. These factors can contribute to the formation of atheromatous plaques even in subjects with perfectly normal levels of LDL and plasma

cholesterol [27]. Moreover, the association of several risk factors can have a multiplicative effect: two associated risk factors increase the risk by 4 times. However, the absence of risk factors does not give immunity [30].

From a biomechanical point of view, formation of atherosclerotic plaques is related to wall shear stress values, which can alter both morphology and orientation of the endothelial cell layer. Endothelial cells subject to a laminar flow with elevated levels of WSS tend to elongate and align in the direction of flow, while in areas subject to disturbed flow, which causes the absence of a main direction, endothelial cells experience low or oscillatory WSS, they assume irregular shapes, become unorganized without a clear orientation and endothelial lining becomes more permeable [13].

Many studies confirm that the presence of a disturbed flow pattern containing regions with low WSS or marked oscillatory patterns of WSS cause intimal wall thickening, influencing onset and progression of the atherosclerotic disease [32,33].

On the contrary, areas subject to high values of WSS are not submitted to the development of atherosclerotic plaques.

### **2.3.2 Effects of atherosclerosis in coronary arteries**

Atherosclerosis is the most common cause of coronary artery disease (CAD), as ischemic cardiomyopathy and myocardial infarction. They both define the failing condition of the heart muscle. While the first is characterized by a decrease in blood supply to the heart tissue which leads to chest pain or angina pectoris, myocardial infarction is the end point of ischemia that results in death of heart tissue due to absence of blood supply.

Some deaths occur suddenly following an acute coronary occlusion, while others occur in more or less long periods due to a progressive weakening of the propulsive action of the heart.

The decrease of the coronary flow is caused by the development of an atheromatous plaque located in the first centimetres of the major coronary arteries, which causes an obstruction to blood flow. The extent of the cardiac damage that follows, also depends on the collateral circulation that develops as a consequence of the occlusion. When the occlusion occurs suddenly, these anastomoses immediately dilate but, in spite of this, blood flow is not enough to keep the heart tissue alive. When plaque formation is a slow process in time, instead, the collateral circulation is formed more slowly, and the subject never incurs acute episodes of cardiac occlusion.

Myocardial infarction is due to an acute coronary occlusion: blood no longer flows into the vessels downstream of the occlusion, except for that small amount of blood from the collateral circulation. The area of the myocardium in which the flow is scarce or is completely lacking, is called infarcted area. In this portion of tissue, which takes on a bluish colour, the cardiac tissue dies, and revascularization techniques are necessary for the tissue to return to functioning properly <sup>[27]</sup> (Figure 2.7).

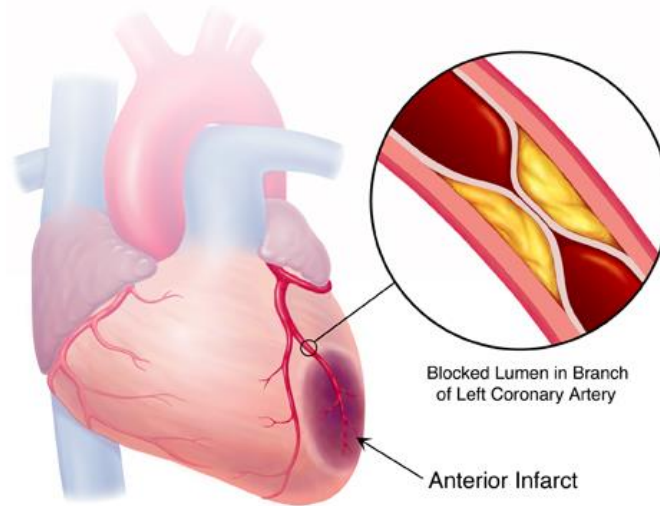


**Figure 2.7** Infarcted heart. Dark area represents the ischemic zone <sup>[34]</sup>

## 2.4 Measurement and classification of coronary stenosis

The severity of coronary arteries stenosis is assessed by the angiographic examination of different characteristics of the lesion, such as the localization, percentage of occlusion, length, morphology, coronary perfusion, vessel diameter distal to the lesion <sup>[35]</sup>.

For the quantitative assessment of stenotic occlusion, the lesion site is compared with the reference site, which is located proximal or distal to the stenosis and it is not involved by the occlusion.

The degree of narrowing is generally expressed as percent lumen diameter stenosis, according to the following formula <sup>[36]</sup>:

$$\% \text{ Stenosis} = 1 - \frac{D_s}{D_0} \times 100$$

Where  $D_s$  is the diameter at stenotic site and  $D_0$  is the reference diameter of the normal vessel without stenosis, as it can be seen in the figure below (Figure 2.8):

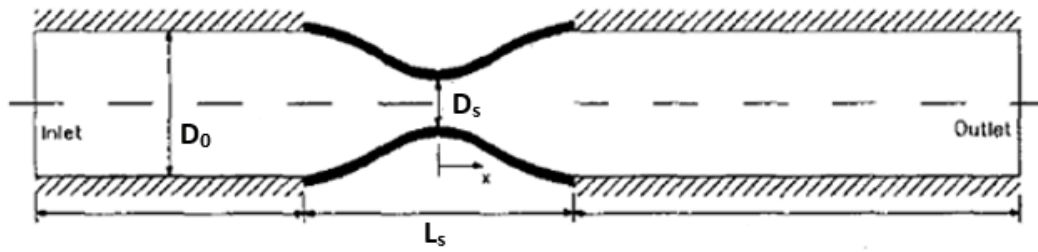


**Figure 2.8** Geometry model of stenotic vessel <sup>[37]</sup>

Traditionally, only diametric measurements have been used for the evaluation of stenosis because the images provided by catheter-based angiography, which for many years has been the standard of reference in this setting, are projection images of the affected vessel, which make stenosis diameter measurable but not stenosis area. The projection image should be generated at a precise angle that allows the correct measurement of the minimum luminal diameter <sup>[38]</sup>. In figure 2.9 it is possible to see how projection images (a, b) and a cross-sectional image (c) are used to measure the diameter of an eccentric arterial stenosis:

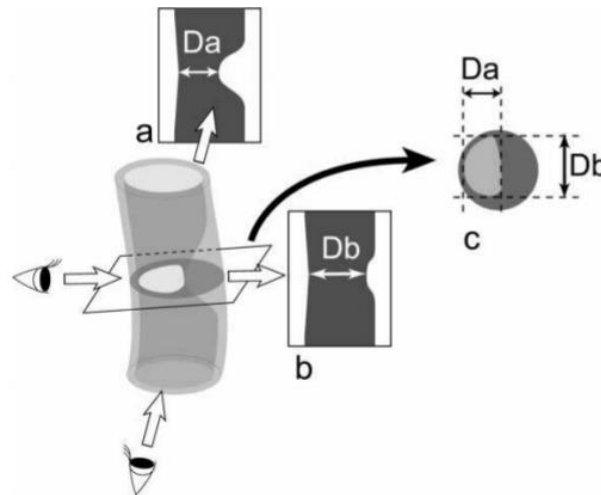


**Figure 2.9** Illustration on how projection images (a, b) and a cross-sectional image (c) are used to measure the diameter of an eccentric stenosis <sup>[38]</sup>

In projection *a*, the minimal lumen diameter ( $D_a$ ) is depicted at the optimal projection angle, so the degree of stenosis can be correctly estimated; conversely, in projection *b* the degree of stenosis is underestimated because the minimal lumen diameter ( $D_b$ ) is depicted at a suboptimal projection angle, making it larger than  $D_a$ . The cross-sectional image *c* is oriented perpendicular to the vessel and accurately depicts lumen morphology, making the minimal lumen diameter easy to measure.

The degree of occlusion can be even measured in terms of the percentage of area reduction, comparing the lumen area at the stenotic site with the lumen area at reference site. Some reports state that a reduction in cross-sectional area correlates better with the hemodynamic effect of stenosis than a reduction in diameter does, therefore, it has been proposed as a more accurate way of measuring arterial stenosis. Moreover, this evaluation is relatively time consuming if the border of the lumen is traced manually and software programs are now commercially available to measure area stenosis automatically, helping in reducing the amount of time required for analysis [38].

It is important to note whether an arterial stenosis is measured in terms of diameter or area because the two percentages do not correspond (Figure 2.10).

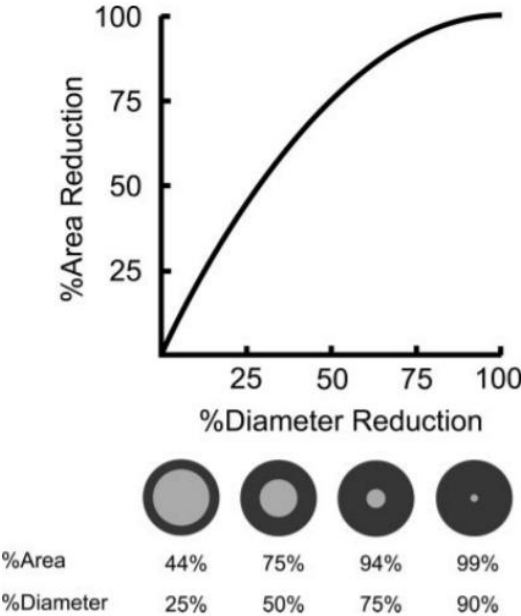


**Figure 2.10** Relationship between area reduction and diameter reduction in cases of completely concentric stenosis [38]

The degree of area reduction is greater than the degree of diameter reduction, and their relationship is described by the following equation:

$$A = D \times \left[ 2 - \left( \frac{D}{100} \right) \right]$$

Where *A* is the percentage of area reduction and *D* is the percentage of diameter reduction.

In cases of eccentric stenosis, this relationship is not constant [38].

The degree of stenosis, considering the occlusion as percentage of diameter reduction, is commonly classified into one of the following categories [35]:

- Normal coronary artery
- $\leq 25\%$ : Irregularities not obstructive
- 25% - 50%: mild stenosis
- 50% - 70%: moderate stenosis
- 70% - 90%: severe stenosis
- 100%: total occlusion

The American Heart Association (AHA) has provided a classification of coronary artery stenosis according to their morphological characteristics. This classification is shown in the figure below (Figure 2.11) [35]:

<p>Type A Lesions</p> <ul style="list-style-type: none"><li>Short (&lt;10 mm)</li><li>Concentric</li><li>Smooth contour</li><li>Nonangulated (&lt;45°)</li><li>No calcification</li><li>Nonostial location</li><li>No side branch involvement</li><li>No thrombus</li></ul> <p>Type B lesions</p> <ul style="list-style-type: none"><li>Tubular (10°–20 mm length)</li><li>Eccentric</li><li>Moderately angulated (&gt;45°, &lt;90°)</li><li>Irregular contour</li><li>Moderate calcification</li><li>Total occlusions &lt;3 months old</li><li>Ostial location</li><li>Bifurcation lesion</li><li>Thrombus present</li></ul> <p>Type C lesions</p> <ul style="list-style-type: none"><li>Diffuse (length &gt;20 mm)</li><li>Extremely angulated (&gt;90°)</li><li>Total occlusion &gt;3 months old</li><li>Inability to protect major side branch</li><li>Degenerated vein grafts with friable lesions</li></ul> <p>Type B1 denotes presence of only one Type B characteristic</p> <p>Type B2 denotes presence of 2 or more Type B characteristics</p>
---

**Figure 2.11** AHA stenosis classification [35]

Furthermore, there is another classification of stenoses based on the circumferential patterns of plaque distribution inside the vessel. In fact, the plaque can be concentric (or diffused) if it is diffused along the whole circular section of the vessel, or it can be eccentric (or focal) if it is localized in a precise area along the section of the vessel. In this second

case the plaque site can have three different orientation: lateral site, myocardium site, pericardium site (Figure 2.12) [39].

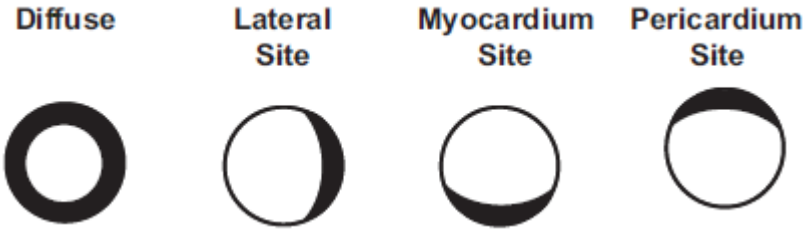


**Figure 2.12** Circumferential patterns of plaque distribution [39]

# CHAPTER 3

## VIRTUAL FRACTIONAL FLOW RESERVE FOR NON-INVASIVE FUNCTIONAL ASSESSMENT OF STENOSIS IN CORONARY ARTERIES

### 3.1 Fractional Flow Reserve

Fractional flow reserve (FFR) is an index widely used in coronary catheterization to estimate stenosis severity in terms of pressure drop, and it has been accepted as the gold standard for detecting functional significance of intermediate coronary stenoses [40]. It expresses the maximal flow down a vessel in the presence of a stenosis compared to the maximal flow in the hypothetical absence of the stenosis [40–42].

The basic physical principle is the proportionality between the pressure and the flow that occurs in a condition of maximal hyperemia.

FFR can be expressed through the ratio between coronary flow during maximal hyperemia in the presence of stenosis ( $Q_{stenosis}$ ) and coronary flow during maximal hyperemia in the absence of stenosis ( $Q_{normal}$ ) [43,44]:

$$FFR = \frac{Q_{stenosis}}{Q_{normal}}$$

The coronary flow  $Q$  is equal to the pressure gradient  $\Delta p$  divided by the myocardial resistance  $R_{myo}$ . Thus,  $Q_{stenosis}$  and  $Q_{normal}$  can be respectively written as follows:

$$Q_{stenosis} = \frac{\Delta p}{R_{myo}} = \frac{P_d - P_v}{R_{myo}} \quad \text{and} \quad Q_{normal} = \frac{\Delta p}{R_{myo}} = \frac{P_a - P_v}{R_{myo}}$$

where  $P_d$  is the pressure downstream of the stenosis,  $P_v$  is the central venous pressure and  $P_a$  is the mean aortic pressure.  $P_v$  is relatively low and subjected to minimal instantaneous changes, therefore it can be neglected. Even  $R_{myo}$  can be omitted because, during hyperemia, resistances are minimal and therefore equal.

Under these assumptions, FFR can be defined as the ratio between the mean distal coronary pressure and the mean aortic pressure, under condition of maximal hyperemia [40–43,45,46] (Figure 3.1):

$$FFR = \frac{P_d}{P_a}$$

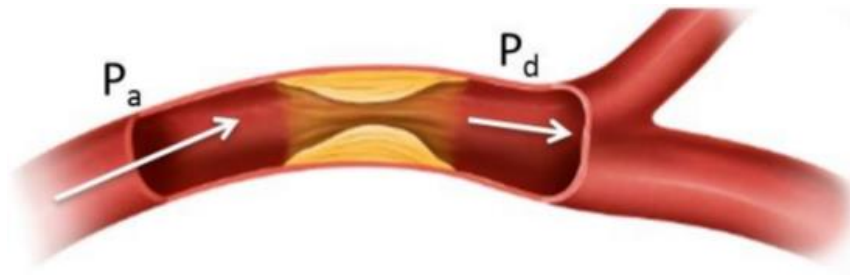


**Figure 3.1** Measure of FFR as ratio of the two values of pressure  $P_d$  and  $P_a$  [46]

The result of this ratio is an absolute number whose value is between 0 and 1. In normal arteries FFR is equal to 1, indicating that no decline of pressure occurs along the length of the vessel, even at hyperemia, while values lower than 1 indicate the presence of an obstacle to blood flow.

The value of FFR equal to 0.8 has been chosen as a threshold to discriminate if a stenosis is significant or not, meaning that the stenosis causes a 20% drop in blood pressure [43,47,48].

For this reason, stenosis with  $FFR \leq 0.8$  are considered as physiologically significant; in particular, if FFR is lower than 0.75 it can be assumed with a certainty of 99% that there is a high risk of ischaemia, while for values between 0.76 and 0.80 clinical judgement based on the physician's experience and the clinical history of the patient are necessary to take a decision. On the other hand, stenosis with  $FFR > 0.8$  are not physiologically significant and the percentage of ischaemia is reduced by less than 5% [49]. (Figure 3.2)

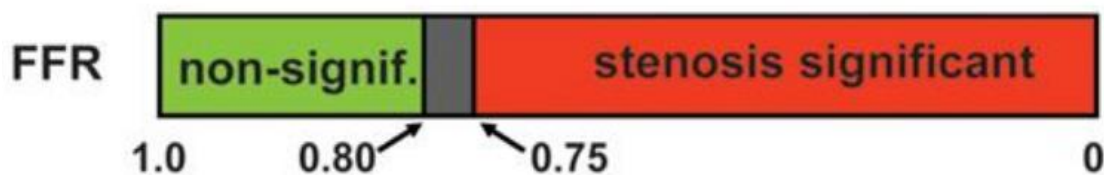


**Figure 3.2** Threshold values of FFR for discriminating stenosis significance [49]

The reason for which the use of FFR investigation became necessary, derives from the limitations of coronary angiography in determining the physiologic significance of coronary stenosis. In fact, despite the introduction of quantitative coronary angiography (QCA), stenosis estimation remains operator-dependent; moreover, coronary angiography alone does not provide any information on the functional criticality of coronary lesions [43]. Conversely, the measurement of FFR in angiographic context can give important information on the analysed stenosis, useful to decide in which way it is necessary to intervene according to the value provided by this parameter. For example, in case of patients suffering from stable coronary artery disease, the information obtained from FFR allows to understand if a stenosis is functionally significant or not and, consequently, it allows to decide if a percutaneous coronary revascularization procedure (PCI) must be planned to restore the correct vascularization of tissues, or if the intervention can be deferred.

Numerous studies have confirmed the efficacy and usefulness of the functional evaluation of coronary disease through the use of FFR. In particular, DEFER (Deferral Versus Performance Without Documented Ischemia) was the first randomized trial published in 2001, that demonstrated the safety of coronary revascularization based on FFR values: the 5-year follow-up recently published confirms that deferring treatment of a functionally non-significant lesion is safe even in long term and does not lead to phenomena of late recovery [43,50]. The study that validated FFR clinical use in large scale was the FAME (FFR VS Angiography in Multivessel Evaluation) study published in 2009, which was conducted on 1005 patient with multivessel coronary artery disease. Its purpose was to compare FFR-guided PCI to angiography-guided PCI, to understand which one of them was more accurate in assessing the functional significance of a coronary stenosis. The salient result of this study was that the rate of adverse events greater than one year was lower in the FFR group compared to the group subjected to angiography. Furthermore, angiography resulted inaccurate in assessing the functional significance of a coronary stenosis when compared with FFR, not only in stenosis with medium severity but also in stenosis with 70% to 90% reduction in diameter [50,51].

Subsequently, the FAME 2 study, halted in 2012, was conducted on 1220 patients with stable coronary artery disease who had at least one functionally significant stenosis. Because in this type of patients the preferential treatment consists in optimal medical therapy, the purpose of this study was to verify if, in the stenosis considered functionally significant by the measurement of the FFR, the coronary revascularization by FFR-guided

PCI associated with the optimal medical treatment was superior than the only optimal medical therapy. The result of this study has shown that in this type of patients, the FFR-guided PCI reduces the need for a new urgent revascularization compared to the strategy based on the only optimal medical therapy<sup>[50,52]</sup>.

Thus, FFR represents the method with more scientific evidence for the functional evaluation of coronary stenosis. This procedure significantly improves the clinical outcome and reduces the mortality rate caused by multivessel coronary artery disease (CAD).

### 3.1.1 Measurement of FFR

A well-established method of assessing the hemodynamic severity of single stenosis in coronary arteries uses pressure wires to measure FFR<sup>[42,53]</sup> (Figure 3.3).

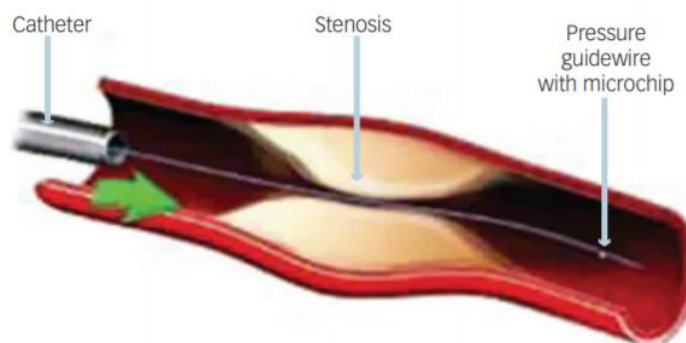


**Figure 3.3** Measure of FFR with the use of a pressure wire<sup>[50]</sup>

The measurement of FFR is generally performed using a guiding catheter but can also be performed with a diagnostic catheter. However, the former presents more advantages: it allows easier handling of the pressure guide by reducing the friction linked to the passage of the catheter guide; it offers a greater internal lumen, interfering less in the measurement of the aortic reference pressure; finally, it makes possible the direct execution of a PCI, using the same pressure guide as a PCI guide.

For a correct measurement of FFR, the pressure guide must be kept inside its container filled with saline solution and placed on a flat surface at the height of the pressure transducer. Subsequently, the pressure guide is advanced into the guiding catheter and the pressure sensor is placed immediately at the exit of the guiding catheter. In this position, equalization between the aortic pressure and the pressure read from the guide must be performed, keeping the pressure sensor at the catheter ostium upstream of the

stenosis. After performing the equalization, the pressure guide with the transducer advance into the coronary, passing the stenosis that must be evaluated. Then, intracoronary nitrates are administered to eliminate any component of epicardial dynamic stenosis due to vasospasm, maximal hyperemia is induced by adenosine administration, and finally the FFR measurement is performed.

Adenosine can be administered either in continuous infusion, through a central or peripheral vein, or with intracoronary injection. The standard dosage for induction of hyperemia with adenosine in continuous infusion is of  $140 \mu\text{g} / \text{kg} / \text{min}$  [43,53]. The administration of adenosine can cause rapidly reversible symptoms (flushing, empty head feeling, difficulty breathing, etc.), electrocardiographic changes (bradycardia) and a mild drop in blood pressure. Furthermore, in the presence of a stenosis, induction of hyperemia determines a characteristic modification of the pressure curves with progressive deviation between the aortic pressure from the distal coronary artery; the curves and pressure values stabilize when stable hyperemia is reached [43].

### 3.1.2 FFR in the most common coronary stenosis location

The correct measurement of FFR may involve special measures depending on the coronary anatomy, the location of the stenosis and the presence of multiple stenoses in a single vessel or multiple vessels [43].

The most common cases are (Figure 3.4):

- Aorto-ostial lesions;
- Common trunk lesions;
- Ostial lesions (except aorto-ostial lesions);
- Serial lesions.

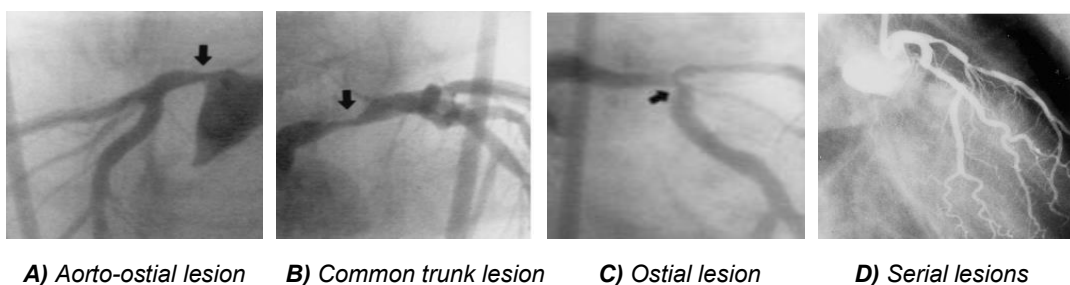


**Figure 3.4** Example of most common stenosis location in the left coronary artery

A) Ostium of LMCA [54]; B) Shaft of LMCA [54]; C) Ostium of LCX [54]; D) Two serial stenoses in the proximal LAD [42]

### **Aorto-ostial lesions**

These lesions, whether they are localized on the ostium of the right coronary artery or of the common trunk, present specific difficulties in the evaluation of their severity. Angiography can hardly discriminate the criticality of intermediate stenosis and even optical coherence tomography (OCT) does not provide optimal imaging. An alternative could be the use of intravascular ultrasound, but it is not yet able to define a minimum luminal diameter cut-off that correlates with the functional significance of the stenosis. Therefore, even in this case, the evaluation with FFR can provide important information in determining if a stenosis is critical or not, provided that a correct equalization and a correct positioning of the catheter during the evaluation of the lesion are performed. The choice of the catheter is crucial: in fact, catheters that allow non-selective cannulation must be used and avoided those built for aggressive or deep cannulation. To perform FFR assessment in these lesions, it is preferable to induce hyperaemia by continuous adenosine infusion, and not by intracoronary administration<sup>[43]</sup>.

### **Common trunk lesions**

Lesions located on the common trunk are not always easily assessed on the basis of coronary angiography, for three reasons: the common trunk is often short and emerges from the coronary sinus with variable angles; the presence of diffuse atherosclerosis makes difficult the identification of healthy reference segments; finally, the visualization of the lesion is often difficult. Non-invasive diagnostic tests are not useful in orienting the diagnosis and the possibility of underestimate the severity of these stenoses may lead the interventional cardiologist to decide to perform revascularization even in case of non-significant stenosis, which exposes the patient to unjustified surgical risk. Thus, functional evaluation using FFR represents a valid possibility in the case of equivocal stenosis of the common trunk<sup>[43]</sup>.

### **Ostial lesions (except aorto-ostial lesions)**

Ostial lesions can make FFR assessment complex. In case of stenosis that involves the anterior intraventricular artery ostium or the circumflex ostium, it is important to verify that the distal common trunk is not involved. If the angiography is not enough to eliminate any doubt, it is recommended the FFR evaluation both at the intraventricular artery level and at the circumflex artery level.

Different difficulties can arise in case of lesions involving the ostium of collateral branches such as diagonal branches, branches at the obtuse margin or distal branches of the right

coronary artery. In these cases, if the collateral branch with ostial lesion emerges from a tortuous trait and with unfavourable angle, the use of the pressure guide can be particularly complex. In fact, pressure guides are less "navigable" than the coronary PCI guides and the manipulation of the tip can cause a malfunction in the measurement phase. It is necessary to handle the guide carefully where the pressure detector is located, to avoid damaging it [43].

### **Serial stenoses**

When multiple sequential stenoses are present in the same coronary artery, the hemodynamic significance of each stenosis is influenced by the others and there is a more gradual decrease in pressure that is proportional to the severity of each stenosis. In this case, FFR provides a value that reflects the functional impact given by their sum on the blood flow. Therefore, if  $FFR > 0.8$  downstream of the most distal lesion, the angioplasty of the lesions may be deferred, whereas in case of  $FFR \leq 0.8$  it is necessary to define the impact of the individual lesions on the total value of the FFR, to evaluate whether all lesions should be treated or if the angioplasty of some of them can be deferred [43].

FFR is an index validated for single stenosis but, theoretically, it can be calculated individually for each stenosis. Considering two sequential stenoses (Figure 3.5), two values of FFR are obtained: the first is the ratio between the pressure after ( $P_m$ ) and before ( $P_a$ ) the proximal stenosis, the second is the ratio between the pressure after ( $P_d$ ) and before ( $P_m$ ) the distal stenosis.

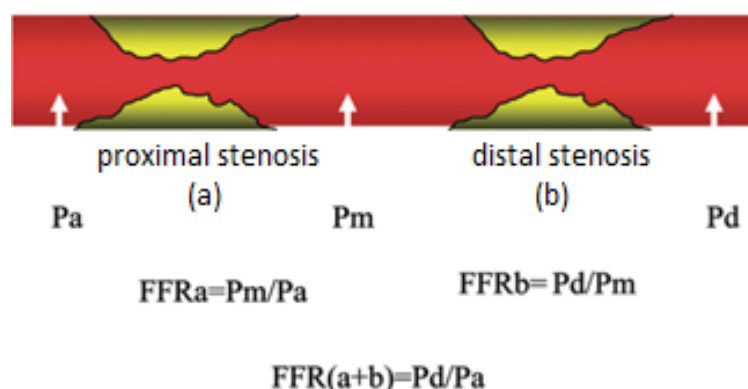


**Figure 3.5 FFR in serial stenoses** [55]

These two values do not account of stenoses interactions and they are expected to underestimate the true severity of each stenosis. This inaccurate estimation is more

pronounced for the proximal lesion than for the distal one, and this problem is more marked when the stenosis in sequence is more severe or when the collateral flow is higher<sup>[42]</sup>.

However, this approach is laborious so in clinical practice another method is used: the pressure guide is slowly retracted during maximal hyperemia, and subsequent increments of the FFR value are observed, which grossly reflect the impact of each individual lesion.

If the pull-back is not decisive in identifying the lesion with greater impact on FFR, it is advisable to proceed as follows:

1. Treat angiographically more critical stenosis.
2. Perform a new evaluation with FFR downstream of each stenosis
3. If  $FFR > 0.8$  the residual lesions can be deferred;
4. If  $FFR \leq 0.8$  the angiographically more significant residual lesions are treated in succession.

Then, in case of further residual lesion in the same vessel, the FFR evaluation is repeated: if  $FFR > 0.9$  the procedure ends, while if  $FFR \leq 0.9$  the result is optimized (example: post-dilation, additional stent implant upstream or downstream, etc) and FFR is repeated until a value greater than 0.9 is obtained<sup>[43]</sup>.

### **3.1.3 Limits of FFR and current solutions**

Despite the advantages of this procedure, the measure of FFR is also characterized by some problems which limit its clinical applications. The introduction of a pressure wire is an invasive method to measure FFR; moreover, this measurement can be applied only through coronary angiography, which is an equally invasive treatment because it requires to expose the patient to an important dose of radiation. In addition to its invasive nature, other limits are due to its cost and the need to induce hyperemia through adenosine infusion.

To solve these problems numerous studies have shown that FFR can also be assessed in a non-invasive way, thanks to a new diagnostic test which has demonstrated high diagnostic performances:  $FFR_{CTA}$  analysis. Starting from coronary images acquired by multidetector angio-CT (CTA) and from some patient parameters, it is now possible to obtain the FFR of the coronary tree using specific software.  $FFR_{CTA}$ , even called virtual FFR (vFFR), has replaced invasive FFR for the assessment of severity of intermediate coronary lesion, thanks to its operational and economic benefits<sup>[40,56]</sup>.

### 3.2 Computation of vFFR through Computational Fluid Dynamics

Virtual FFR utilizes computational fluid dynamics (CFD) to compute the hemodynamic on a reconstructed patient-specific coronary artery model [40]. CFD is a branch of fluid mechanics that uses numerical methods and algorithms to simulate and analyse fluid flow.

It allows to obtain coronary blood flow and pressure field in the three-dimensional region of interest by solving the governing equations of fluid dynamics, known as Navier-Stokes equations, that in vector form are written as follows [53,57]:

$$\nabla \bar{u} = 0$$
$$\rho \frac{\partial \bar{u}}{\partial t} + \rho \bar{u} \cdot \nabla \bar{u} = -\nabla p + \mu \nabla^2 \bar{u} + \rho \bar{g}$$

These equations are solved for the unknown pressure and for three components of blood velocity, all functions of position and time. Blood properties, as density and viscosity, are known to solve them and, although blood exhibits complex rheological properties, it can be approximated as a Newtonian fluid with a constant viscosity in large arteries.

The governing equations are insufficient to solve blood flow problems; in fact, to compute coronary flow and pressure, CFD requires anatomical and physiological inputs, that is the definition of a geometrical 3D model of the coronary and the application of realistic boundary conditions.

The geometric model of interest is extract from image data (CTA) through segmentation and reconstruction algorithms which extract the luminal surface of the vessels, the topology of the artery tree, the anatomy of lesions eventually present and the luminal boundaries, up to the limits imposed by the resolution of CTA (Figure 3.6); then the geometric model is discretized with a finite element mesh with millions of vertices and elements [53] (Figure 3.7).

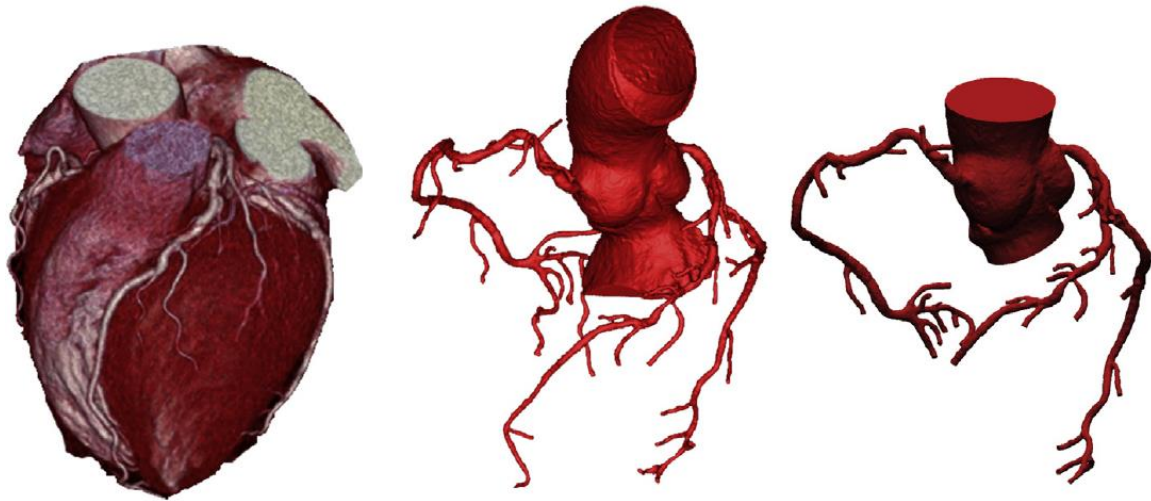


**Figure 3.6** Example of image segmentation steps for computing  $FFR_{CTA}$ .  
 From left: volume-rendered image, lumen boundary surface segmented from image data, 3D model <sup>[53]</sup>.

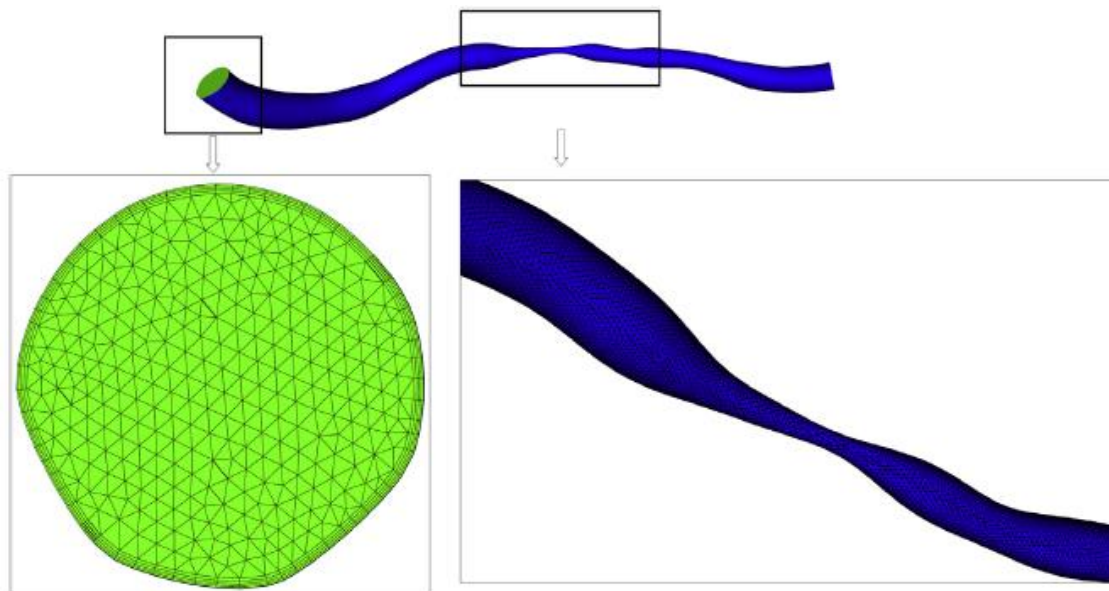


**Figure 3.7** Example of Finite Element Mesh used for Simulations.  
 Detail of the wall (blue) and inlet (green) are shown <sup>[58]</sup>

Once extract the model it is possible to incorporate boundary conditions representing cardiac output, aortic pressure, microcirculatory resistance, coronary flow at rest and at hyperemia. Boundary conditions are mathematical relationship between the variables of interest (flow and pressure) defined on the boundaries of the mathematical model, that is

the lateral surface, the inlet and the outlet boundaries. Furthermore, it is necessary to describe the conditions at the interface of the model of interest and the rest of the system [53].

After the definition of the 3D geometrical model and the boundary conditions, the CFD solver simulates the distribution and dynamics of blood pressure, flow and shear stress within the artery over time, and the data generated are used to calculate vFFR at any point of the vessel [57]. All the stages are shown in the following image (Figure 3.8):

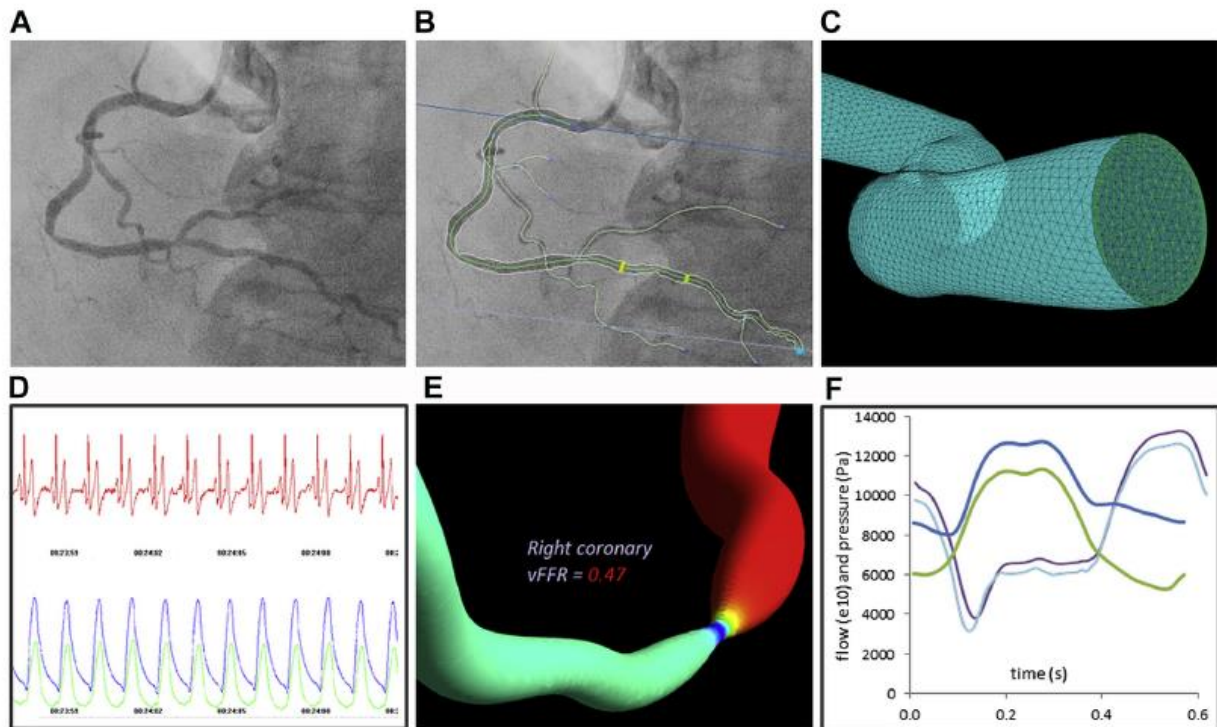


**Figure 3.8** Stages of developing a typical vFFR workflow [57].

**A)** Coronary angiogram; **B)** Segmentation and reconstruction into an anatomical 3D model; **C)** Surface and volumetric mesh; **D)** Boundary conditions; **E)** CFD simulation computes pressure gradient, using the 3D model and the boundary conditions; **F)** Results validation against invasive measurements.

Theoretically, computing the pressure drop across a stenosis is an elementary CFD problem. However, due to practical and clinical limitations, the geometric and hemodynamic factors that influence blood flow and energy loss along a diseased coronary artery are complex [57].

### 3.2.1 Boundary conditions

For vFFR computation, the physical conditions that affect each boundary (inlet, outlets and vessel walls) must be accurately represented in the model, to obtain the best approximation of the vessels physiology. However, the identification of a non-invasive technique to parametrize these boundary conditions represent the greatest challenge. The boundaries of a generic vascular model ( $\Omega$ ) can be classified into three groups (Figure 3.9):

- Vessel wall boundary ( $\Gamma_s$ )
- Inlet boundary ( $\Gamma_g$ )
- Outlet boundary ( $\Gamma_h$ )

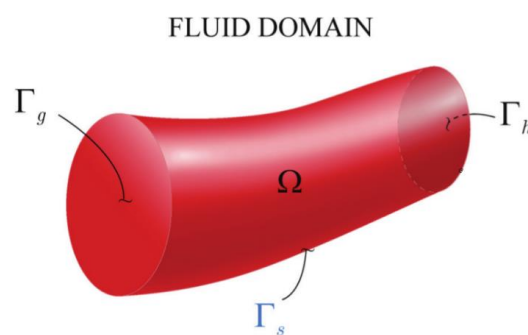


**Figure 3.9** Inlet, outlet and wall boundaries for a cylindrical vessel <sup>[59]</sup>

Vessel wall boundary represents the interface between the fluid domain and the vessel wall. Different conditions can be applied, based on the assumption that the surface can be considered rigid, in most of the simulation, or deformable.

Inlet boundary conditions are relatively easy to determine; for example, pressure can be determined either from direct measurement of aortic pressure in a Coronary Angiography-based model, or from cuff-pressure with a transfer function in the case of coronary CTA <sup>[57]</sup>. As inlet boundary condition, a flat velocity profile can be applied <sup>[60]</sup> or a prescribed pattern of aortic blood pressure obtained using a typical waveform of the aortic pressure <sup>[61]</sup>.

Distal outlet boundary conditions require a characterization of distal impedance and they are difficult to determine because coronary microvasculature circulation (CMVC) is heterogeneous both in healthy and diseased condition and require direct invasive measurement, problem that would be preferable to avoid in minimally invasive modelling <sup>[57]</sup>.

The electrical model in the figure below (Figure 3.10), shows the importance of the distal boundary conditions during vFFR computation:

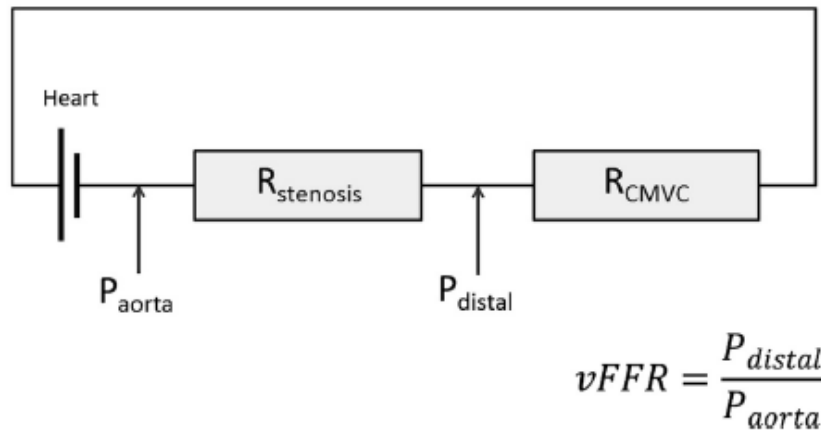


**Figure 3.10** System analogous electrical model<sup>[57]</sup>

Pressure, flow and resistance are analogous to electrical potential difference, current, and resistance, respectively. Stenosis resistance ( $R_{stenosis}$ ) and coronary microvasculature circulation resistance ( $R_{CMVC}$ ) are effectively two resistors arranged in series. The distal pressure is determined by  $R_{CMVC}$ , so even if the aortic pressure ( $P_{aorta}$ ) and stenosis resistance are known or computed, computation of vFFR is wholly dependent on the microvasculature resistance. If CMCV resistance is overestimated, even vFFR is overestimated and lesion severity results underestimated, as well as the potential benefit from revascularization<sup>[57]</sup>.

To overcome these issues a lower-order model can be used to represent the physiological conditions of the outlet boundaries<sup>[60]</sup>: a 0D lumped parameter model is used for each outlet and coupled to the 3D coronary model (Figure 3.11):

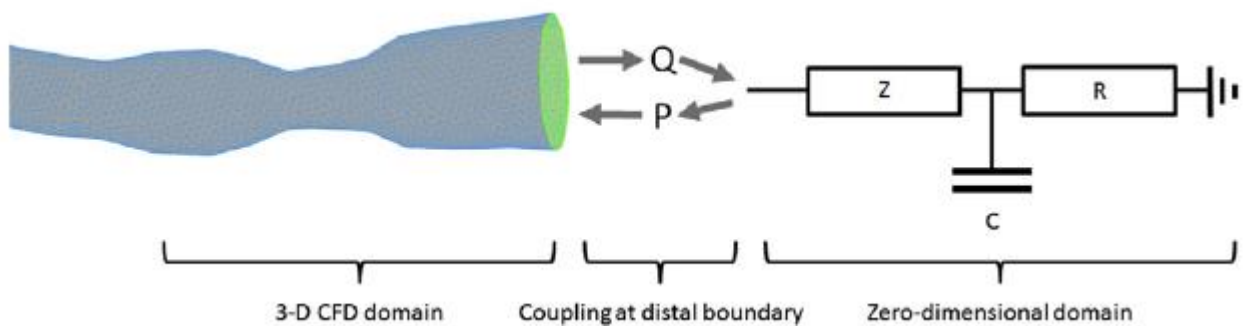


**Figure 3.11** 3D model coupled to 0D model to determine the distal coronary boundaries<sup>[57]</sup>

The lumped parameter model (LPM) corresponds to an electrically analogous Windkessel model which represents the impedance  $Z$ , the resistance  $R$  and the capacitance  $C$  of the distal coronary microvasculature circulation<sup>[57]</sup>.

In many studies, methods based on coupling the 3D model with an LPM were used. For example, in 2010 Kim et al. <sup>[62]</sup> used a 3D model for the hemodynamic of the aorta and coronary arteries, coupled with a LPM of the entire cardiovascular system to consider the interaction between the heart and the arterial system. This method showed clinical relevance and usefulness but, including the aorta in the CFD model and the entire cardiovascular system in the LPM, resulted computationally complicated and required the identification of many model parameters. This represented a problem because the uncertainties of the simulation increase.

Another example is Morris et al. <sup>[48]</sup> study in 2013, in which the attention was focused in the determination of the downstream microvascular resistance and compliance for each patient. Because determination of these parameters normally requires the invasive pressure measurement, they used an optimization process by averaging the resistance and compliance values to produce a generic value applicable to the whole cohort.

In the same year, Taylor et al. <sup>[53]</sup> implemented a more sophisticated strategy with the definition of a mathematical relationship among resistance, flow, and vessel diameter. Considering that coronary arteries dilate or constrict to modulate blood flow according to different physiological states (rest, exercise), the idea was to create “form-function” relationships to describe this adaptive mechanism, which takes place even in presence of atherosclerosis.

Although both models demonstrated impressive accuracy, they were prone to errors linked to variability in hyperemic CMVC resistance and this represents a problem for vFFR calculation. Applying flow as a boundary condition is a sensible alternative, because this accounts for CMVC resistance <sup>[57]</sup>. However, measurement of absolute hyperemic coronary flow is invasive, challenging, and requires induction of hyperemia. Estimating mean flow rate from TIMI (Thrombolysis in Myocardial Infarction) frame count yields respectable results that correlate to Doppler wire analysis, but this is only apposite for steady-flow analysis and cannot easily be applied to a transient CFD analysis. For this reason, a strategy that provides personalized estimation of the distal boundary conditions, using non-invasive clinical data, is required <sup>[57]</sup>.

In 2014, a simpler method was proposed by Kwon et al. <sup>[61]</sup> to overcome the issues related to Kim et al. model. Their method included only the coronary arteries in the geometry of the CFD model, and the coupled LPM was not based on the entire cardiovascular system, but only on the coronary circulation. Coronary circulation involved three compartments: coronary arteries, capillaries and veins. To couple the two systems, the computed flow

rate ( $Q$ ) at the outlet of the CFD model was passed to the LPM. Afterward, pressure and flow rate in the three compartments were computed by solving the ordinary differential equations and the computed value of the coronary artery pressure was then passed to the CFD model. Here, this value was used to compute the outlet pressure as the outlet boundary condition of the CFD model. This kind of coupling method effectively solves the local fluid dynamics of large vessels coupled with microvascular circulation.

### **3.2.2 vFFR computation: steady VS transient analysis**

The optimal method of CFD simulation is also yet to be determined. The coronary circulation is a dynamic pulsatile system, for this reason transient (time dependent) 3D CFD simulation is considered the most representative and accurate method. This involves solving nonlinear partial differential equations, simultaneously and repeatedly for hundreds or thousands of time for each cardiac cycle. Although pulsatile flow is considered to be the most accurate model to simulate coronary blood flow in circulation, the computation expense in terms of time and hardware requirements restricts its clinical applicability. An alternative is the steady-state CFD analysis; even if it does not represent the accelerative, time-dependent behaviour of pulsatile blood flow, it is considered as a more practical approach because it requires much less computational time. Steady-state analysis has demonstrated to simulate similar flow and shear stress patterns, and the negligible difference between data obtained with steady and pulsatile flow, indicates that steady flow can be used in vFFR computation. In fact, comparing vFFR obtained with steady and pulsatile simulation, steady state vFFR demonstrates respectable accuracy [40,57].

In the transient analysis, vFFR is a function of 9 parameters which include proximal pressure, coefficients of pressure loss, microvascular resistance and compliance, and additional parameters that describe myocardial systolic contractions. In the steady-state computation, all these parameters are reduced to a single time average value of resistance, and vFFR becomes a function of 4 parameters which are the mean pressure, coefficients of pressure loss and the total resistance. It is thanks to these fewer parameters that less computational power and time are required for the simulation [45,58].

### 3.3 Relationship between FFR and WSS

Wall shear stress (WSS) in stenosed coronary arteries is an important hemodynamic parameter related to atherosclerotic inflammation, vascular spasms and rupture.

Since  $WSS_{max}$  beyond a critical value can induce inflammatory reactions, patients with high  $WSS_{max}$  may be worsening even though their stenotic severity is not excessively significant.

In general, as coronary stenosis becomes severe, FFR value decreases while maximum WSS ( $WSS_{max}$ ) value increases. However, the way in which these values can change according to stenotic severity has not previously been investigated.

Recently, it was observed that  $WSS_{max}$  and FFR are inversely proportional to each other, meaning that  $WSS_{max}$  increases proportionally with the increase of pressure drop through stenotic lesion <sup>[36]</sup>. The slope of the linear correlation line varies by patient, indicating that it may represent a hemodynamic characteristic of the patient; thus, understanding the slope of this correlation line may help clinicians to design treatment plans for patients.

Both FFR and  $WSS_{max}$  are critical factors in the diagnosis and treatment of coronary artery disease. Therefore, estimating variations in FFR and WSS according to the progression of stenotic severity will be helpful for assessing the severity of coronary lesions <sup>[36]</sup>.

### 3.4 Advantages and disadvantages of vFFR

In addition to improving quality of life and economic benefits, virtual FFR offers some additional advantages. It provides a virtual pullback in which pressure is demonstrated at all points within a branched coronary arterial tree in a single analysis, allowing the physiological significance of serial lesions to be evaluated accurately and individually, process that is much more challenging with invasive FFR. It can also provide a “virtual stenting”, that is testing in silico some experimental strategies to observe their physiological effects before applying them in vivo. Furthermore, it allows to assess any segment of coronary tree, including those to which it might be challenging to pass a pressure wire <sup>[57]</sup>.

On the other hand, vFFR even presents some limits. Numerous artifacts may affect CTA interpretability, including calcification, motion and misregistration. Because  $FFR_{CTA}$  requires accurate anatomic models, these artifacts may limit accuracy, so it is necessary the adherence to protocols that ensure good quality data and facilitate accurate lumen boundary descriptors. Another limitation is related to the assumptions made on the

physiological model, which includes population-specific data instead of patient-specific data. The problem in this assumption is that some parameters vary among patients. For example, the relationship relating myocardial mass to total coronary flow can change, as well as the microvasculature resistance or the reduction of resistance in hyperemic condition. The consequence is that  $FFR_{CTA}$  values obtained result incorrectly estimated [53]. In general,  $FFR_{CTA}$  tends to give an overestimation of stenosis severity and an underestimation of lesion length. However, the accuracy of the measure is high with a mean error lower than 1% and correlation coefficient between  $vFFR$  and  $FFR$  of 0.99, while for  $FFR < 0.8$  the accuracy is 100% [45].

# CHAPTER 4

## METHODS

### 4.1 Geometry model and generation of stenosis

The model used in this study derives from a previously reconstructed model of the complete left coronary tree. It is composed of the left circumflex coronary artery (LCX) characterized by a bifurcation from which the marginal artery, the one with smaller diameter, branches off (Figure 4.1):



*Figure 4.1 Model used during the study*

As it can be seen in the figure above, the model consists of a proximal main branch (the proximal LCX), a distal main branch (the distal LCX) and a side branch (the marginal artery).

This domain was obtained in VMTK® as a succession of inscribed spheres, arranged as to form the geometry of the vessel.

To obtain a robust characterization of the model, a Python code was created to carry out a geometric analysis based on centerlines. Centerlines represent an approximation of vessel axis and are determined as weighted minimal action paths traced between two extremal points of the vessel [63,64], which are the inlet and the outlet (two outlets in this case). To ensure that the final lines were central, the paths were defined along the inner vertices of Voronoi diagram of the vessel model (Figure 4.2). Voronoi diagram is a non-manifold surface, that is a surface where different sheets can meet at one edge, and it is the place where the centers of maximal inscribed spheres are defined. A sphere inscribed in an object is maximal when there's no other inscribed sphere that contains it [63,64]. The envelope of maximal inscribed spheres along centerlines produce a canal surface inscribed inside the vessel and tangent to it at discrete locations [64]. A problem which characterizes Voronoi diagram is its noise; this does not affect centreline computation but provides an irregular surface that must be filtered to eliminate some parts of the diagram classified as unstable and retain the remaining stable parts related to salient geometric features.

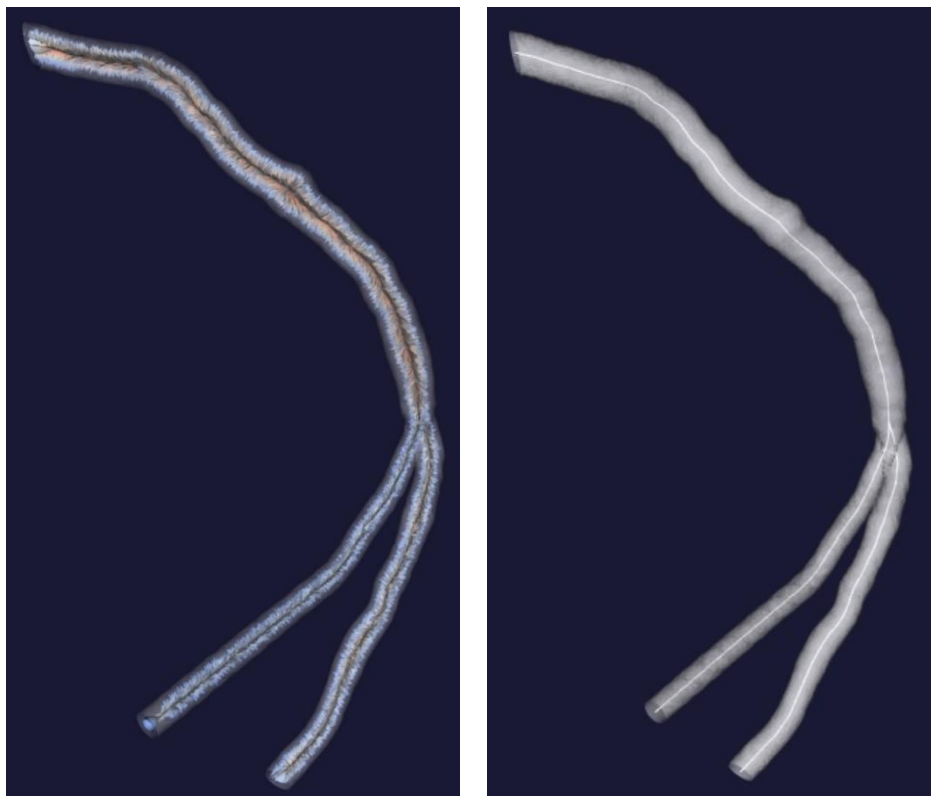


**Figure 4.2** Voronoi diagram (left) and resulting centerlines (right)

Centerlines are determined by propagating a wave from a source point using the inverse of the maximum inscribed sphere radius as the wave speed and recording the wave arrival time on all the points of the Voronoi diagram; then the line is backtraced from a target point down along the gradient of arrival times. Operatively, centerlines are computed by solving the Eikonal equation from a seed point on the Voronoi Diagram domain:

$$|\nabla T| = R(u)^{-1}$$

where  $R(u)$  is the maximal inscribed sphere radius field defined on the Voronoi diagram,  $u$  is its parametric space and  $T$  is the solution representing the arrival times of a wavefront traveling on the Voronoi diagram with speed equal to  $R(u)$ . After solving  $T$ , a centreline is generated by following the path of steepest descent of  $T$  on the Voronoi diagram from each target point by solving the following trajectory equation:

$$\frac{dc}{ds} = -\nabla T$$

where  $s$  is the centreline parametric space taken as its curvilinear abscissa <sup>[64]</sup>.

From the Voronoi diagram which describes the model, all points associated to spheres with a diameter lower than a certain threshold were eliminated, obtaining a filtered Voronoi diagram on which Gaussian stenosis was applied. After stenosis creation the surface of the stenotic model obtained was reconstructed and filtered to remove all the irregularities related to Voronoi diagram.

In this study, symmetric and concentric Gaussian stenosis were introduced (Figure 4.3), whose characteristics were attributed based on the data found in literature. In particular, two parameters were considered:

- Degree of occlusion
- Extension of the stenosis

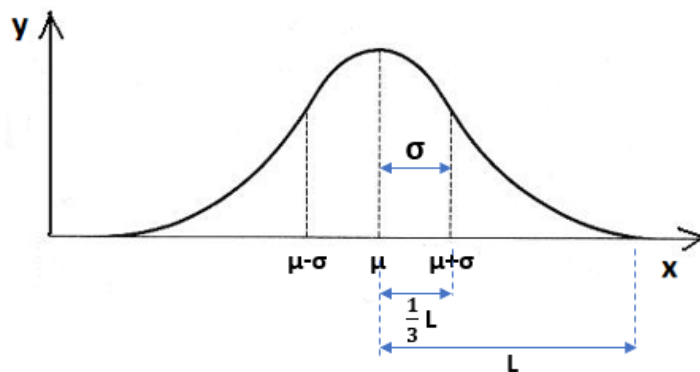


**Figure 4.3** Gaussian stenosis

In many studies it has been observed that the proximal portion of the left circumflex artery is one of the parts most affected by lepidic deposition and consequent formation of atherosclerotic plaque [47,56,61,65,66]. For this reason, it was decided to locate all the stenosis in the proximal circumflex artery, approximately in the central part of the main branch.

Regarding stenosis severity, three different degrees of occlusion were simulated, to observe the effects given by a non-obstructive stenosis, an intermediate stenosis and an obstructive stenosis. The degrees of narrowing were defined as percentage in reduction of diameter:

- 30% stenosis -> non-obstructive
- 50% stenosis -> intermediate
- 75% stenosis -> obstructive

Finally, three different lengths of stenosis were chosen, one for each typology according to the AHA classification [35]:

- Length = 3 mm -> type A (<10 mm)
- Length = 15 mm -> type B (from 10 to 20 mm)
- Length = 25 mm -> type C (>20 mm)

To generate these Gaussian stenoses, the code required the specification of 3 parameters: the mean value, the scaled radius and the variance.

The mean value ( $\mu$ ) indicates the position of the Gaussian stenosis in the vessel. The stenosis has been centered in correspondence of the sphere number 24 from inlet, which is about the middle of the main branch considering that the total number of spheres which characterise the main branch is 40.

The scaled radius represents the percentage of radius reduction compared to its initial value in the original non-stenotic model. Considering that the percentage of diameter reduction studied are 30%, 50% and 75%, the radius result reduced of the same quantity, so the values of the scaled radius are respectively: 0.3, 0.5, 0.75.

The variance ( $\sigma^2$ ) represents the extension of the Gaussian stenosis and these values were calculated considering that the standard deviation ( $\sigma$ ) is given by  $\frac{1}{3}$  of the Gaussian half-length (Figure 4.3). The values of variance obtained for the three values of length are respectively: 0.25 – 6.25 – 16.

Overall, 9 stenosis were generated in the proximal LCX, given by the combination of the 3 percentages of occlusion and the 3 extension values (Figure 4.4 – 4.5 – 4.6).

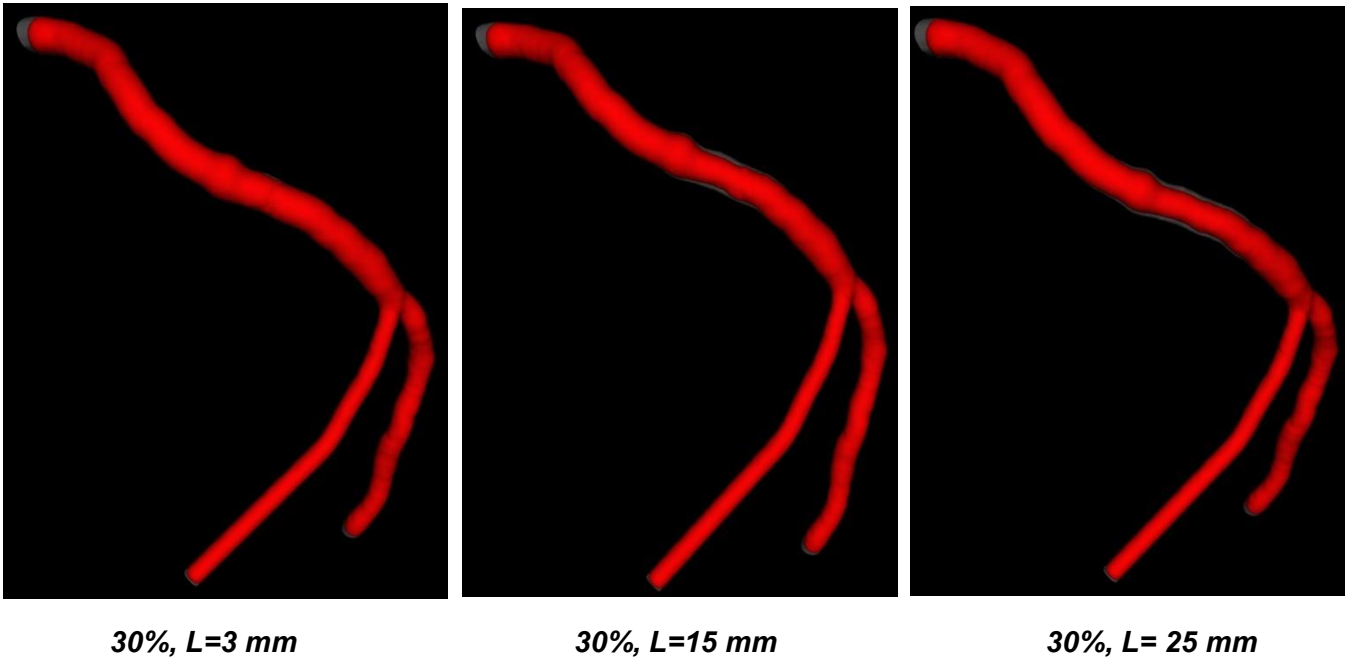


*Figure 4.4 Models with 30% reduction of diameter with the three lengths*

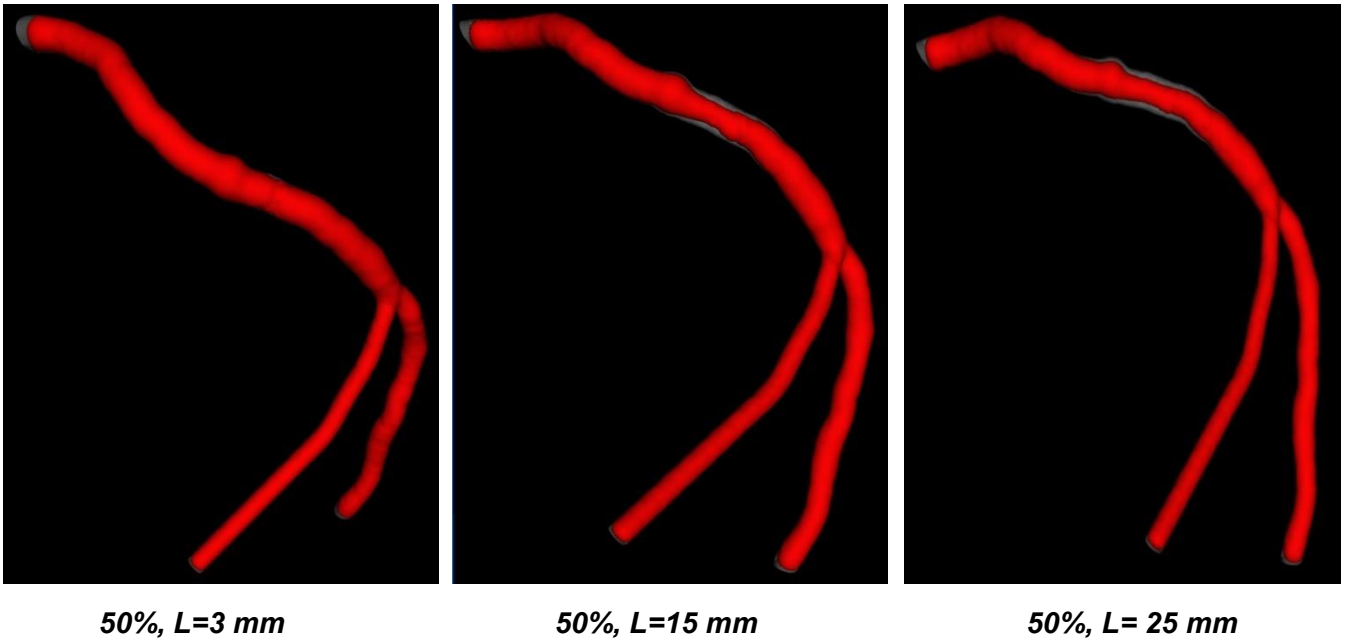


*Figure 4.5 Models with 50% reduction of diameter with the three lengths*

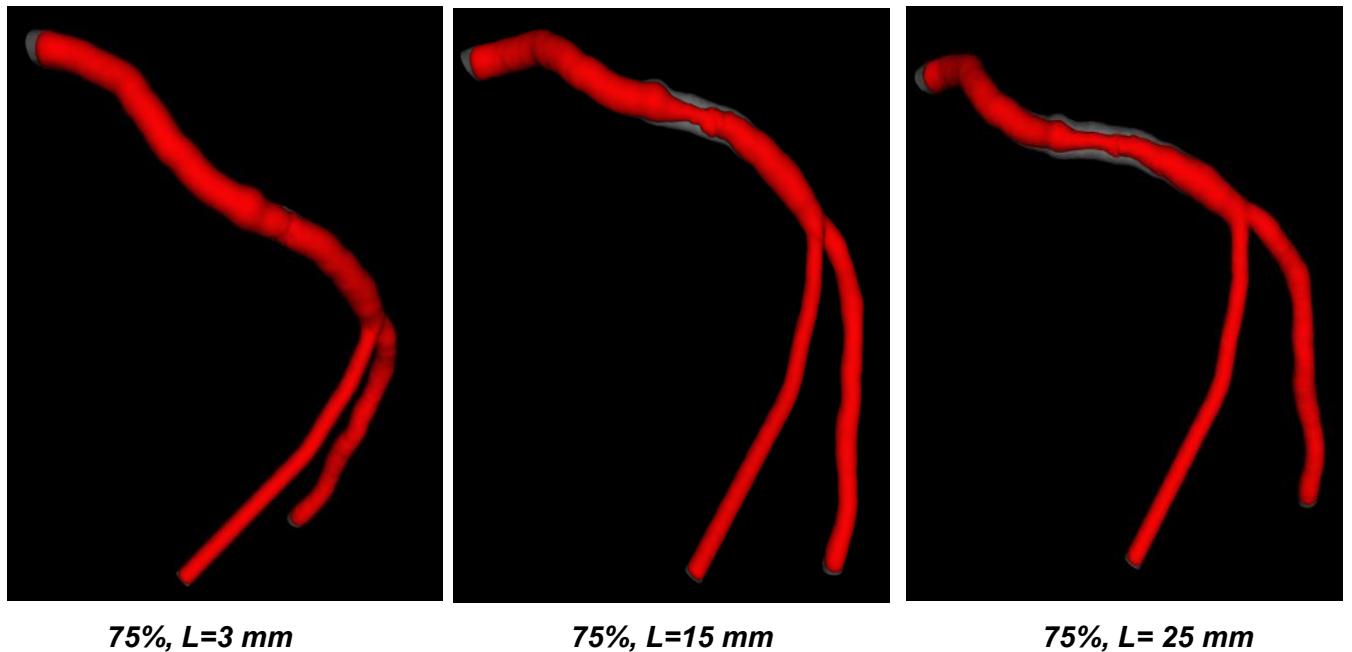


*Figure 4.6 Models with 75% reduction of diameter with the three lengths*

## 4.2 Pre-processing

The software VMTK® and ANSYS ICEM® were used in order to prepare the models for being meshed before the CFD simulation (Figure 4.7 to 4.15).

The steps of this pre-processing phase were:

1. Inlet and outlets clipping (a)
2. Creation of centerlines (b)
3. Calculation of flow extensions (c)
4. Definition of the fluid zone and the surfaces that delimit the volume: wall, inlet and the two outlets (d)

The generation of flow extensions is necessary to ensure a fully developed flow at the inlet of models, which means that the velocity profile does not change towards the downstream coordinate. In these coronary models the generation of flow extensions 1 diameter long were enough for this purpose.

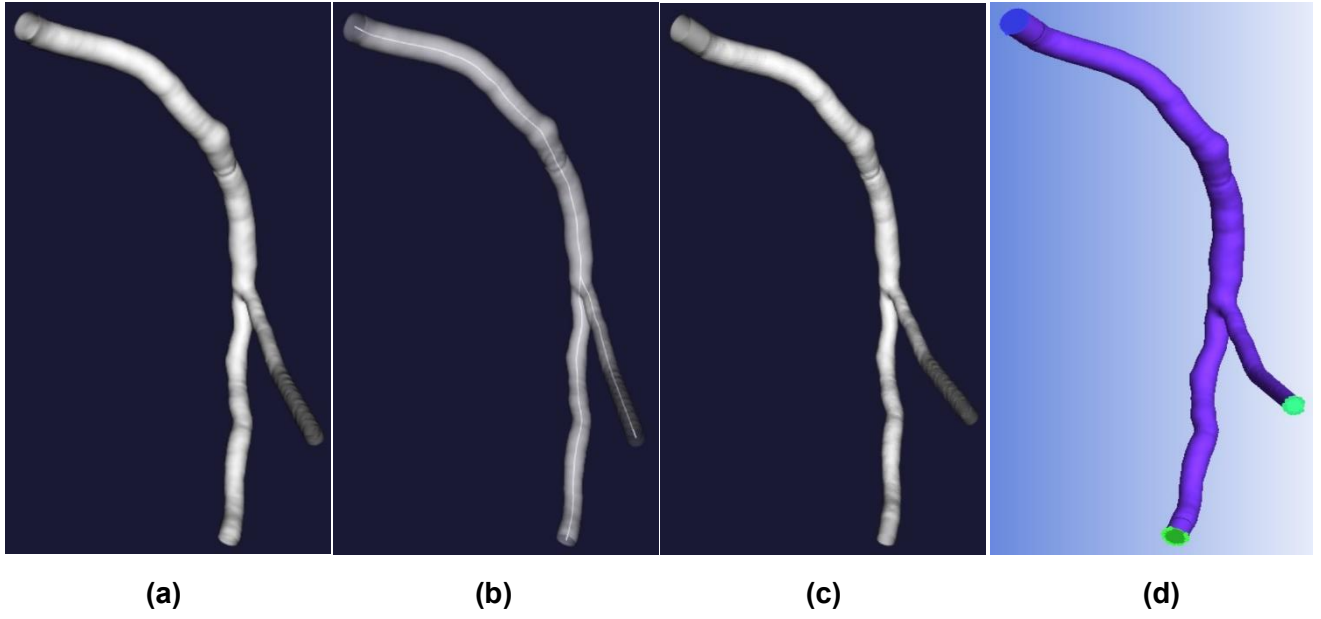


**Figure 4.7** Model: 30%,  $L = 3 \text{ mm}$

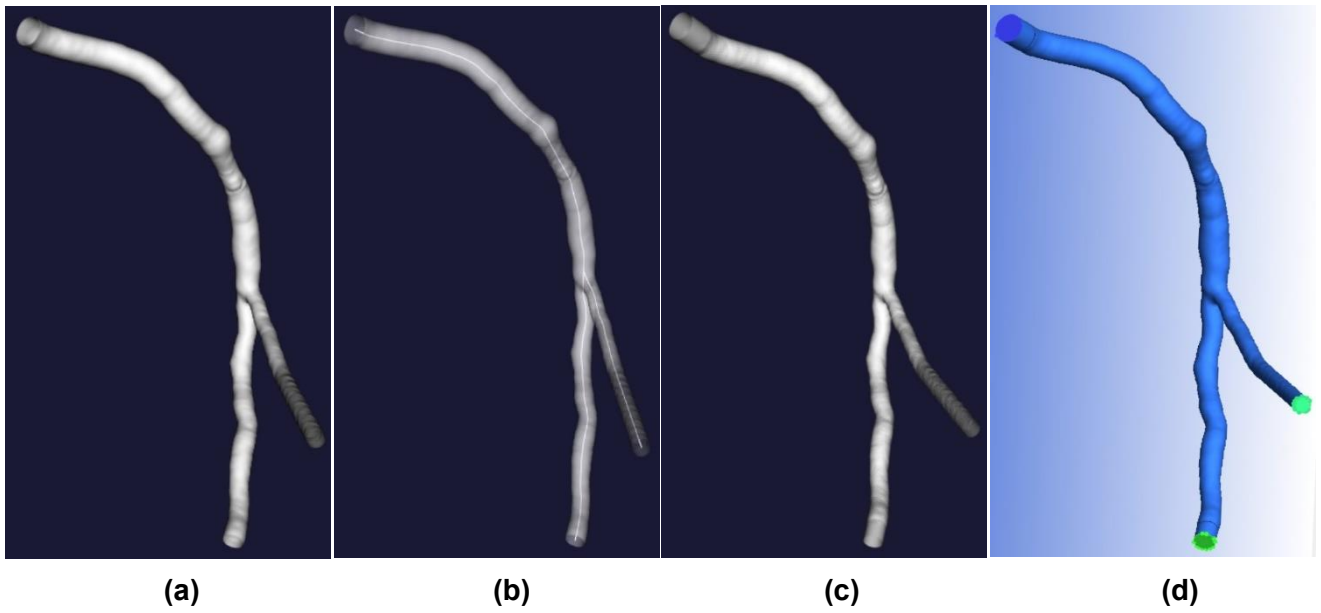


**Figure 4.8** Model: 30%,  $L = 15 \text{ mm}$

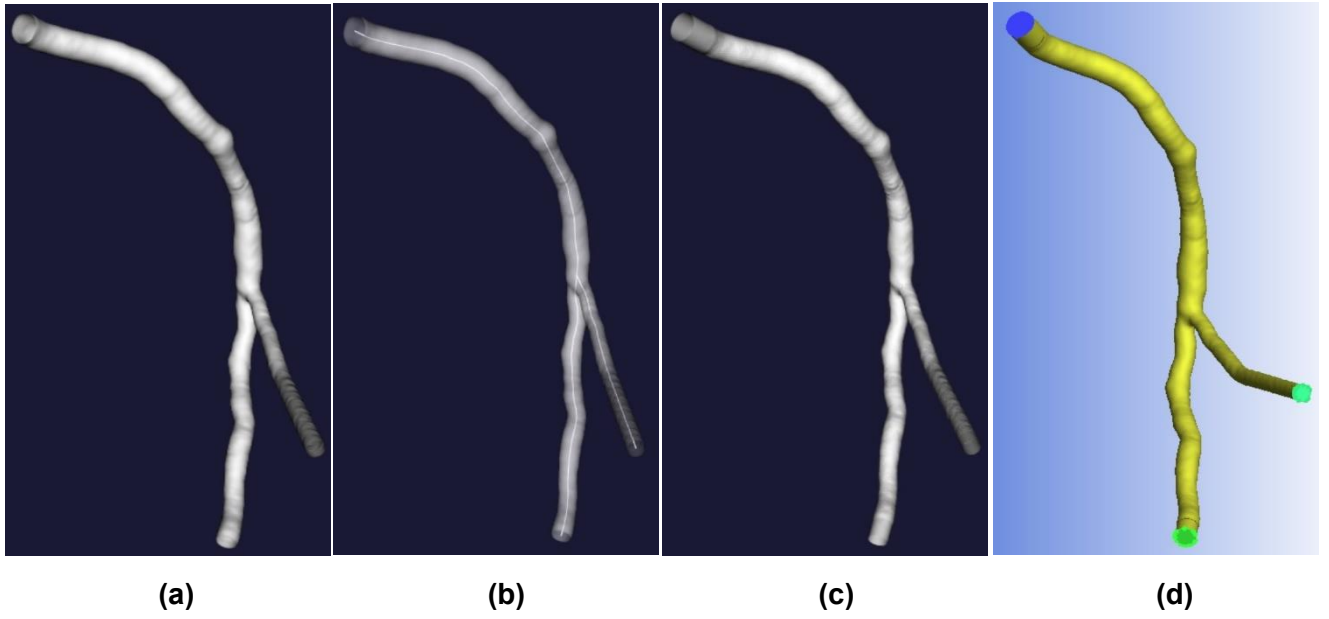


**Figure 4.9** Model: 30%,  $L = 25$  mm

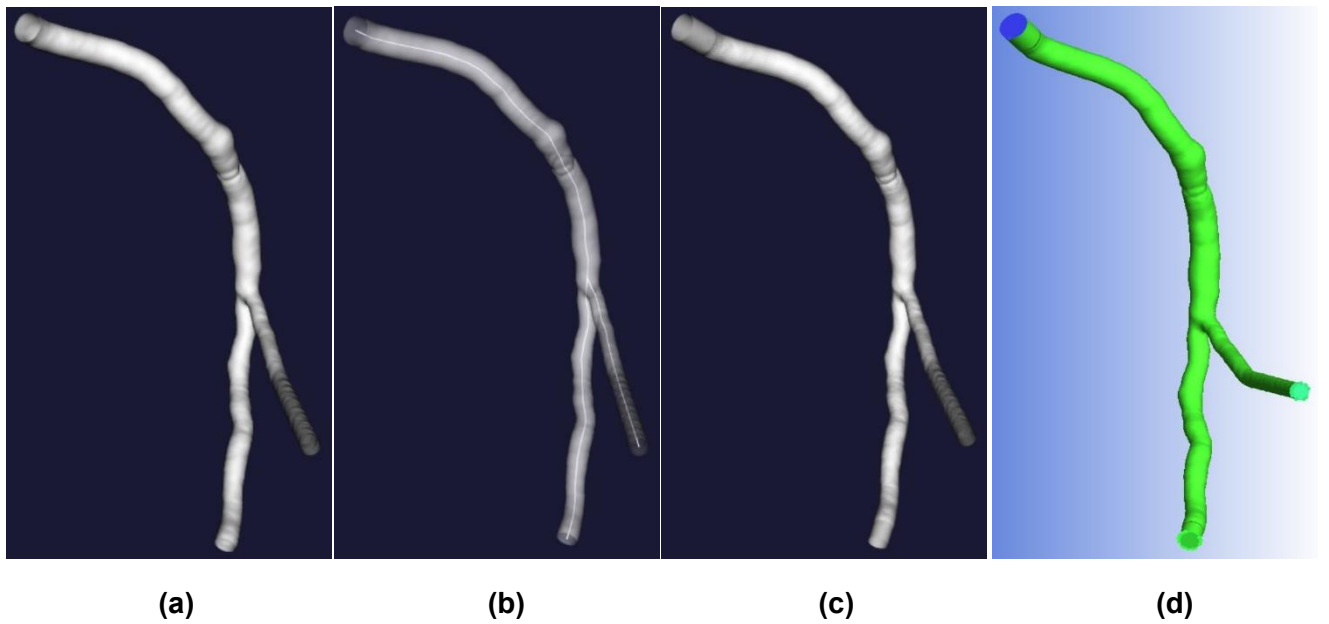


**Figure 4.10** Model: 50%,  $L = 3$  mm

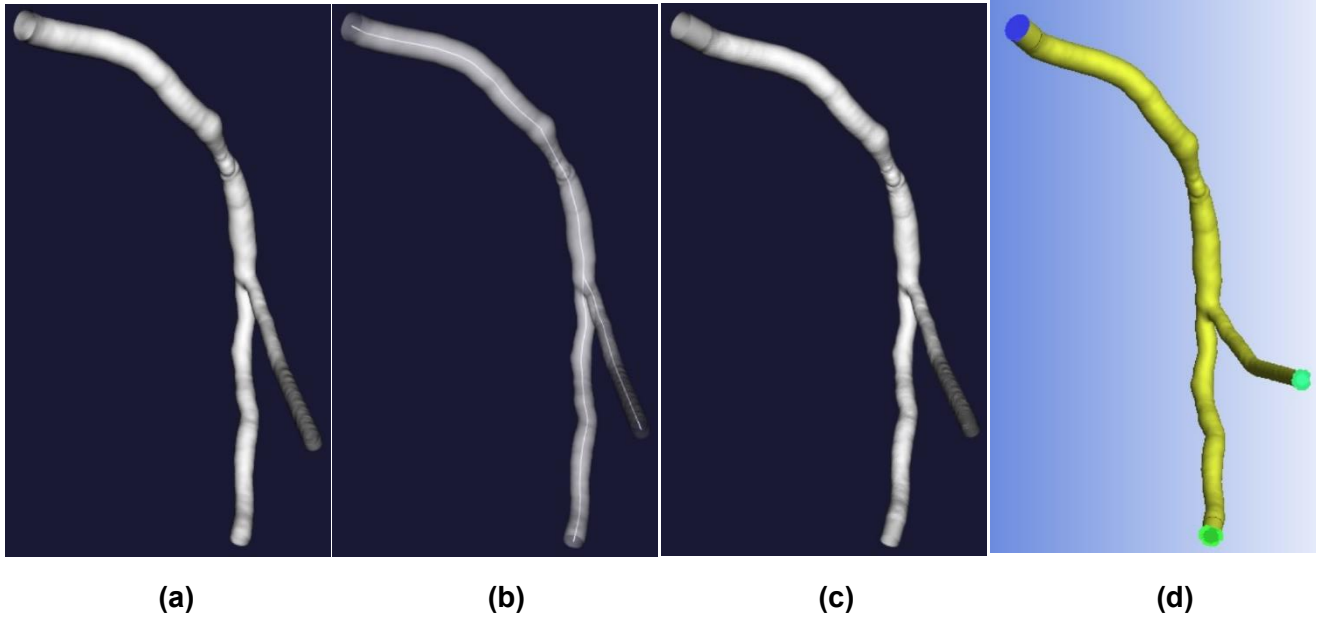


**Figure 4.11** Model: 50%,  $L = 15$  mm

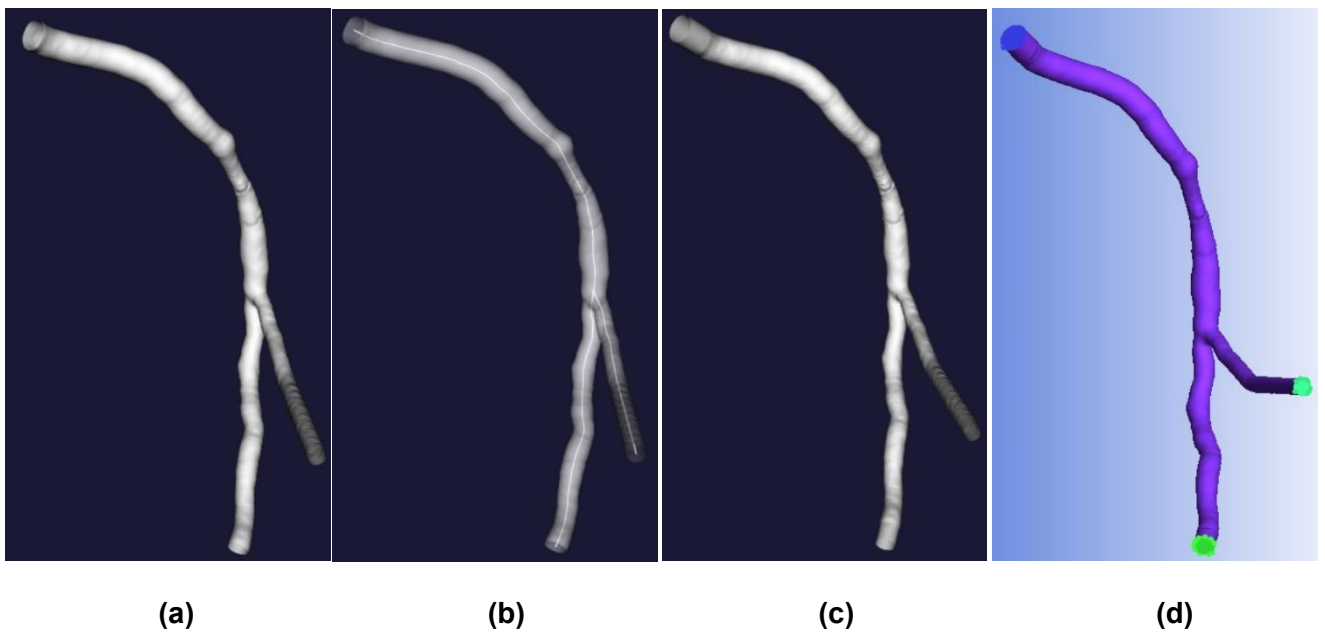


**Figure 4.12** Model: 50%,  $L = 25$  mm

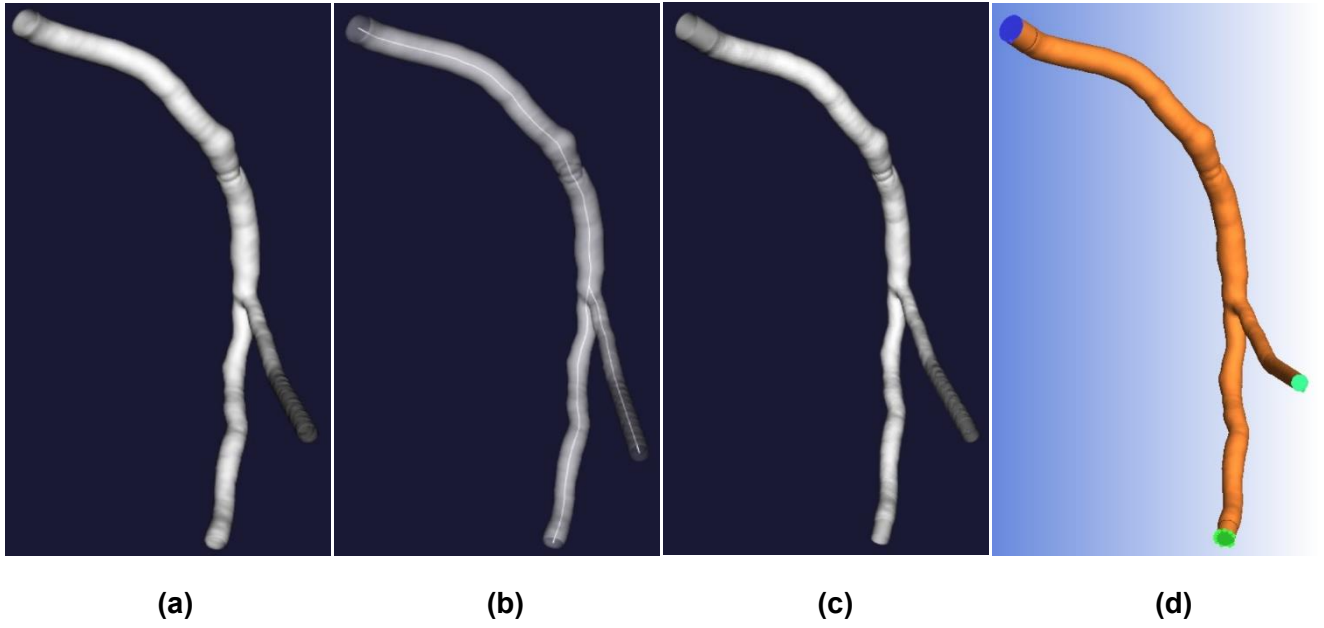


**Figure 4.13** Model: 75%,  $L = 3 \text{ mm}$

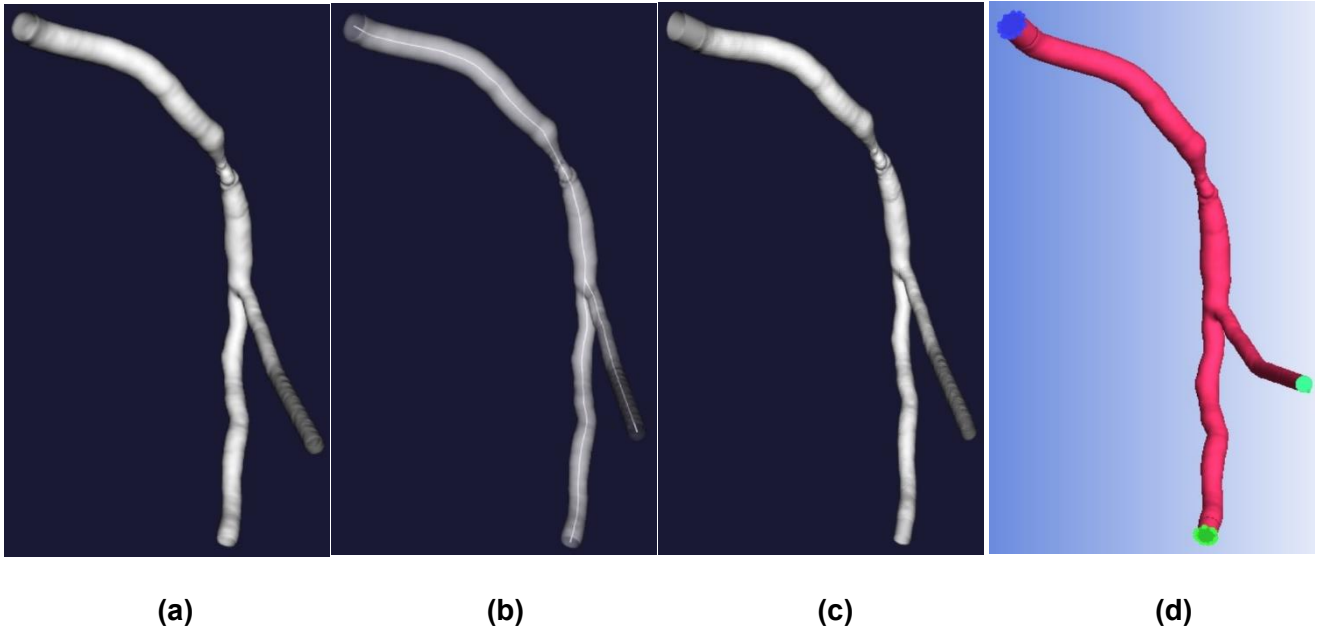


**Figure 4.14** Model: 75%,  $L = 15 \text{ mm}$

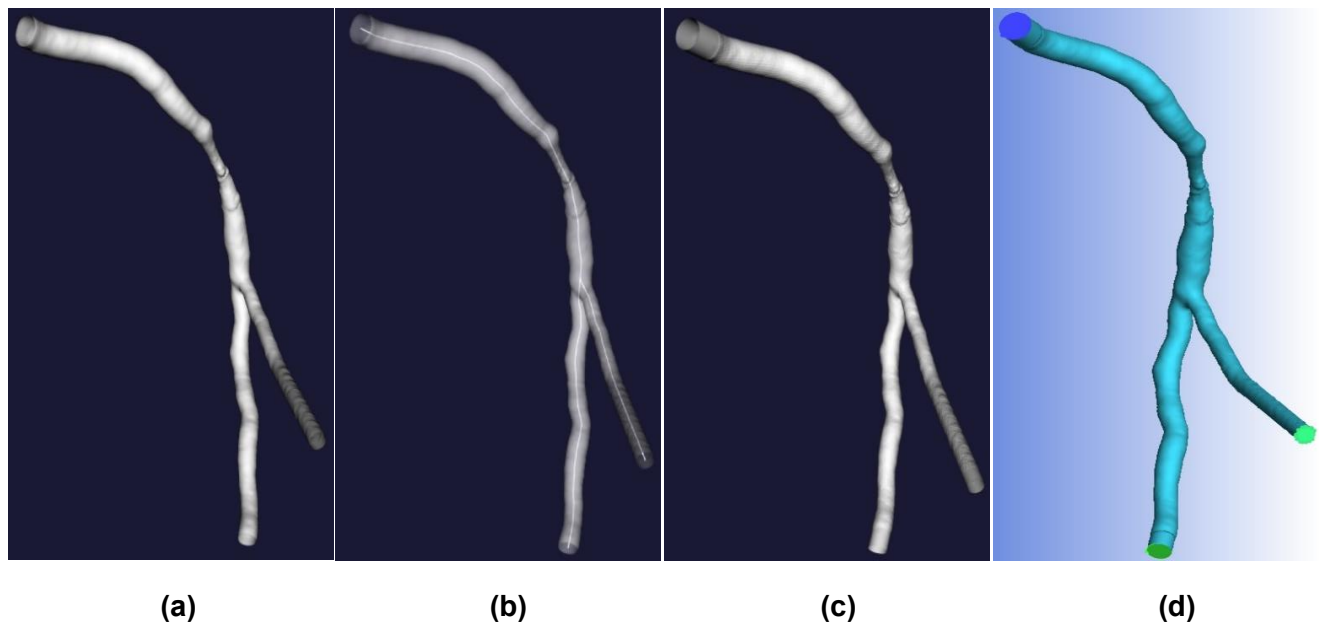


**Figure 4.15** Model: 75%, L = 25 mm

Then, the geometrical characteristics of the models were calculated through VMTK®, necessary to determine the setting parameters for the successive simulations. The values of diameters and areas at inlet, outlets and in correspondence of the stenotic sites are shown in the table below (Table 4.1):

	<b>Diameter [m]</b>	<b>Area [m<sup>2</sup>]</b>
<b>Inlet</b>	$2.76 \cdot 10^{-3}$	$5.98 \cdot 10^{-6}$
<b>Outlet distal LCX</b>	$2.04 \cdot 10^{-3}$	$3.26 \cdot 10^{-6}$
<b>Outlet marginal artery</b>	$1.63 \cdot 10^{-3}$	$2.09 \cdot 10^{-6}$
<b>30% stenosis</b>	$2.10 \cdot 10^{-3}$	$3.46 \cdot 10^{-6}$
<b>50% stenosis</b>	$1.50 \cdot 10^{-3}$	$1.77 \cdot 10^{-6}$
<b>75% stenosis</b>	$0.75 \cdot 10^{-3}$	$0.44 \cdot 10^{-6}$

**Table 4.1** Geometric parameters of the models

### 4.3 Sensitivity Analysis

The sensitivity analysis is necessary to decide which is the most appropriate mesh that must be used for the CFD simulations. For this purpose, two aspects must be considered:

- 1) Finding which number of elements is needed to obtain a spatial resolution that makes any result independent from the number of the elements of the mesh.
- 2) Ensuring a reasonable computational time.

When the number of elements decreases, there is a reduction of computational time and cost, whereas when the number of elements increase there is a growth of accuracy. For these reasons it is important to find a mesh that guarantees a compromise between a good accuracy and a good computational time.

This analysis was performed on the most important stenotic model, that is the one characterized by a 75% degree of occlusion and the greatest extension ( $L = 25$ ).

In this model, three different tetrahedral meshes were created with ANSYS ICEM®, importing the geometry as an STL file. Each one was created using the Robust (Octree) method and curvature refinement, useful to improve the mesh quality. The three meshes were generated by varying the global element size and the surface meshing parameters, in order to create a spatial grid increasingly denser.

In the table below, the three meshes created and their quality parameters are shown (Table 4.2):

Mesh	Total number of elements	Minimum quality value	Maximum quality value
$4 \cdot 10^6$	4'604'182	0.268773	0.999982
$6 \cdot 10^6$	6'736'129	0.249951	0.999982
$10 \cdot 10^6$	10'677'525	0.232293	0.999945

**Table 4.2** Mesh details

As quality parameter, the “EquiAngle Skewness” was calculated, which is an index of cells angles symmetry, to evaluate the distortion degree of tetrahedron. This parameter ranges from 0 to 1, where 0 is the worst element (most distorted) and 1 is the best. Minimum values lower than 0.15 indicate low mesh quality.

To understand which one of the three meshes was more appropriate, their performances were compared making a comparison between their respective WSS and pressure data, extracted after performed a steady state simulation for each mesh. These simulations

were performed using an inflow value of 60 ml/min, which is the mean inflow for the left circumflex artery at rest condition. This value was found by Pietrabissa et al. [67] in their computational study based on lumped parameter models, in which it was observed what was the inflow trend for the main branches of the coronary tree, in case of stenosis in the left anterior descendent artery (LAD). As it can be seen in the figure below, from zero degree of occlusion up to 75% of narrowing in the LAD, the inflow value for the LCX is 60 ml/min (Figure 4.16).

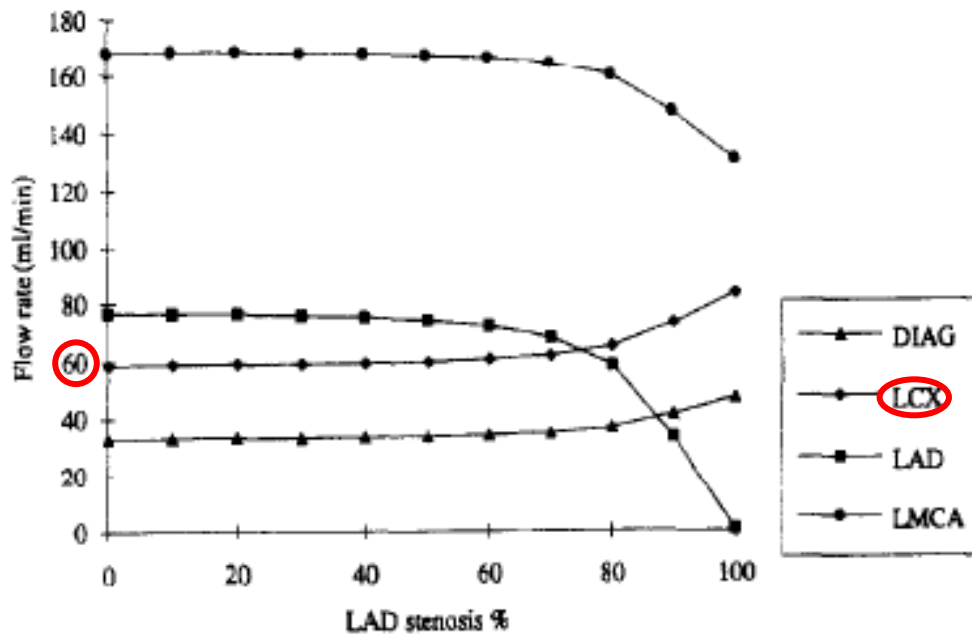


**Figure 4.16** Blood flow rate in the main branches of the coronary tree [67]

DIAG: diagonal; LCX: left circumflex; LAD: left anterior descending; LMCA: left main coronary artery.

To establish the regime of flow in the stenotic models during simulations, the Reynolds numbers (Re) were calculated.

The Reynolds number is a dimensionless quantity which is useful to determine if flow is laminar or turbulent: if it is higher than a critical Reynolds number, the flow is turbulent, if it is lower, the flow is laminar. The critical value changes according to the kind of geometry, and for flows in rough pipe the values which discriminate the flow regime are:

- Laminar regime if  $Re < 1000$
- Turbulent regime if  $Re > 2000$
- Transition regime if  $1000 < Re < 2000$

In general, the Reynolds number is defined by the following formula:

$$Re = \frac{\rho_b v d}{\mu_b}$$

Where:

- $\rho_b$  is the blood density.
- $\mu_b$  is the blood viscosity.
- $d$  is the diameter of the vessel in which the Reynolds number is calculated.
- $v$  is the mean blood velocity throughout the vessel and it can be expressed as the ratio between the mean incoming flow ( $Q$ ) and the inlet area ( $A$ ):  $v = \frac{Q}{A} = \frac{4Q}{\pi d^2}$

Since these parameters were known, Reynolds numbers were calculated at rest condition both for the non-stenotic model and in correspondence of the 3 stenotic diameters, to see if these three degrees of stenosis may promote a laminar flow or cause a turbulent flow. The values obtained are reported in the following table (Table 4.3):

<b>Q<sub>rest</sub> = 60 ml/min</b>				
	<b>Non-stenotic model</b>	<b>30% stenosis</b>	<b>50% stenosis</b>	<b>75% stenosis</b>
<b>Re</b>	95.45	137.79	192.90	385.81

**Table 4.3** Reynolds numbers at rest condition

In this condition of flow, all stenotic models are characterized by a Reynolds number lower than 1000, meaning that blood flow at rest condition promotes a regime of laminar motion.

Therefore, the set parameters defined for the three simulations are the following ones:

- Flow type: laminar
- Blood characteristics: Newtonian fluid behaviour with a density of 1060 Kg/m<sup>3</sup> and viscosity of 0.0035 Pa·s.

Density value is obtained considering a plasma density ( $\rho_b$ ) of 1035 kg/m<sup>3</sup>, a corpuscular density ( $\rho_{gr}$ ) of 1090 Kg/m<sup>3</sup> and a haematocrit value of 45%.

Viscosity value was supposed to be 0.0035 Pa·s, obtained for a plasma viscosity ( $\mu_p$ ) of 0.00165 Pa·s

- Boundary conditions:
  - Inlet condition: velocity = 0.167 m/s, obtained for a mean flow Q = 60 ml/min
  - LCX and marginal outlets conditions: pressure = 0

After performed the three steady simulations, WSS and static pressure data were extracted from ANSYS FLUENT®. For both WSS and pressure, average and maximum values were calculated for the three meshes, and the values obtained were reported on bar diagrams. Then, the absolute value of the percentage differences with respect to the greatest mesh were calculated and plotted, so that it would be easier to compare the values and decide which mesh would be more appropriate. Their trends are reported in the following graphs (Figure 4.17 to 4.20).

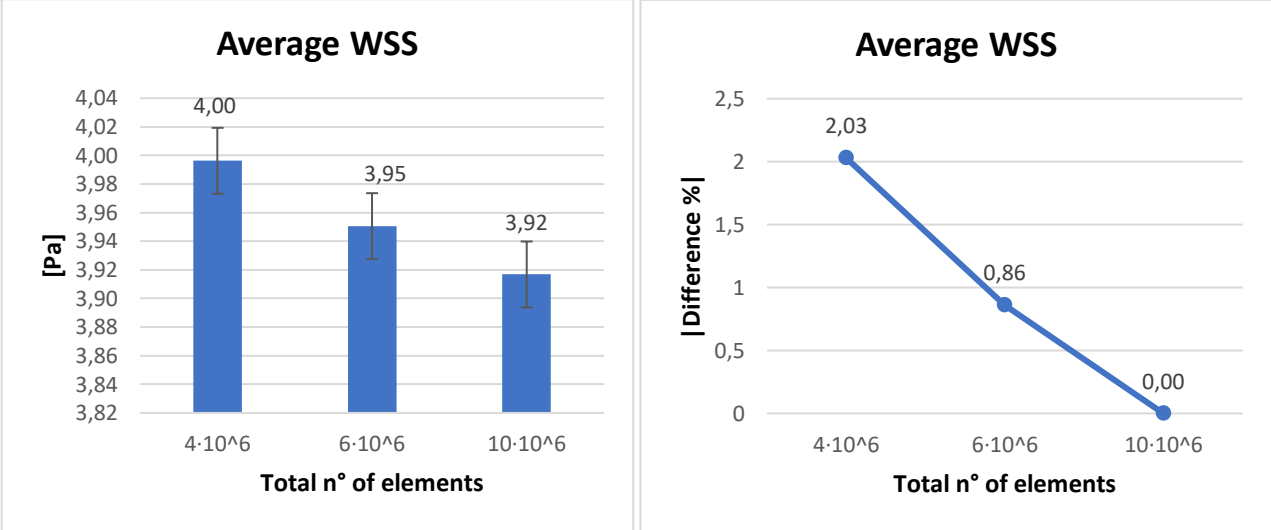


Figure 4.17 Average WSS

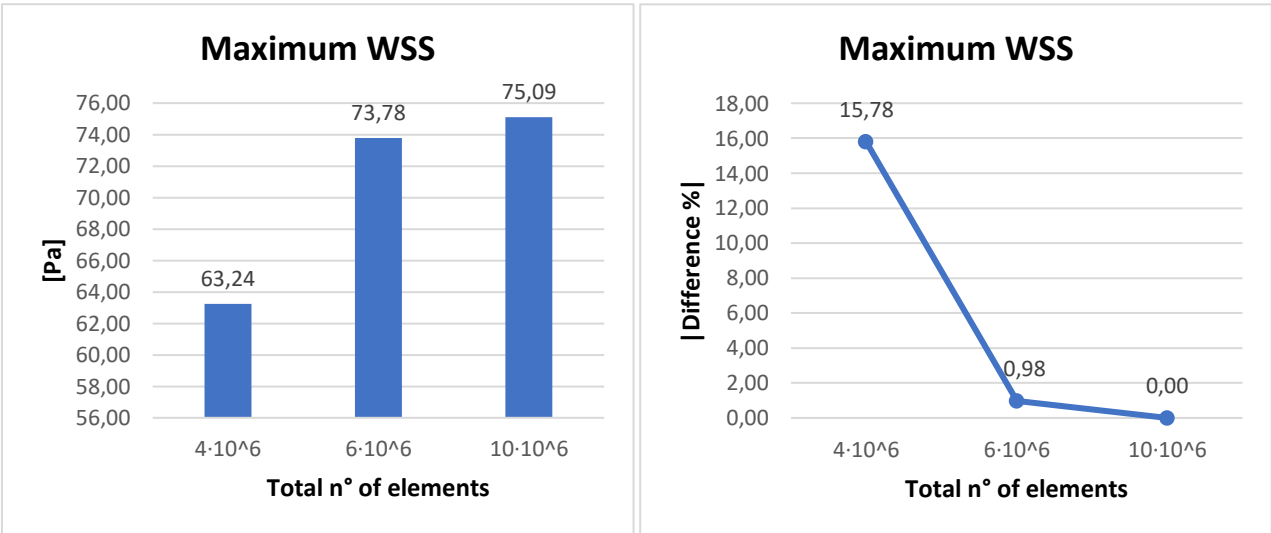
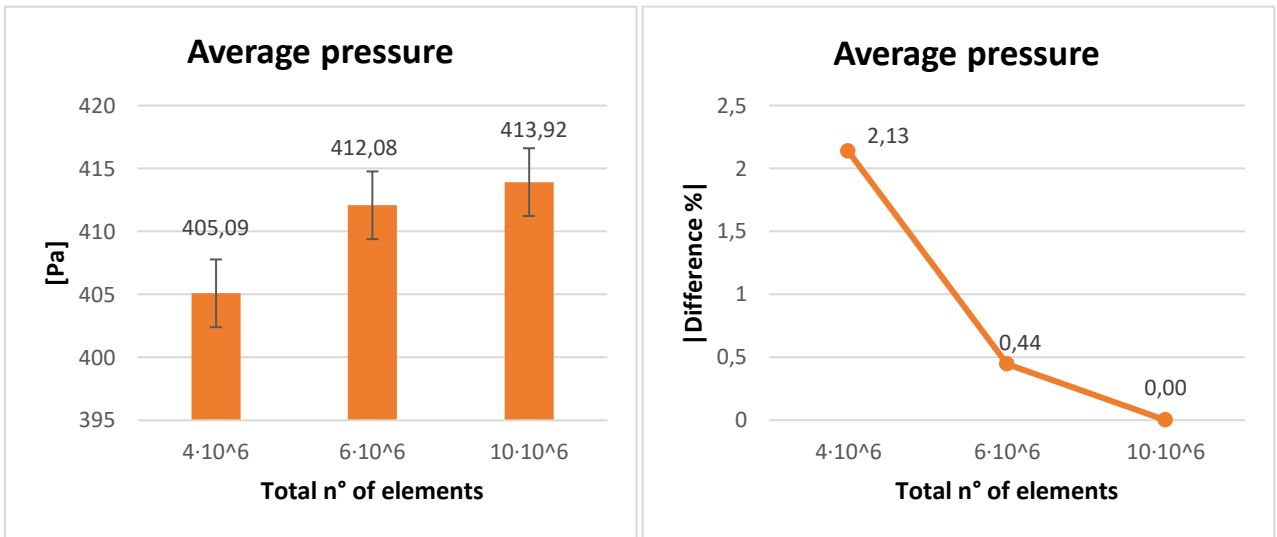
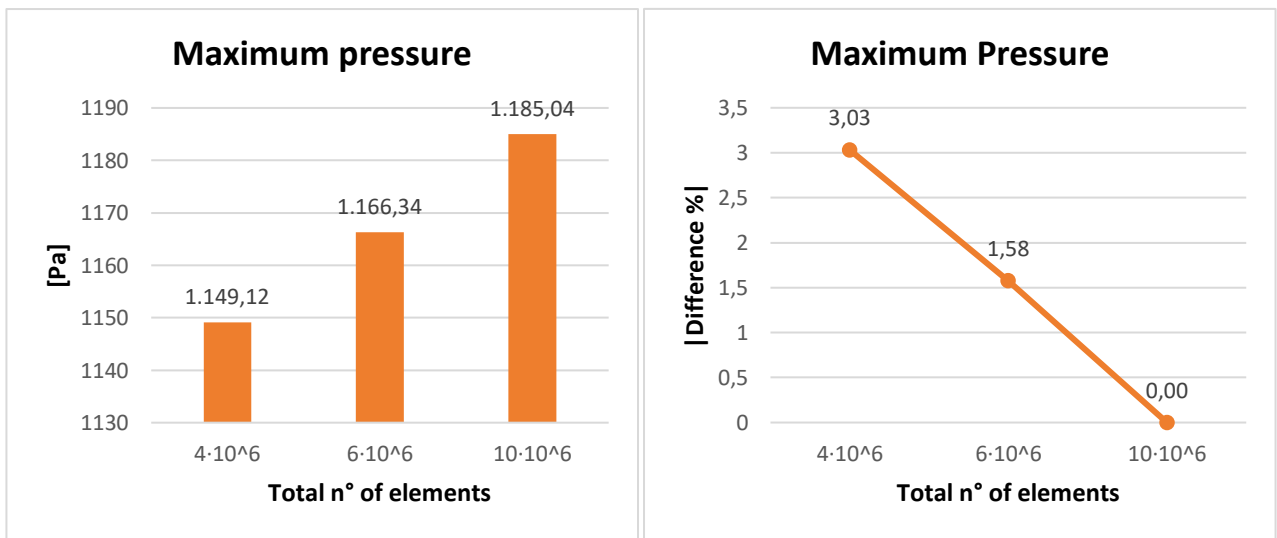


Figure 4.18 Maximum WSS



**Figure 4.19** Average pressure



**Figure 4.20** Maximum pressure

The mesh which defines the necessary spatial resolution is the one whose percentage differences from the mesh with the highest number of elements are negligible.

According to the results, the maximum WSS and the average pressure show that the mesh with  $6 \cdot 10^6$  elements is the one with the smallest percentage difference compared to the one with  $10 \cdot 10^6$  elements: in fact, the absolute values of the percentage differences are respectively 0.98 and 0.44, indicating that the mesh with  $6 \cdot 10^6$  elements should be the most appropriate. Instead, as regards the average WSS and the maximum pressure, percentage differences of the mesh with  $4 \cdot 10^6$  and  $6 \cdot 10^6$  of elements compared to the one with  $10 \cdot 10^6$  do not allow to decide which mesh is more appropriate for this application.

To have a greater certainty in the choice of the mesh, it was decided to focus the sensitivity analysis only on the stenosis area. To do this, the model was clipped upstream and downstream of the stenosis, in order to isolate the stenosis from the rest of the model (Figure 4.21).

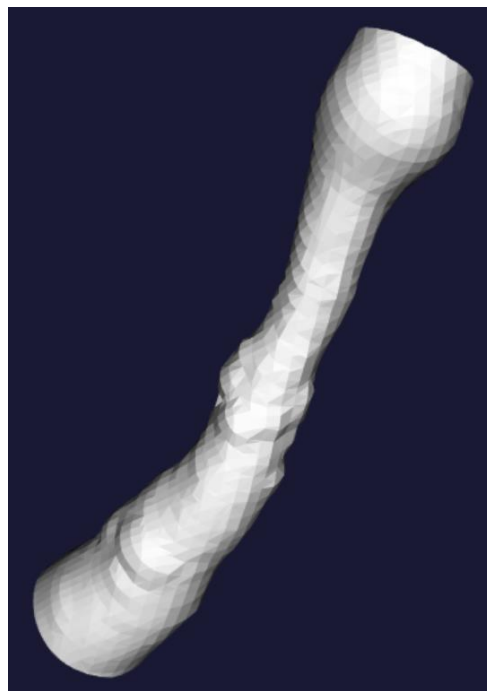


**Figure 4.21** *Clipped model to isolate the stenosis*

Then, the same procedure was repeated on the isolated stenosis and the related graphs were analysed (Figure 4.22 to 4.25).

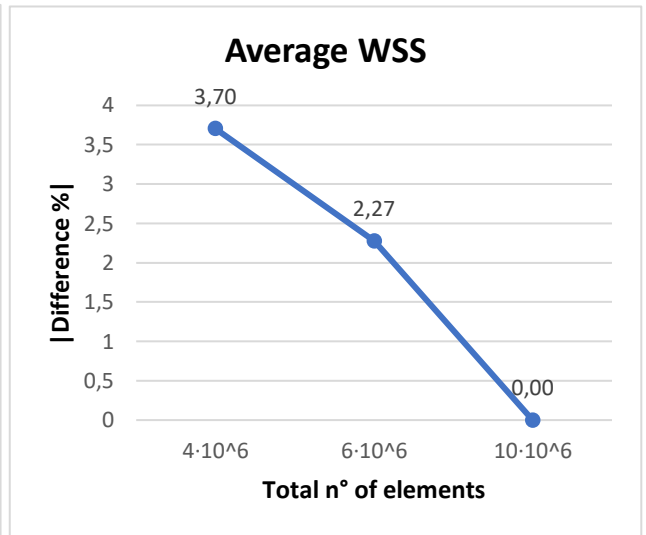
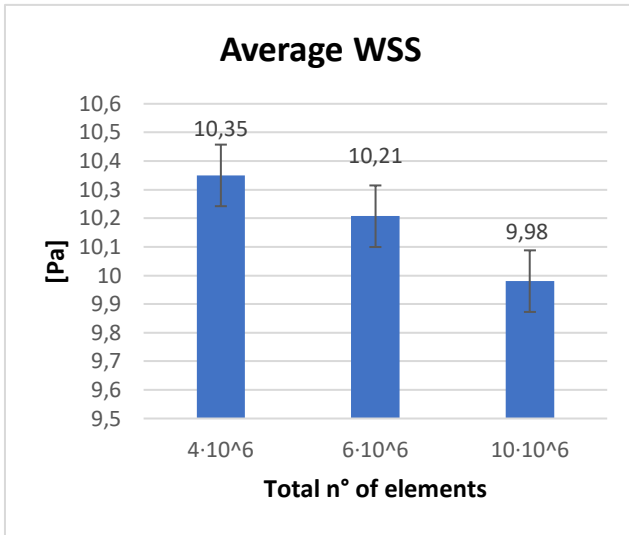


Figure 4.22 Average WSS on the stenosis

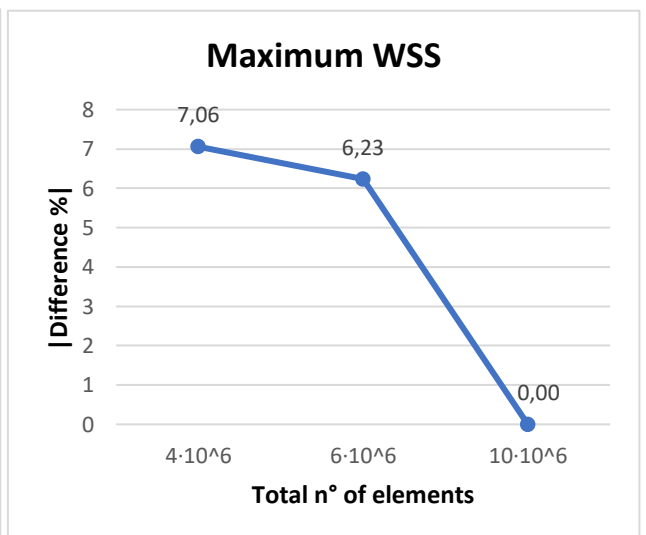
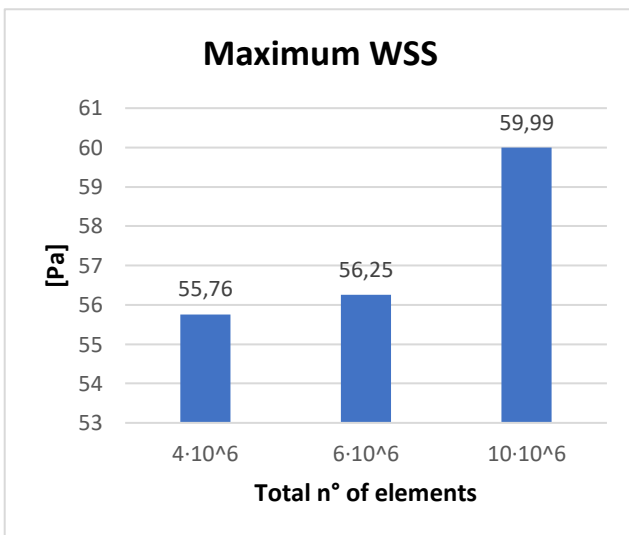
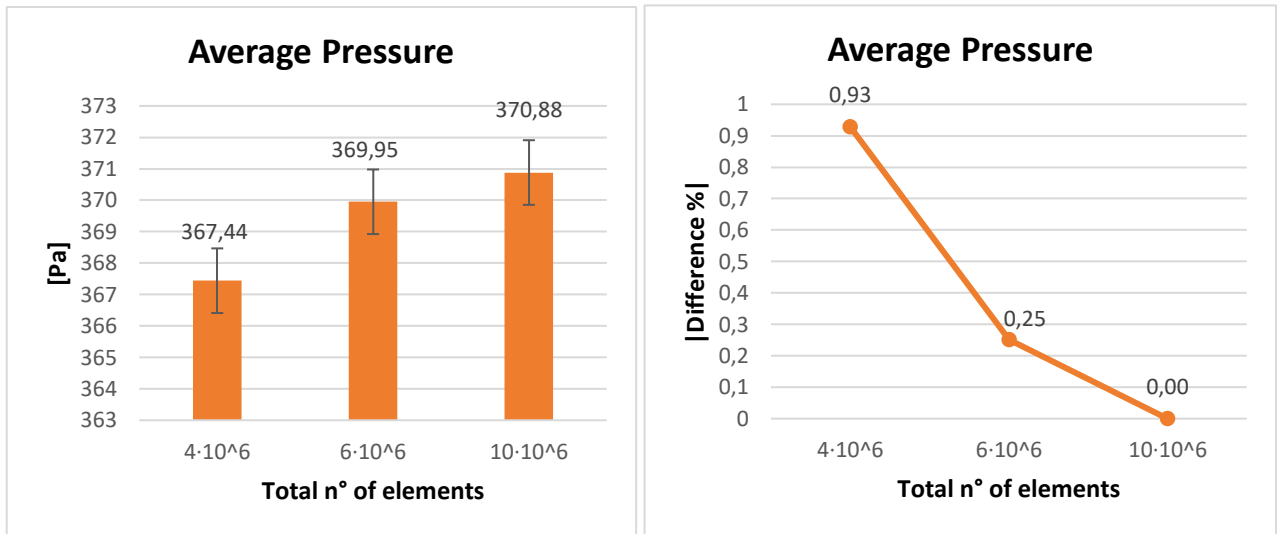
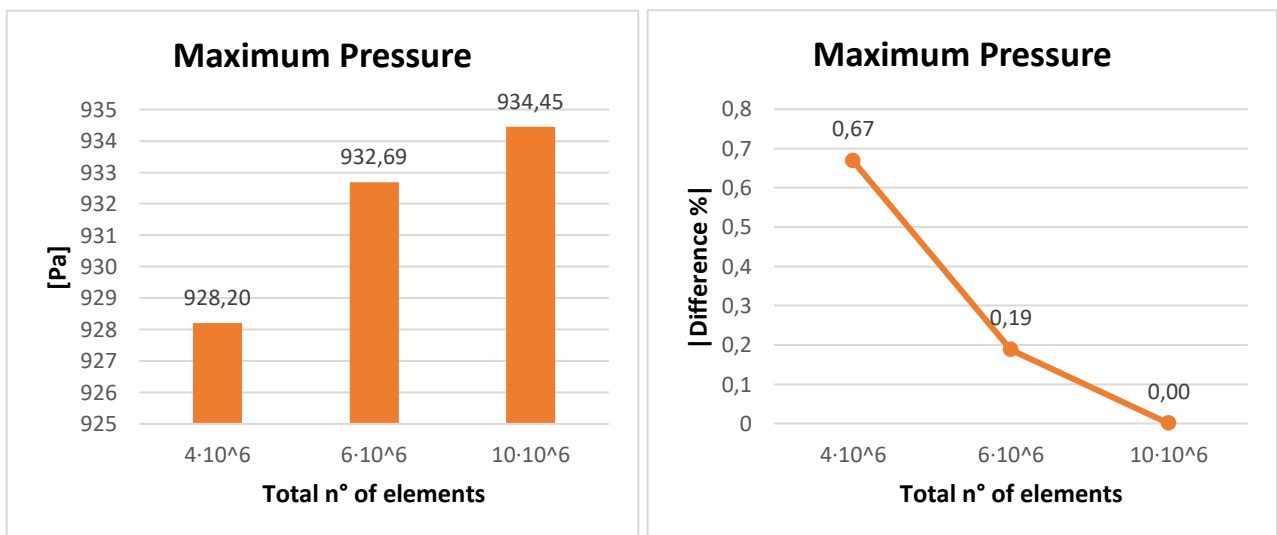


Figure 4.23 Maximum WSS on the stenosis



*Figure 4.24 Average pressure on the stenosis*



*Figure 4.25 Maximum pressure on the stenosis*

According to the results, the average and maximum WSS do not give useful information because the two meshes with  $4 \cdot 10^6$  and  $6 \cdot 10^6$  show high percentage differences compared with the mesh with  $10 \cdot 10^6$  elements. In reverse, both pressure graphs show negligible percentage differences between the mesh with  $6 \cdot 10^6$  elements and  $10 \cdot 10^6$  elements, meaning that the one with  $6 \cdot 10^6$  elements should be the most appropriate: in fact, the absolute value of percentage differences are 0.25 and 0.19 for the average and maximum pressure respectively.

Considering that the final aim of this thesis is the computation of FFR, which is an index given from the ratio between two values of pressure, it has been decided to give more importance to pressure data than to WSS data, to decide which mesh defines the necessary spatial resolution. For this reason, the mesh with  $6 \cdot 10^6$  elements was chosen as the most suitable for this fluid dynamic application (Figure 4.26). Moreover, this mesh guarantees a good compromise between accuracy and computational time.

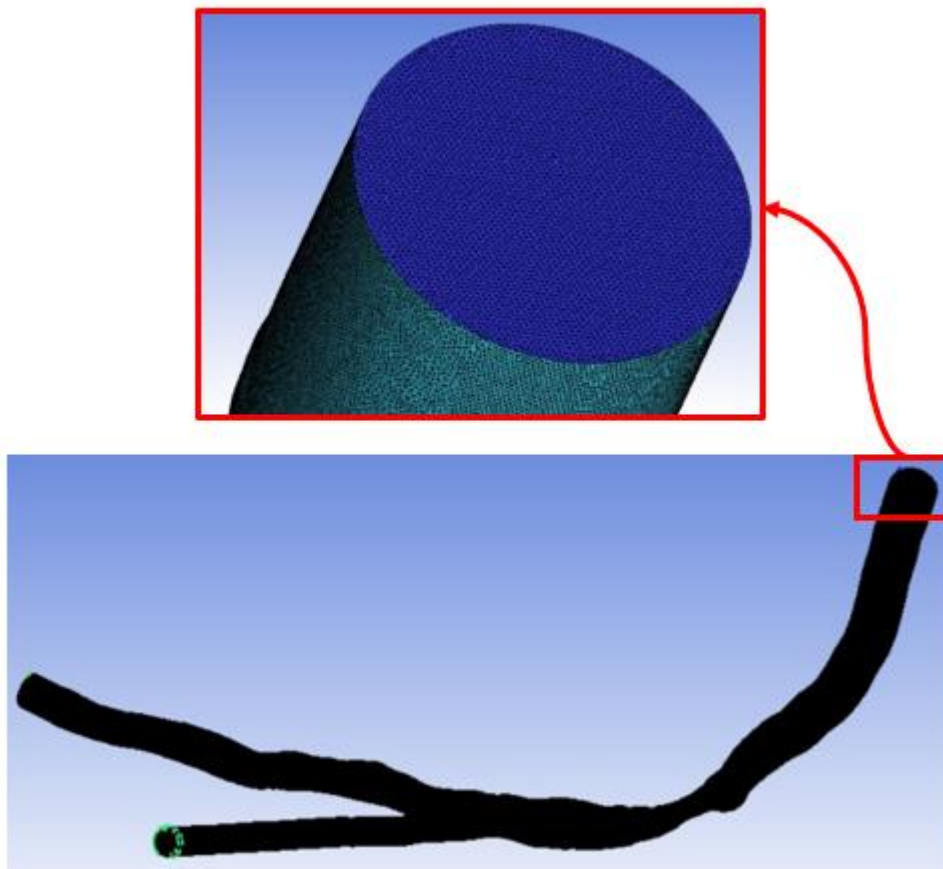


**Figure 4.26** Mesh  $6 \cdot 10^6$  elements with inlet details above

The global and surface setting parameters used to create this  $6 \cdot 10^6$  elements mesh in the model analysed, were used to create meshes in all the other models.

## 4.4 CFD simulations

After models' discretization, the fluid domains were studied under steady flow conditions, using two values of mean flow to simulate two different conditions: rest and hyperemia. As already mentioned above, the mean inflow value at rest for the left circumflex coronary artery is 60 ml/min [67], while at hyperemia it increases by approximately 3.5 times [53,62]. The rest flow regime has already been established to be laminar, while to define the regime at hyperemia the Reynolds number was calculated again. The values obtained for the non-stenotic model and in correspondence of the 3 stenotic diameters are reported in the following table (Table 4.4):

	$Q_{\text{hyperemia}} = 3.5 Q_{\text{rest}}$			
	Non-stenotic model	30% stenosis	50% stenosis	75% stenosis
Re	334.08	482.27	675.15	1350.33

**Table 4.4** Reynolds numbers at hyperemic condition

At hyperemia models with 30% and 50% of occlusion are characterized by a Reynolds number lower than 1000, so they promote a laminar flow, while model with 75% of reduction in diameter shows a Reynolds number of 1350.33, which is higher than the laminar critical value. Thus, the condition of motion in this case should be part of the transition regime but, considering that this value does not exceed the threshold excessively, in the following simulations it has been assumed a laminar flow even for this model.

Thus, to perform CFD simulations the regime of flow used is laminar in both conditions of flow, blood characteristics are the same used for the steady simulations performed during sensitivity analysis, while the boundary conditions are the following:

- Inlet condition at rest -> velocity = 0.167 m/s, obtained for  $Q_{\text{rest}} = 60$  ml/min
- Inlet condition at hyperemia -> velocity = 0.585 m/s, obtained for  $Q_{\text{hyperemia}} = 3.5 Q_{\text{rest}}$
- The outlets conditions both at rest and at hyperemia were defined as the flow rates outgoing from the two branches of the bifurcation. These values were derived from the following equation [68] (Figure 4.27):

$$\frac{Q_{\text{marg}}}{Q_{\text{LCX}}} = \left( \frac{d_{\text{out marg}}}{d_{\text{out LCX}}} \right)^{2.27}$$

This equation indicates that the ratio between the flow values outgoing from the marginal and the distal LCX branches is equal to the ratio of their outlet diameters, with exponent 2.27.

Solving this equation, the results obtained are:

- Outflow from the distal LCX outlet = 62.5% of the inflow value
- Outflow from the marginal outlet = 37.5% of the inflow value

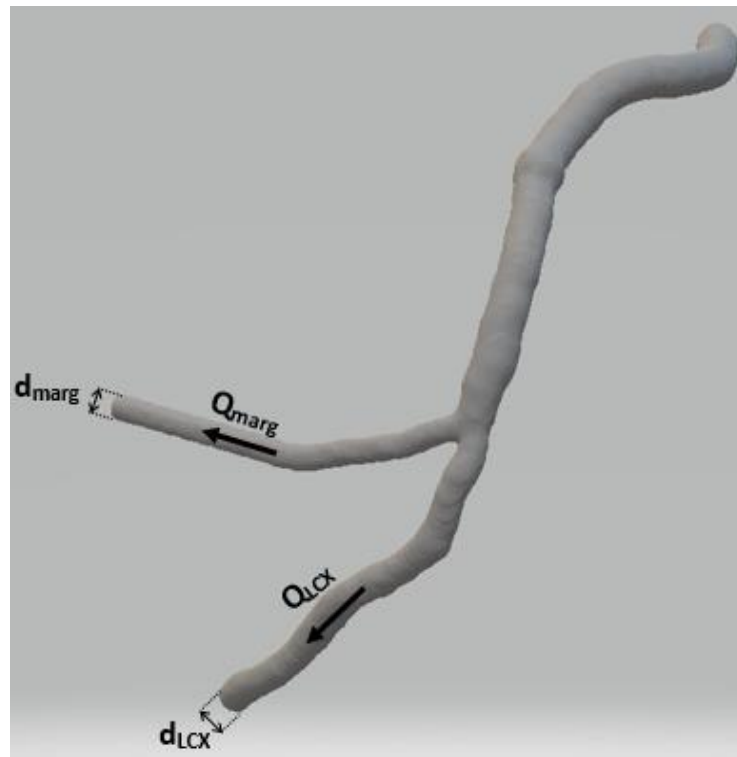


**Figure 4.27** Reference image for outflow rates calculation

## 4.5 Post-processing

Once performed the simulations on all the models, the post-processing phase was based on the computation of FFR index.

To do this, a custom function was created on ANSYS FLUENT®, which allows to visualize the value of this index at any point of the vessel. This function was obtained in two steps:

- 1) The static pressure ( $P_{static}$ ) of the vessel was added to the ostium pressure ( $P_{ostium}$ ) calculated relatively to the mean aortic pressure ( $P_a$ ), obtaining all pressure values along the vessel relative to the mean aortic pressure:

$$P_{relative} = P_{static} + (P_a - P_{ostium})$$

- 2) the function to visualize the distribution of FFR values was obtained by the ratio between the relative pressure of the vessel and the mean aortic pressure:

$$FFR = \frac{P_{relative}}{P_a}$$

The mean aortic pressure is given by the following relationship:

$$P_{aortic} = \frac{1}{3} P_{systolic} + \frac{2}{3} P_{diastolic}$$

For systolic ( $P_{systolic}$ ) and diastolic ( $P_{diastolic}$ ) pressure, the reference values of 120 mmHg and 80 mmHg were chosen respectively, obtaining a mean aortic pressure of 93.3 mmHg. This value was used for both conditions of flow. In fact, considering that hyperemia acts mostly by lowering the capillary resistance through vasodilating mechanisms, it can be assumed that the variation in aortic pressure is negligible compared to rest condition.

# CHAPTER 5

## RESULTS AND DISCUSSION

In this section results from post-processing data of the steady simulations are reported. For all the stenotic models, WSS distribution and the static pressure gradient along the vessel, calculated with respect to inlet pressure, were analysed at rest and hyperemia; then Fractional Flow Reserve values were computed in the two conditions of flow. The values obtained were compared in the two cases to understand the relationship between stenoses geometric features and the pressure drop they caused, relatively to the mean aortic pressure, in the two conditions of flow.

### **5.1 WSS and static pressure gradient at rest and hyperemia**

The distribution of WSS and of the absolute value of static pressure gradient in all stenotic models are reported in the following figures (Figure 5.1 to 5.4).

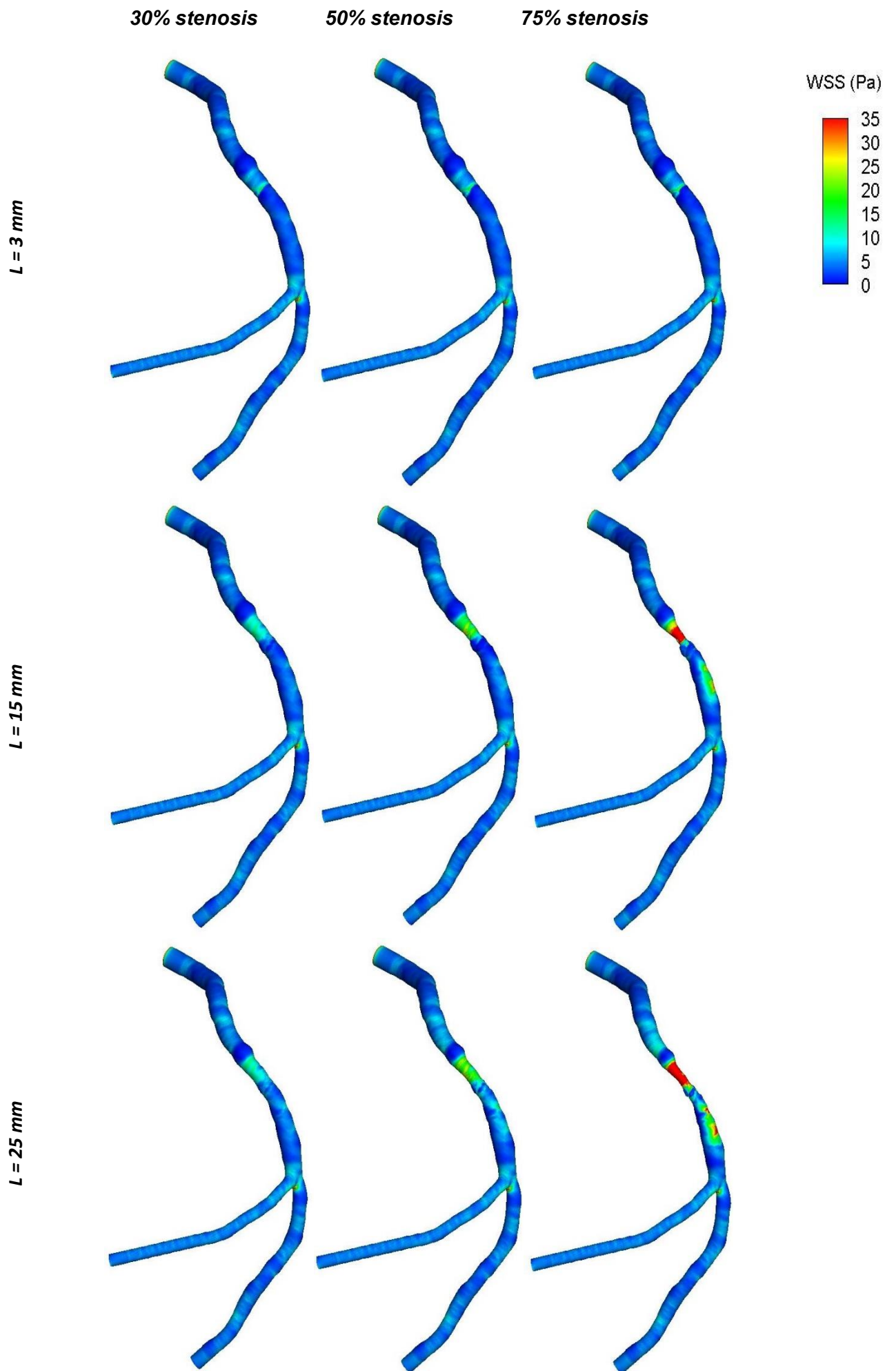
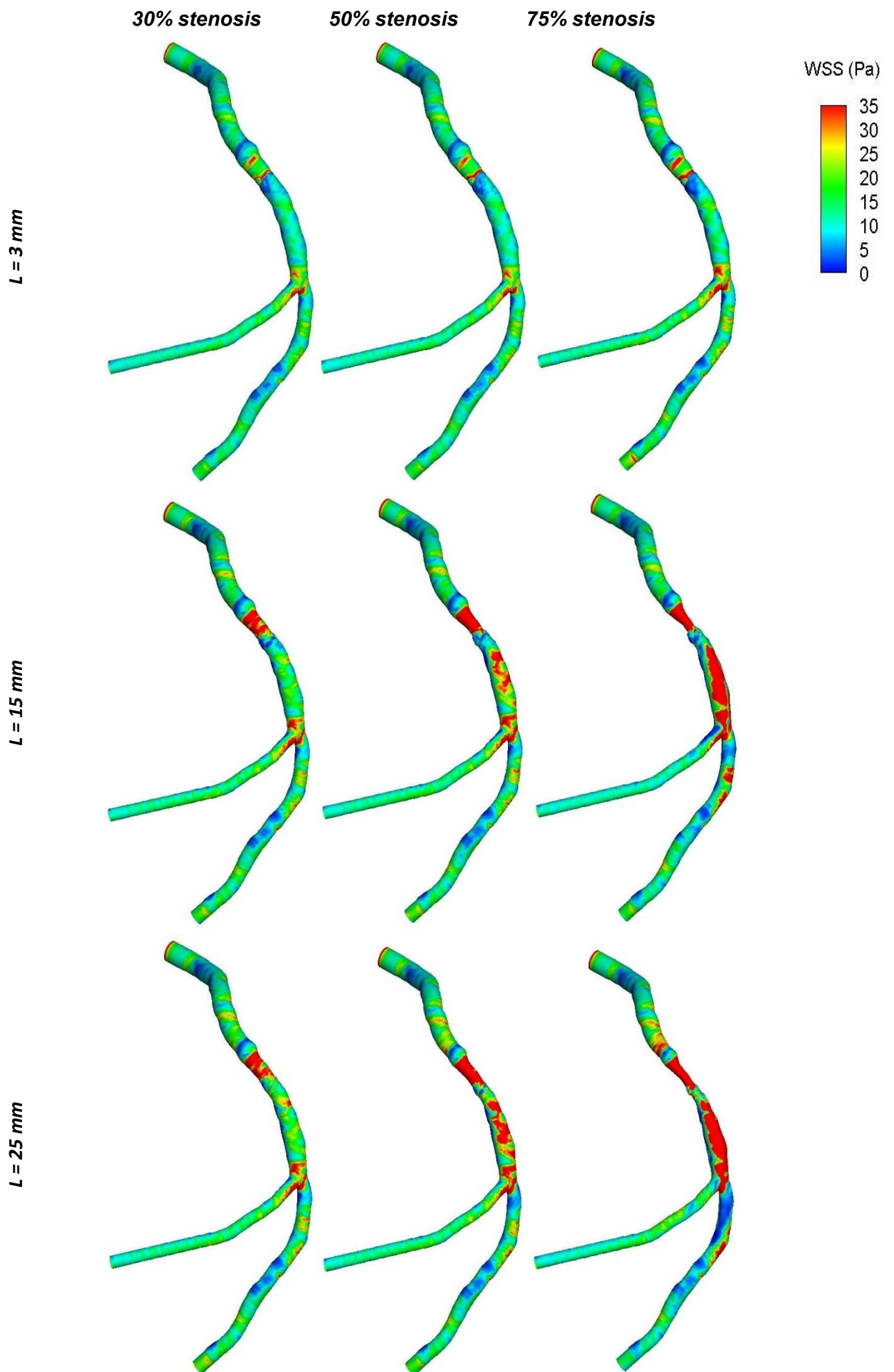


Figure 5.1 WSS at rest



**Figure 5.2** WSS at hyperemia

As it can be seen from the figures, both at rest and hyperemia, the highest values of WSS in all models are found in correspondence of the stenosis and the bifurcation because, due to their morphology, they are subject to a greater impact by blood flow.

As regards the stenotic sites, WSS grows as the percentage of occlusion and stenosis extension increase in both conditions of flow, but at hyperemia WSS values are higher than at rest because the flow is greater and the wall result much more stressed.

The average values of WSS in the stenosis of all models at rest and hyperemia are reported in the following table (Table 5.1):

<b>Model</b>	<b>WSS<sub>mean</sub> at rest [Pa]</b>	<b>WSS<sub>mean</sub> at hyperemia [Pa]</b>
<b>30%, L = 3 mm</b>	2.54	14.07
<b>50%, L = 3 mm</b>	2.59	14.14
<b>75%, L = 3 mm</b>	2.76	15.59
<b>30%, L = 15 mm</b>	2.73	15.79
<b>50%, L = 15 mm</b>	3.61	22.37
<b>75%, L = 15 mm</b>	7.99	49.57
<b>30%, L = 25 mm</b>	2.97	16.79
<b>50%, L = 25 mm</b>	4.52	26.49
<b>75%, L = 25 mm</b>	10.22	62.61

**Table 5.1** Mean WSS values in stenotic sites

These results show how WSS changes according to the entity of stenosis, in terms of percentage of occlusion and extension, and to the value of blood flow.

The dependence of WSS on these parameters can be expressed through the relationship between WSS, flow and diameter of the vessel <sup>[69]</sup>:

$$WSS = \frac{32 \mu Q}{\pi d^3}$$

where  $\mu$  is fluid viscosity,  $Q$  is flow rate and  $d$  is vessel diameter.

This relationship demonstrates that WSS increase as the value of flow increases and the cube of the vessel diameter decrease. This explains why WSS values are greater at hyperemia and grow as the percentage of occlusion and the extension of lesion increase.

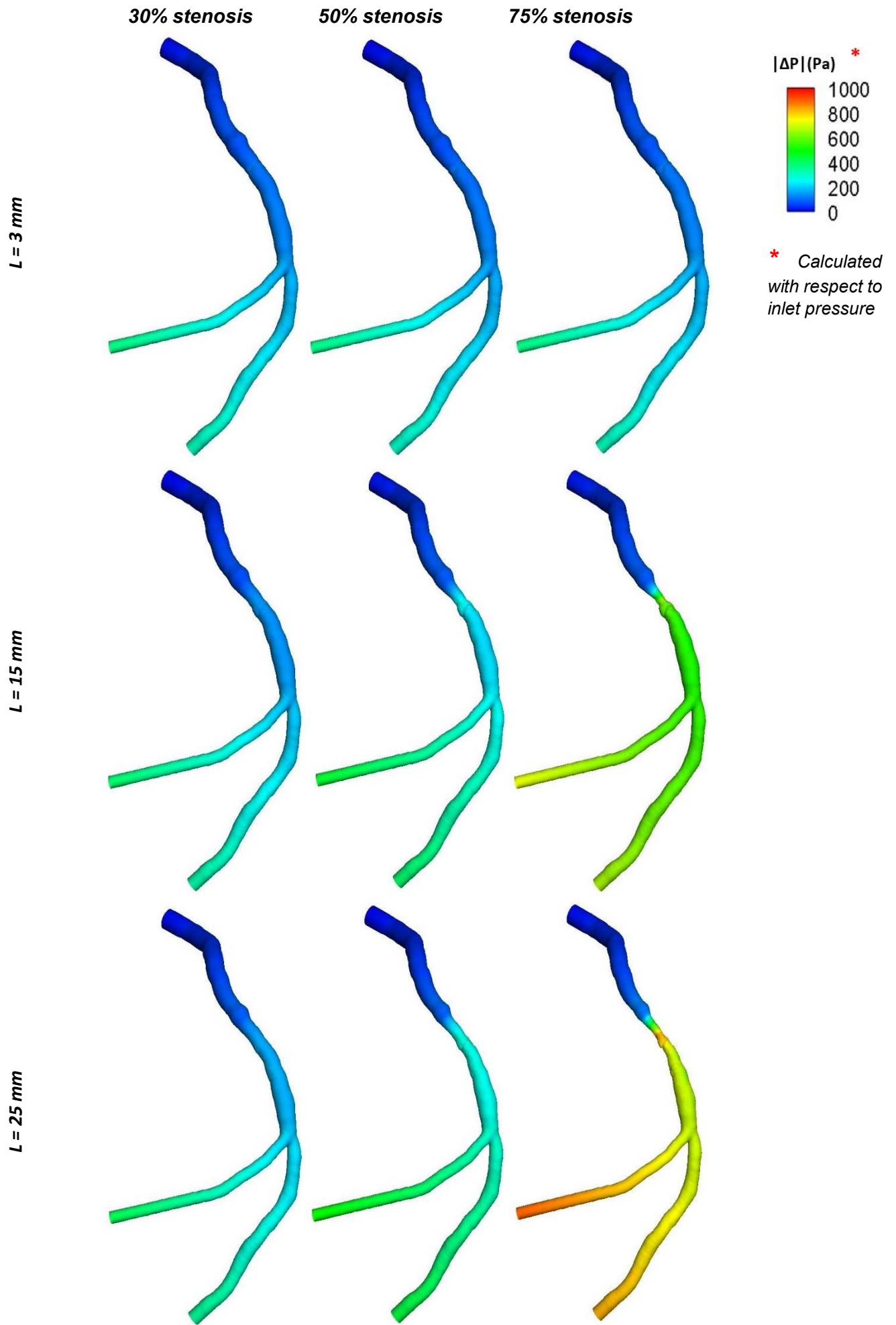


Figure 5.3 Pressure gradient at rest

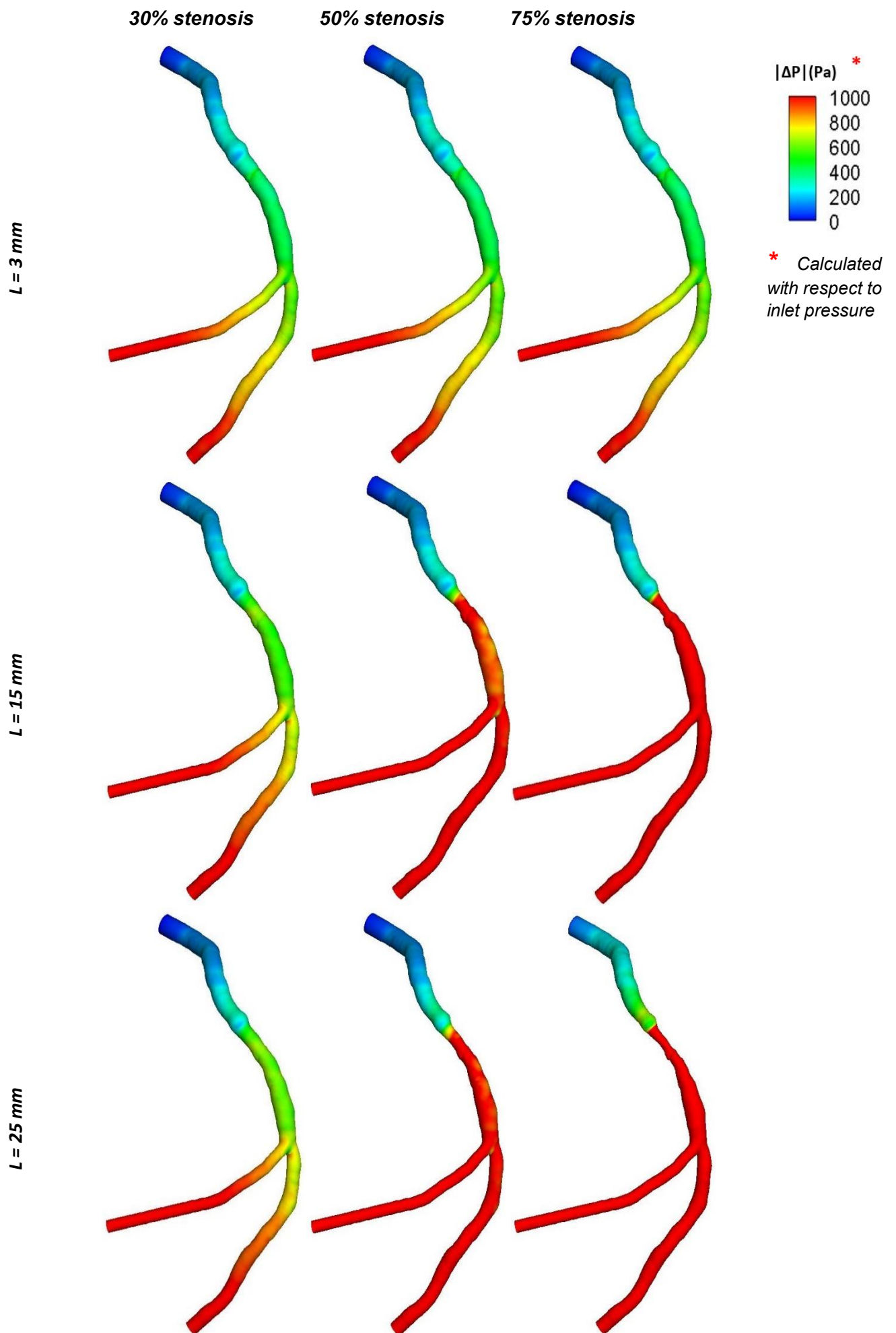


Figure 5.4 Pressure gradient at hyperemia

As it can be seen from the figures, both at rest and at hyperemia, the absolute value of the static pressure gradient, calculated with respect to inlet pressure, increases along the vessel indicating a decrease of pressure values. The decrease of pressure is more evident as the percentage of occlusion and stenosis extension increase in both conditions of flow but results more drastic at hyperemia where the value of flow along the vessel is higher.

This can be explained through Poiseuille relation, which expresses the relationship between the pressure drop ( $\Delta P$ ), flow and the diameter of the vessel [13]:

$$\Delta P = \frac{128 \mu L Q}{\pi d^4}$$

where  $\mu$  is fluid viscosity,  $L$  is the length of the vessel over which the pressure drop takes place,  $Q$  is the flow rate and  $d$  is vessel diameter.

This relationship demonstrates that pressure drop increases as the flow increases and the diameter of the vessel decreases. This explains why the decrease of pressure downstream of the stenosis is much more evident at hyperemia, resulting more drastic as the degree of occlusion and extension of lesion increase.

## **5.2 FFR at rest and hyperemia**

The distribution of FFR values at rest and hyperemia are reported in the following figures (Figure 5.5 and 5.6).

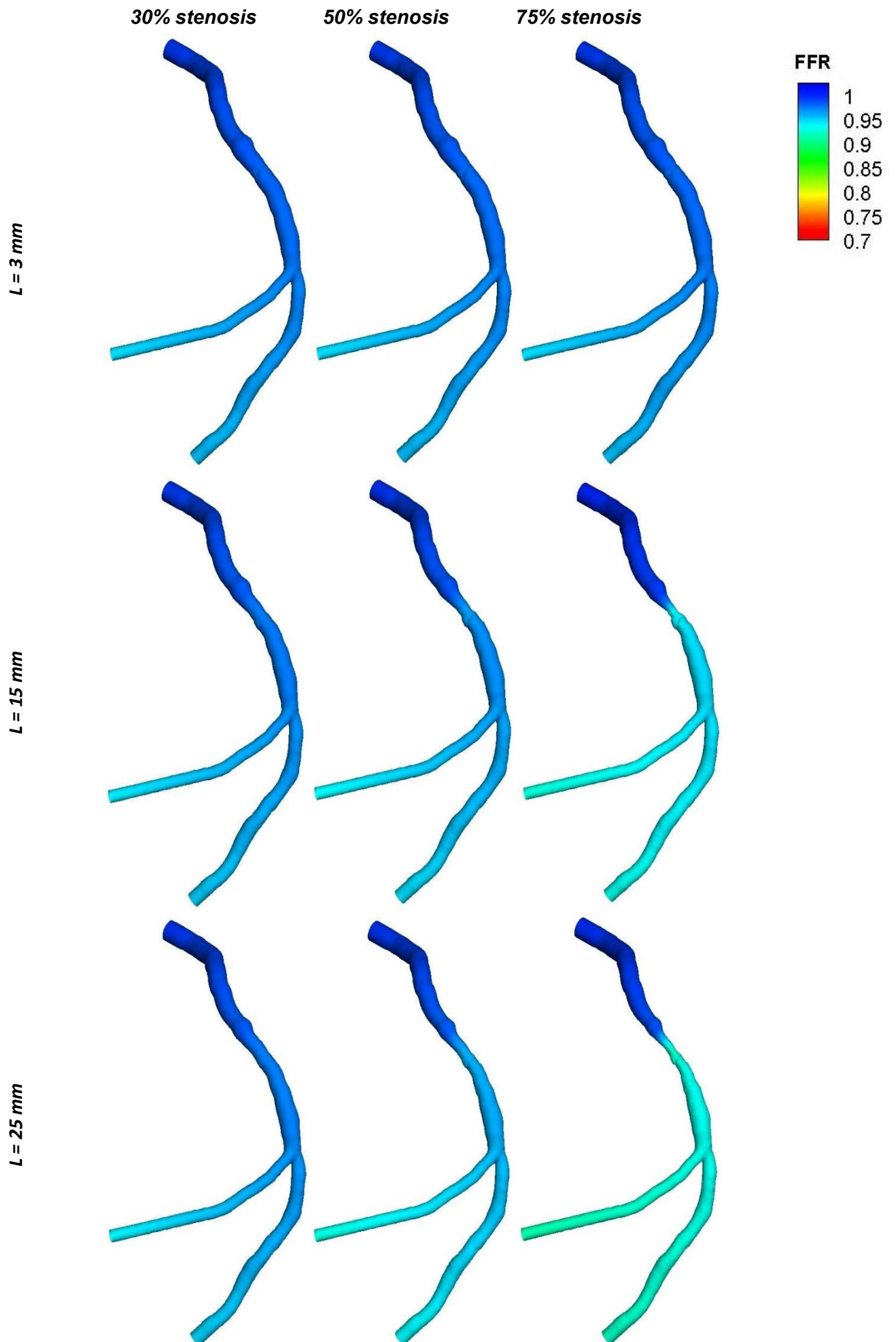
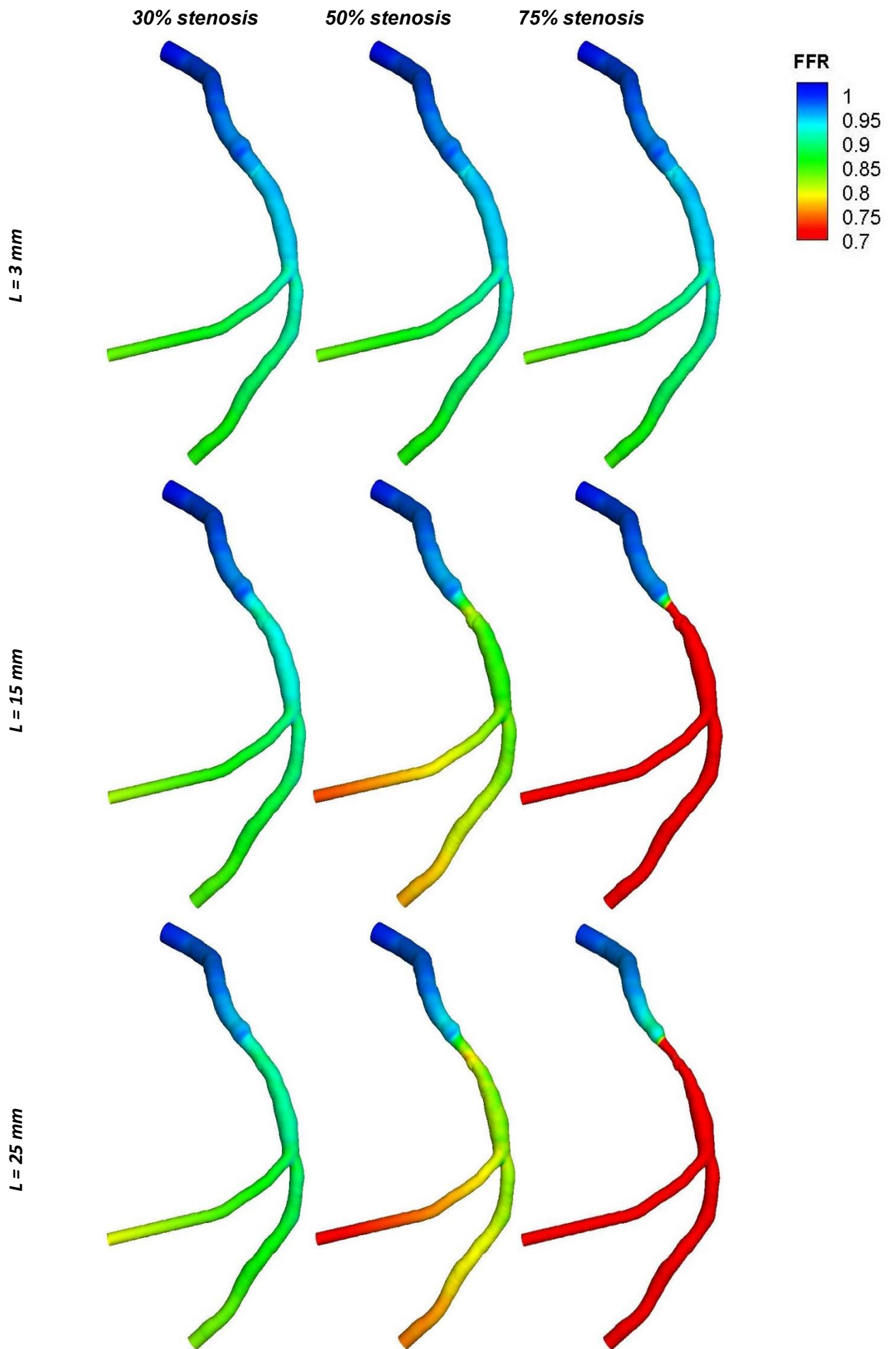


Figure 5.5 FFR at rest



**Figure 5.6** FFR at hyperemia

As it can be seen from the images, in all models the value of FFR is equal to 1 in correspondence of the ostium, then it decreases along the vessels according to stenosis severity.

All models at rest are characterised by high values of this index, which is greater than the cut-off value of 0.8 for all their length. Conversely, among the models at hyperemia, some of them show values greater than 0.8 downstream of the stenosis, while there are in particular two models characterized by values lower than 0.8, that occur starting from the stenotic site. These two models are the ones characterised by 75% of occlusion with a length of 15 mm and 25 mm.

To assess more precisely the severity of each stenotic model at rest and hyperemia, the values that FFR assumes in correspondence of the stenoses were observed and reported in the following table (Table 5.2). The trend of these values, according to the percentage of occlusion and stenosis extension in both conditions of flow, is shown in figure 5.7.

<b>Model</b>	<b>FFR at rest</b>	<b>FFR at hyperemia</b>
<b>30%, L = 3 mm</b>	0.988	0.931
<b>50%, L = 3 mm</b>	0.987	0.933
<b>75%, L = 3 mm</b>	0.987	0.932
<b>30%, L = 15 mm</b>	0.985	0.902
<b>50%, L = 15 mm</b>	0.976	0.825
<b>75%, L = 15 mm</b>	0.924	0.446
<b>30%, L = 25 mm</b>	0.984	0.887
<b>50%, L = 25 mm</b>	0.972	0.782
<b>75%, L = 25 mm</b>	0.905	0.247

*Table 5.2 FFR values in stenotic sites at rest and hyperemia*

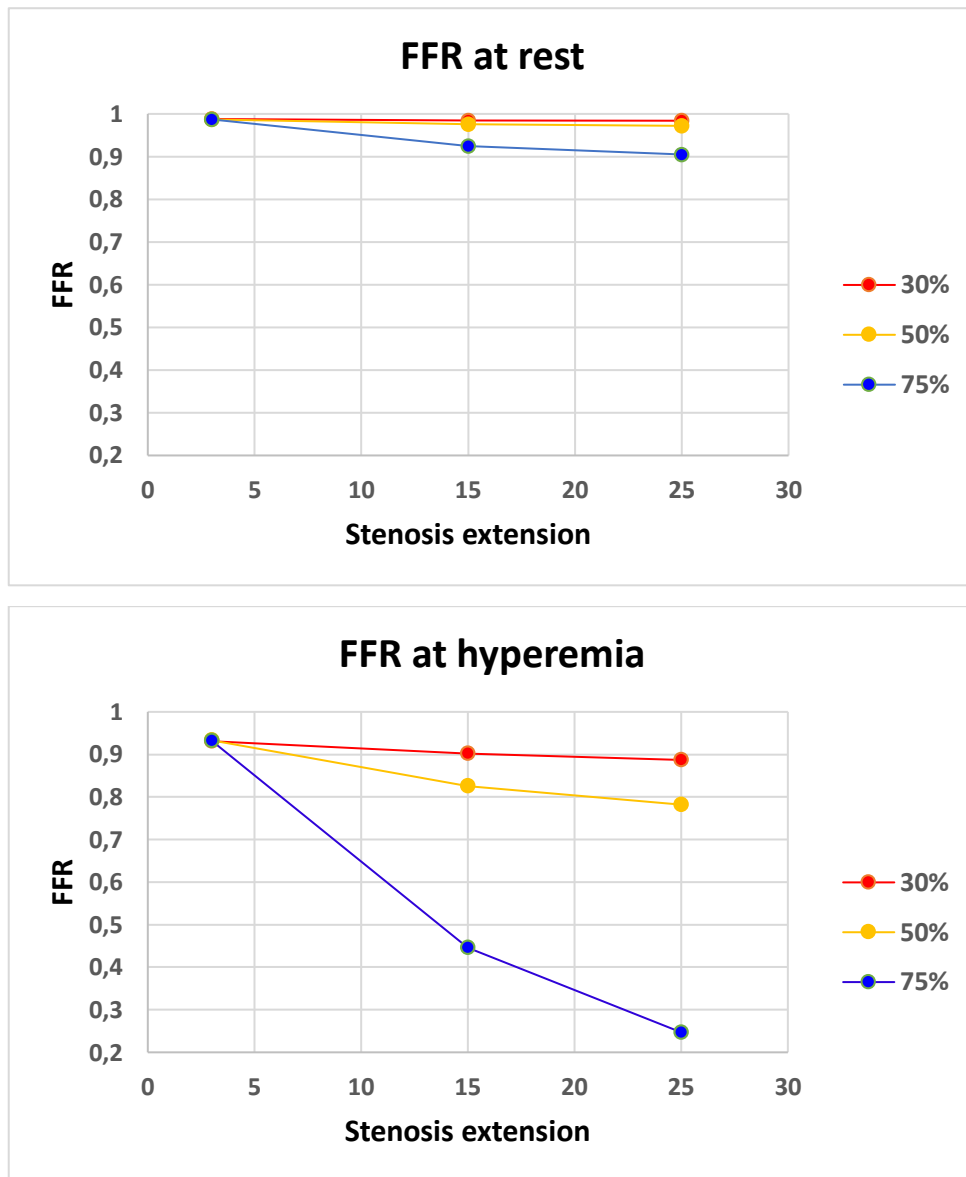


**Figure 5.7** Trend of FFR values in stenotic sites at rest and hyperemia

In all the models simulated at rest condition, FFR values are greater than 0.9, meaning that this condition of flow does not involve any significant pressure drop even in case of stenosis characterised by high degree of occlusion and extension.

Conversely, as regards the models simulated at hyperemic condition, it is possible to observe that consequences caused by stenoses for this value of flow, becomes dependent on the level of narrowing of the lesion and their extension. FFR is greater than 0.9 in all the models with  $L = 3$  mm, meaning that short stenoses are not significant even though their degree of occlusion is important. Value greater than 0.8 are also present in the stenotic models with 30% and 50% of occlusion characterized by  $L = 15$  mm, meaning that even if the extension is intermediate, these two degrees of narrowing are not

excessively important. Finally, FFR greater than 0.8 can be observed even in the model with 30% of occlusion and  $L = 25$  mm, which means that, even though this stenosis is quite extensive, the degree of occlusion is not so important to involve a significant pressure drop downstream of the stenosis.

On the other hand, in 3 cases it is possible to observe FFR values lower than 0.8. These models are the one with 75% of occlusion and  $L = 15$  mm, and the two models with 50% and 75% with  $L = 25$  mm. In these cases, pressure drops are important meaning that these three stenoses result as significant at this condition of flow. In particular, among these three models, the one with 50% of occlusion and  $L = 25$  mm has a FFR which is lower than 0.8 but greater than 0.75, meaning that physician's experience and the clinical history of the patient are necessary to take a decision in assessing the severity of this stenosis. As regards the other two models, the ones with 75% of occlusion, are characterized by a FFR much lower than 0.75, equal to 0.446 and 0.247 respectively for  $L = 15$  mm and  $L = 25$  mm, meaning that they are responsible for a high risk of ischaemia.

These results demonstrate that at rest the value of flow at the entrance of the vessel is not high enough to determine significant pressure drops, regardless of the morphological characteristics of the stenosis. Conversely, at hyperemia, as the degree of occlusion and the extension of the stenosis grow, the pressure drop downstream of the stenosis is more evident. Overall it can be deduced that pressure drop becomes more significant in presence of high values of flow showing a greater impact of stenoses geometric features on FFR values.

# CONCLUSIONS

The aim of this thesis was to observe the impact of stenoses geometric features on clinical parameters. This method was based on the calculation of virtual Fractional Flow Reserve (vFFR), an index which allows to quantify stenosis severity in terms of the pressure drop caused downstream of the stenosis itself. This parameter is useful to understand if a stenosis is critical or not and thus if it may involve ischemic events that must be prevented to avoid the worsening of patient clinical conditions.

First, a concentric Gaussian stenosis was created in the proximal left circumflex coronary artery, obtained by varying the percentage of occlusion (30, 50, 75%) and the extension along the vessel (3, 15, 25 mm), obtaining a total of nine stenotic models. Then, all models were meshed to perform CFD simulation. Mesh creation represents a critical step because a mesh which guarantees high accuracy must be chosen but it must not involve excessive computational times, so it is necessary to find a right compromise.

Subsequently, all models were simulated through steady-state CFD simulations setting two different values of flow at the entrance of the vessel, to evaluate the influence of stenosis to flow obstruction at rest and hyperemic conditions.

After performed steady simulations, WSS and static pressure gradient distribution were analysed in all the stenotic models and the FFR was calculated in the two conditions of flow, to understand the relationship between stenoses geometric features and the pressure drop they cause according to the condition of flow used.

WSS values are higher in the stenotic sites than in the other parts of the main branch, because stenosis represents an obstacle to blood flow and the stenotic wall undergoes higher shear stress. As regards pressure gradient, calculated with respect to inlet pressure, it increases along the vessel meaning a decrease of pressure values.

Both WSS values in the stenosis and the decrease of pressure downstream depend on stenosis morphology and on the value of flow through the vessel. In fact, WSS in the stenotic sites increases as the degree of occlusion and stenosis extension increase and this growth is greater at hyperemia because the walls are stressed by a higher flow. Pressure gradient, instead, undergoes a slight increase at rest which becomes more drastic at hyperemia as the entity of the stenosis increases.

Evaluating the distribution of FFR values, it is possible to affirm the dependence of pressure drop on stenosis geometry and on blood flow values. At rest FFR is always

greater than 0.9, meaning that this condition of flow does not involve any significant pressure drops whatever the entity of stenosis is. Conversely, at hyperemia blood flow is greater and the FFR results dependent on the level of occlusion and extension of the stenosis. This happens because stenosis hampers a greater flow with the result that the pressure drop is much higher. In particular, if a stenosis is characterized by a high degree of occlusion but it is not particularly extensive, the pressure drop it causes is quite negligible. On the other hand, a stenosis characterized by a high degree of occlusion and a wide extension provides very low FFR values indicating a high risk of ischaemia.

Overall, if the value of flow at the entrance of the vessel is low as at rest condition, pressure drops are not significant in any case, while if the value of flow is high as at hyperemia the pressure drop becomes dependent on the degree of occlusion and extension of stenosis. Thus, at hyperemia the impact of stenoses geometric features on FFR values is more evident.

Thanks to the robustness of CFD modelling, it has been possible to simulate the functional significance of different coronary stenoses, allowing to understand the relationship between stenoses morphology and their severity.

# BIBLIOGRAPHY

- [1] <https://www.britannica.com/science/circulatory-system>.
- [2] [http://www.vascularconcepts.com/content/pages.php?pg=patients\\_cardio\\_system&page=the\\_heart](http://www.vascularconcepts.com/content/pages.php?pg=patients_cardio_system&page=the_heart).
- [3] <https://www.thoughtco.com/the-heart-wall-4022792>.
- [4] [http://www.vascularconcepts.com/content/pages.php?pg=patients\\_cardio\\_system&page=cardiac\\_cycle](http://www.vascularconcepts.com/content/pages.php?pg=patients_cardio_system&page=cardiac_cycle).
- [5] [http://www.vascularconcepts.com/content/pages.php?pg=patients\\_cardio\\_system&page=blood\\_pressure](http://www.vascularconcepts.com/content/pages.php?pg=patients_cardio_system&page=blood_pressure).
- [6] <http://myheartandfitness.com/high-blood-pressure-cause-and-prevention/>.
- [7] <http://superagatoide.altervista.org/vasi-sanguigni.html>.
- [8] <https://www.britannica.com/science/blood-vessel>.
- [9] [http://www.vascularconcepts.com/content/pages.php?pg=patients\\_cardio\\_system&page=circulation](http://www.vascularconcepts.com/content/pages.php?pg=patients_cardio_system&page=circulation).
- [10] <https://www.ncbi.nlm.nih.gov/pubmedhealth/PMH0072434/>.
- [11] Azer K, Peskin CS. A one-dimensional model of blood flow in arteries with friction and convection based on the Womersley velocity profile. *Cardiovasc Eng*. 2007;7(2):51-73. doi:10.1007/s10558-007-9031-y.
- [12] <http://www.innerbody.com/image/cardov.html>.
- [13] BMSCV A.A 2016/2017.
- [14] [https://training.seer.cancer.gov/images/anatomy/cardiovascular/artery\\_wall.jpg](https://training.seer.cancer.gov/images/anatomy/cardiovascular/artery_wall.jpg).
- [15] <https://sites.google.com/site/zaneandnickcirculatorysystem/arteries-veins-and-capillaries>.
- [16] <https://www.medicinapertutti.it/argomento/struttura-dellarteria/>.
- [17] <https://www.medicinapertutti.it/argomento/arterie-di-grosso-calibro-di-tipo-elastico/>.

- [18] <https://medicinaonline.co/2017/01/23/differenza-tra-arterie-vene-capillari-arteriole-e-venule/>.
- [19] <http://geoface.info/ebff/e5578a68bff2/the-cardiovascular-system-blood-vessels-part-a-ppt-downl-07d73f>.
- [20] <https://www.britannica.com/science/blood-biochemistry>.
- [21] Johnston BM, Johnston PR, Corney S, Kilpatrick D. Non-Newtonian blood flow in human right coronary arteries: Steady state simulations. *J Biomech.* 2004;37(5):709-720. doi:10.1016/j.jbiomech.2003.09.016.
- [22] <http://www.panvascular.com/pagine/info/pazienti/common/coronarie.html>.
- [23] <http://www.ricercheradiologiche.it/CD/2005/ANATOMIA.HTM>.
- [24] <https://www.britannica.com/science/coronary-circulation>.
- [25] [https://www.hopkinsmedicine.org/healthlibrary/conditions/cardiovascular\\_diseases/anatomy\\_and\\_function\\_of\\_the\\_coronary\\_arteries\\_85,P00196](https://www.hopkinsmedicine.org/healthlibrary/conditions/cardiovascular_diseases/anatomy_and_function_of_the_coronary_arteries_85,P00196).
- [26] Pavone P., Fioranelli M., “Malattia Coronarica: Fisiopatologia e Diagnostica Non Invasiva con TC”. Springer-Verlag, Italia 2008.
- [27] Guyton A.C., Hall J.E., “Fisiologia Medica”, Tredicesima Edizione, Edra S.p.a., Milano,2017.
- [28] [http://www.med.unipg.it/ccl/Materiale%20Didattico/Fisiologia%20\(Grassi\)/Circolo%20coronarico.pdf](http://www.med.unipg.it/ccl/Materiale%20Didattico/Fisiologia%20(Grassi)/Circolo%20coronarico.pdf).
- [29] <https://myhealth.alberta.ca/Health/pages/conditions.aspx?hwid=hw139808>.
- [30] <http://articoli-medicina.blogspot.it/2009/09/arteriosclerosi.html>.
- [31] Della Rocca DG, Pepine CJ. Endothelium as a predictor of adverse outcomes. *Clin Cardiol.* 2010;33(12):730-732. doi:10.1002/clc.20854.
- [32] Friedman MH, Hutchins GM, Brent Barger C, Deters OJ, Mark FF. Correlation between intimal thickness and fluid shear in human arteries. *Atherosclerosis.* 1981;39(3):425-436. doi:10.1016/0021-9150(81)90027-7.
- [33] Steinman DA, Poepping TL, Tambasco M, Rankin RN, Holdsworth DW. Flow patterns at the stenosed carotid bifurcation: Effect of concentric versus eccentric stenosis. *Ann Biomed Eng.* 2000;28(4):415-423. doi:10.1114/1.279.

- [34] [https://www.informazionimediche.com/2011/09/ischemia\\_miocardica\\_sintomi\\_fattori\\_di\\_rischio\\_cause\\_e\\_terapie.html](https://www.informazionimediche.com/2011/09/ischemia_miocardica_sintomi_fattori_di_rischio_cause_e_terapie.html).
- [35] Lanzer P., Topol E.J., "PanVascular Medicine: Integrated Clinical Management", Springer-Verlag, 2002.
- [36] Lee KE, Kim GT, Lee JS, Chung JH, Shin ES, Shim EB. A patient-specific virtual stenotic model of the coronary artery to analyze the relationship between fractional flow reserve and wall shear stress. *Int J Cardiol.* 2016;222:799-805. doi:10.1016/j.ijcard.2016.07.153.
- [37] Shim EB, Kamm RD, Heldt T, Mark RG. Numerical analysis of blood flow through a stenosed artery using a coupled, multiscale simulation method. *Comput Cardiol.* 2000;27:219-222. doi:10.1109/CIC.2000.898496.
- [38] Ota H, Takase K, Rikimaru H, et al. Quantitative Vascular Measurements in Arterial Occlusive Disease. *RadioGraphics.* 2005;25(5):1141-1158. doi:10.1148/rg.255055014.
- [39] Oviedo C, Maehara A, Mintz GS, et al. Intravascular ultrasound classification of plaque distribution in left main coronary artery bifurcations where is the plaque really located? *Circ Cardiovasc Interv.* 2010;3(2):105-112. doi:10.1161/CIRCINTERVENTIONS.109.906016.
- [40] Li S, Chin C, Thondapu V, et al. Numerical and experimental investigations of the flow–pressure relation in multiple sequential stenoses coronary artery. *Int J Cardiovasc Imaging.* 2017;33(7):1083-1088. doi:10.1007/s10554-017-1093-3.
- [41] Bruyne B De, Pijls NHJ, Heyndrickx GR, et al. Pressure-Derived Fractional Flow Reserve to Assess Serial. 2000:1840-1847. doi:10.1161/01.CIR.101.15.1840.
- [42] Pijls NHJ, De Bruyne B, Bech GJW, et al. Coronary Pressure Measurement to Assess the Hemodynamic Significance of Serial Stenoses Within One Coronary Artery: Validation in Humans. *Circulation.* 2000;102(19):2371-2377. doi:10.1161/01.CIR.102.19.2371.
- [43] Valente S, Mattesini A, Rossini R, et al. Riserva frazionale di flusso : una breve guida pratica all ' utilizzo per l ' interventista e il punto di vista del cardiologo clinico. 2017:3-9.
- [44] Bedogni F, Indolfi C, Ribichini F, et al. Documento di posizione della Società Italiana di Cardiologia Invasiva-Gruppo Italiano Studi Emodinamici (SICI-GISE) sulle basi teoriche, applicazioni pratiche e valutazione economico-sanitaria dell'utilizzo della guida di pressione intracoronarica. *G Ital Cardiol.* 2015;16(2):116-128.

- [45] Kern MJ, Yu JH, Seto AH. Building a Fast Virtual Fractional Flow Reserve: Reductionists or Dreamers? *JACC Basic to Transl Sci.* 2017;2(4):447-449. doi:10.1016/j.jacbts.2017.07.005.
- [46] Siogkas PK, Sakellarios AI, Papafaklis MI, et al. Assessing the hemodynamic influence between multiple lesions in a realistic right coronary artery segment: A computational study. *Conf Proc . Annu Int Conf IEEE Eng Med Biol Soc IEEE Eng Med Biol Soc Annu Conf.* 2014;2014:5643-5646. doi:10.1109/EMBC.2014.6944907.
- [47] Kruk M, Wardziak Ł, Demkow M, et al. Workstation-Based Calculation of CTA-Based FFR for Intermediate Stenosis. *JACC Cardiovasc Imaging.* 2016;9(6):690-699. doi:10.1016/j.jcmg.2015.09.019.
- [48] Morris PD, Ryan D, Morton AC, et al. Virtual fractional flow reserve from coronary angiography: Modeling the significance of coronary lesions. Results from the VIRTU-1 (VIRTUal fractional flow reserve from coronary angiography) study. *JACC Cardiovasc Interv.* 2013;6(2):149-157. doi:10.1016/j.jcin.2012.08.024.
- [49] Pijls NHJ, Tanaka N, Fearon WF. Functional assessment of coronary stenoses: can we live without it? *Eur Heart J.* 2013;34(18):1335-1344. doi:10.1093/eurheartj/ehs436.
- [50] St. Jude Medical, Fractional Flow Reserve ( FFR ) — Shown to Improve Patient Outcomes and Reduce Costs. 2013;2(October):1-8.
- [51] Tonino PAL, Fearon WF, De Bruyne B, et al. Angiographic Versus Functional Severity of Coronary Artery Stenoses in the FAME Study. Fractional Flow Reserve Versus Angiography in Multivessel Evaluation. *J Am Coll Cardiol.* 2010;55(25):2816-2821. doi:10.1016/j.jacc.2009.11.096.
- [52] Fineschi M, Marzilli M, Huqi A. Lo studio FAME 2. *G Ital Cardiol.* 2013;14(10):636-640. doi:10.1714/1335.14828.
- [53] Taylor CA, Fonte TA, Min JK. Computational fluid dynamics applied to cardiac computed tomography for noninvasive quantification of fractional flow reserve: Scientific basis. *J Am Coll Cardiol.* 2013;61(22):2233-2241. doi:10.1016/j.jacc.2012.11.083.
- [54] Park S-J, Park S-W, Hong M-K, et al. Stenting of Unprotected Left Main Coronary Artery Stenoses: Immediate and Late Outcomes. *J Am Coll Cardiol.* 1998;31(1):37-42. doi:10.1016/S0735-1097(97)00425-7.
- [55] <https://www.cathlabdigest.com/articles/FAQ-FFR>.

- [56] Tu S, Barbato E, Kőszegi Z, et al. Fractional flow reserve calculation from 3-dimensional quantitative coronary angiography and TIMI frame count: A fast computer model to quantify the functional significance of moderately obstructed coronary arteries. *JACC Cardiovasc Interv.* 2014;7(7):768-777. doi:10.1016/j.jcin.2014.03.004.
- [57] Morris PD, Van De Vosse FN, Lawford P V., Hose DR, Gunn JP. "virtual" (Computed) Fractional Flow Reserve Current Challenges and Limitations. *JACC Cardiovasc Interv.* 2015;8(8):1009-1017. doi:10.1016/j.jcin.2015.04.006.
- [58] Morris PD, Silva Soto DA, Feher JFA, et al. Fast Virtual Fractional Flow Reserve Based Upon Steady-State Computational Fluid Dynamics Analysis: Results From the VIRTU-Fast Study. *JACC Basic to Transl Sci.* 2017;2(4):434-446. doi:10.1016/j.jacbts.2017.04.003.
- [59] <http://simvascular.github.io/docsFlowSolver.html>.
- [60] Brown AG, Shi Y, Marzo A, et al. Accuracy vs. computational time: Translating aortic simulations to the clinic. *J Biomech.* 2012;45(3):516-523. doi:10.1016/j.jbiomech.2011.11.041.
- [61] Kwon SS, Chung EC, Park JS, et al. A novel patient-specific model to compute coronary fractional flow reserve. *Prog Biophys Mol Biol.* 2014;116(1):48-55. doi:10.1016/j.pbiomolbio.2014.09.003.
- [62] Kim HJ, Vignon-Clementel IE, Coogan JS, Figueroa CA, Jansen KE, Taylor CA. Patient-specific modeling of blood flow and pressure in human coronary arteries. *Ann Biomed Eng.* 2010;38(10):3195-3209. doi:10.1007/s10439-010-0083-6.
- [63] Antiga L, Ene-lordache B, Remuzzi A. Computational geometry for patient-specific reconstruction and meshing of blood vessels from MR and CT angiography. *IEEE Trans Med Imaging.* 2003;22(5):674-684. doi:10.1109/TMI.2003.812261.
- [64] Antiga L, Piccinelli M, Botti L, Ene-lordache B, Remuzzi A, Steinman DA. An image-based modeling framework for patient-specific computational hemodynamics. *Med Biol Eng Comput.* 2008;46(11):1097-1112. doi:10.1007/s11517-008-0420-1.
- [65] Wertman BM, Cheng VY, Kar S, et al. Characterization of Complex Coronary Artery Stenosis Morphology by Coronary Computed Tomographic Angiography. *JACC Cardiovasc Imaging.* 2009;2(8):950-958. doi:10.1016/j.jcmg.2008.12.032.
- [66] Nakazato R, Park HB, Berman DS, et al. Noninvasive fractional flow reserve derived from computed tomography angiography for coronary lesions of intermediate stenosis severity results from the DeFACTO study. *Circ Cardiovasc Imaging.* 2013;6(6):881-889. doi:10.1161/CIRCIMAGING.113.000297.

- [67] Pietrabissa R, Mantero S, Marotta T, Menicanti L. A lumped parameter model to evaluate the fluid dynamics of different coronary bypasses. *Med Eng Phys.* 1996;18(6):477-484. doi:10.1016/1350-4533(96)00002-1.
- [68] van der Giessen AG, Groen HC, Doriot PA, et al. The influence of boundary conditions on wall shear stress distribution in patients specific coronary trees. *J Biomech.* 2011;44(6):1089-1095. doi:10.1016/j.jbiomech.2011.01.036.
- [69] Friedman MH. Variability of arterial wall shear stress, its dependence on vessel diameter and implications for Murray's Law. 2010;203(1):47-48. doi:10.1016/j.atherosclerosis.2008.07.003.Variability.